

## INFORMATION TO USERS

This manuscript has been reproduced from the microfilm master. UMI films the text directly from the original or copy submitted. Thus, some thesis and dissertation copies are in typewriter face, while others may be from any type of computer printer.

**The quality of this reproduction is dependent upon the quality of the copy submitted.** Broken or indistinct print, colored or poor quality illustrations and photographs, print bleedthrough, substandard margins, and improper alignment can adversely affect reproduction.

In the unlikely event that the author did not send UMI a complete manuscript and there are missing pages, these will be noted. Also, if unauthorized copyright material had to be removed, a note will indicate the deletion.

Oversize materials (e.g., maps, drawings, charts) are reproduced by sectioning the original, beginning at the upper left-hand corner and continuing from left to right in equal sections with small overlaps.

Photographs included in the original manuscript have been reproduced xerographically in this copy. Higher quality 6" x 9" black and white photographic prints are available for any photographs or illustrations appearing in this copy for an additional charge. Contact UMI directly to order.

ProQuest Information and Learning  
300 North Zeeb Road, Ann Arbor, MI 48106-1346 USA  
800-521-0600

UMI<sup>®</sup>



University of Alberta

**The Effect of  $\gamma$ -Dendrotoxin on  
Calcium-Activated Potassium Channels  
in Neuroblastoma Cells**

by

**Victoria Inglis**



A thesis submitted to the Faculty of Graduate Studies and Research  
in partial fulfillment of the requirements for the degree of  
Master of Science

Department of Physiology

Edmonton, Alberta

Spring, 2000



National Library  
of Canada

Acquisitions and  
Bibliographic Services

395 Wellington Street  
Ottawa ON K1A 0N4  
Canada

Bibliothèque nationale  
du Canada

Acquisitions et  
services bibliographiques

395, rue Wellington  
Ottawa ON K1A 0N4  
Canada

*Your file Votre référence*

*Our file Notre référence*

The author has granted a non-exclusive licence allowing the National Library of Canada to reproduce, loan, distribute or sell copies of this thesis in microform, paper or electronic formats.

The author retains ownership of the copyright in this thesis. Neither the thesis nor substantial extracts from it may be printed or otherwise reproduced without the author's permission.

L'auteur a accordé une licence non exclusive permettant à la Bibliothèque nationale du Canada de reproduire, prêter, distribuer ou vendre des copies de cette thèse sous la forme de microfiche/film, de reproduction sur papier ou sur format électronique.

L'auteur conserve la propriété du droit d'auteur qui protège cette thèse. Ni la thèse ni des extraits substantiels de celle-ci ne doivent être imprimés ou autrement reproduits sans son autorisation.

0-612-60131-5

**Canada**

University of Alberta

**Library Release Form**

Name of Author: **Victoria Inglis**  
Title of Thesis: **The Effect of  $\gamma$ -Dendrotoxin on Calcium-  
Activated Potassium Channels in  
Neuroblastoma Cells**  
Degree: **Master of Science**  
Year This Degree Granted: **2000**

Permission is hereby granted to the University of Alberta library to reproduce single copies of this thesis and to lend or sell such copies for private, scholarly or scientific purposes only.

The author reserves all other publication and other rights in association with the copying of the thesis, and except as hereinbefore provided neither the thesis nor substantial portion thereof may be printed or otherwise reproduced in any material form whatever without the author's written permission.


*Victoria Inglis*  
.....  
11340-79 Avenue Edmonton, Alberta

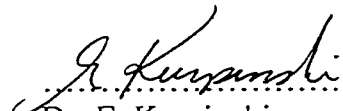
Date: *Jan. 5, 2000*

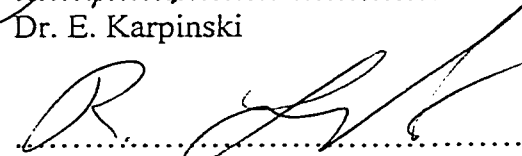
University of Alberta

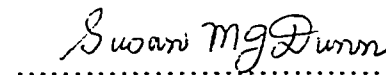
**Faculty of Graduate Studies and Research**

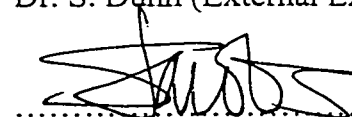
The undersigned certify that they have read, and recommend to the Faculty of Graduate Studies and Research for acceptance, a thesis entitled "The Effect of  $\gamma$ -Dendrotoxin on Calcium-Activated Potassium Channels in Neuroblastoma Cells" submitted by Victoria Inglis in partial fulfillment of the requirements for the degree of **Master of Science**.

  
.....  
Dr. C. Benishin (Supervisor)

  
.....  
Dr. E. Karpinski

  
.....  
Dr. R. Lewanczuk

  
.....  
Dr. S. Dunn (External Examiner)

  
.....  
Dr. S. Jacobs (Committee Chair)

Date: December 9, 1999.

## Abstract

Potassium currents in undifferentiated N1E 115 neuroblastoma cells were found to be sensitive to  $\gamma$ -dendrotoxin (DTX).  $\gamma$ -DTX-induced block was thought to be dependent upon the presence of calcium-activated potassium currents. The structurally related toxin  $\beta$ -DTX had a variable effect, while neither  $\alpha$ - nor  $\delta$ -DTX had any effect on recorded  $K^+$  currents.

Single channel studies using outside-out patches from undifferentiated N1E 115 cells confirmed that  $\gamma$ -DTX directly blocked one class of  $Ca^{2+}$ -activated  $K^+$  channel found in the patches: large conductance  $Ca^{2+}$ -activated  $K^+$  (BK(Ca)) channels. Another channel type found in the patch, intermediate conductance  $Ca^{2+}$ -activated  $K^+$  (IK(Ca)) channels was  $\gamma$ -DTX-insensitive. Both channels were insensitive to  $\alpha$ -DTX. The IK(Ca) channel, unlike the BK(Ca) channels in these patches, were weakly voltage-dependent, TEA- and IbTX-insensitive. These studies represent the first indication that any member of the DTX family can block  $Ca^{2+}$ -activated  $K^+$  channels, and that IK(Ca) channels are present in this cell line.

## Acknowledgments

I owe a great debt of gratitude to my supervisor, Dr. Christina Benishin for her support and guidance. Without her endless patience and encouragement I would not have been able to finish this thesis. I have benefited from her enthusiasm, generosity, and creativity.

I also thank Dr. Edward Karpinski for teaching me the finer points of the patch clamp technique and for his valuable technical support. Over the course of preparing this thesis he has answered endless silly questions with equanimity and has always been willing to provide thoughtful criticism and suggestions.

I also am grateful to Dr. Richard Lewanczuk for his creative suggestions and thought-provoking questions during both the experimental stage and the preparation of the thesis itself. Without his input I would not have considered all the possible implications of this work.

I am thankful to Lei Zhang, Bing Li, Ren Jun for their help in learning the patch clamp technique; they have all generously devoted their time to teaching me and helping to solve any technical problems. I also wish to thank Lienan Gu, Haiyan Jiao, and Fang Ba for all their help with tissue culture, in both teaching me the techniques and helping to maintain the cells. I also thank Teresa Labedz and Soly Sawada for their friendship and support—they have patiently listened to me, and were always ready to suggest possible solutions, or direct me to an alternative approach. Dr. Loren Kline has also been a great source of technical support. I also wish to thank all the members of Dr. Pang, Dr. Karpinski, and Dr. Benishin's labs for warmly accepting me and making this such a



valuable experience. They have all contributed to making me feel welcome and helping me to cope with the process of preparing and writing this thesis.

I also thank Michelle Evans and Annette Aarbo for all their help with the administrative side of this process.

Finally, I am indebted to my family for their unstinting support and unfailing belief in me. I would not have been able to finish this thesis without them. I thank my brother Thomas, my sister Laura, my mother and father, who have all contributed so much to the preparation and writing of this thesis. I dedicate this thesis to my mother, Elizabeth Hollis Berry and my grandmother Lillian Berry, who are a source of inspiration, and whose strength and love guide me.

# Table of Contents

## Chapter I Introduction and Literature Review

1.1	Introduction.....	1
1.2	Voltage-gated potassium channels.....	4
	1.2.1 Channel structure.....	4
	1.2.2 Channel kinetics.....	7
	1.2.3 Inactivation.....	8
1.3	Calcium-activated potassium channels.....	12
	1.3.1 Large conductance $\text{Ca}^{2+}$ -activated $\text{K}^{+}$ channels.....	13
	1.3.2 Small conductance $\text{Ca}^{2+}$ -activated $\text{K}^{+}$ channels.....	19
	1.3.3 Intermediate conductance $\text{Ca}^{2+}$ -activated $\text{K}^{+}$ channels.....	20
1.4	$\text{K}^{+}$ channel blockers from venoms.....	23
	1.4.1 Charybdotoxin.....	24
	1.4.2 Dendrotoxins.....	26
1.5	Neuroblastoma N1E 115 cell line.....	31
1.6	Objectives.....	34

## Chapter II Materials and Methods

2.1	Cell culture of neuroblastoma (N1E 115) cells.....	39
2.2	Whole-cell version of the patch clamp technique.....	40
	2.2.1 Electrodes.....	40
	2.2.2 Solutions.....	41
	2.2.3 Experimental procedures.....	41
	2.2.4 Data analysis.....	43
2.3	Single channel recording.....	44
	2.3.1 Electrodes.....	44
	2.3.2 Solutions.....	45
	2.3.3 Experimental procedures.....	45
	2.3.4 Data analysis.....	46
2.4	Measurement of free calcium.....	47
2.5	Chemicals and their preparation.....	48

2.6	Statistics.....	49
-----	-----------------	----

### **Chapter III Whole-cell results**

3.1	Introduction.....	51
3.2	Experimental design.....	51
	3.2.1 Characterization of outward currents.....	51
	3.2.2 Pharmacology of potassium currents.....	52
	3.2.3 Effect of dendrotoxins on potassium currents.....	52
3.3	Results.....	53
	3.3.1 Characterization of outward currents.....	53
	3.3.2 Pharmacology of whole-cell potassium currents.....	56
	3.3.3 Effect of dendrotoxins on whole-cell potassium currents.....	56

### **Chapter IV Single channel results**

4.1	Introduction.....	80
4.2	Experimental design.....	80
	4.2.1 Characterization of single channels.....	80
	4.2.2 Pharmacology of single channels.....	81
	4.2.3 Effect of $\gamma$ -DTX on single channels.....	82
4.3	Results.....	82
	4.3.1 Characterization of the single channels.....	82
	4.3.2 Pharmacology of the single channels.....	83
	4.3.3 Effect of $\gamma$ -DTX on single channels .....	85

### **Chapter V Discussion**

5.1	Whole-cell results.....	114
5.2	Single channel results.....	116
5.3	Implications and significance.....	119

<b>References.....</b>	<b>122</b>
------------------------	------------

## List of Tables

- Table III-1. The population of deactivation time constants fitted by one exponential from tail current decay from +20 mV to the holding potential of -80 mV can be divided into three main groups: fast, medium and slow.....60
- Table III-2. The effect of  $\beta$ - and  $\gamma$ -DTX on whole-cell  $K^+$  currents is dependent on the presence of saturating currents in control recordings.....61

## List of Figures

Figure I-1. Hypothetical arrangement of the K <sup>+</sup> channel subunit for (A) voltage-gated, (B) inward rectifier, and (C) minimal K <sup>+</sup> (minK <sup>+</sup> ) channels.....	36
Figure I-2. A scheme showing the classification of K <sup>+</sup> channels, showing the six transmembrane (6TM), and two transmembrane (2TM) subunit structural classes and their division into K <sup>+</sup> channel families and subfamilies.....	37
Figure I-3. Models of channel N-type and C-type, and $\beta$ -subunit inactivation.....	38
Figure II-1. A diagram showing how outside-out patches were prepared.....	50
Figure III-1. Voltage protocols given, and the resultant outward currents showing cell-to-cell variation among recorded currents in the presence of pipette EGTA, ATP and Ca <sup>2+</sup> .....	62
Figure III-2. Tail current decay and examples of curve fitting by one and two exponentials.....	63
Figure III-3. Plots of tail current decay versus voltage and tail current deactivation time constants versus voltage are used to determine the potential at which all K <sup>+</sup> channels are active.....	64
Figure III-4. The reversal potential of whole-cell currents recorded in the presence of EGTA, ATP and Ca <sup>2+</sup> .....	65
Figure III-5. Effect of 20 mM TEA application on whole-cell K <sup>+</sup> currents recorded in the presence of pipette EGTA, ATP and Ca <sup>2+</sup> .....	66
Figure III-6. Effect of 1 mM TEA application on whole-cell K <sup>+</sup> currents recorded in the presence of pipette EGTA, ATP and Ca <sup>2+</sup> .....	67
Figure III-7. Effect of 1 mM 4-AP application on whole-cell K <sup>+</sup> currents recorded in the presence of pipette EGTA, ATP and Ca <sup>2+</sup> .....	68
Figure III-8. Effect of 50 $\mu$ M 4-AP application on whole-cell K <sup>+</sup> currents recorded in the presence of pipette EGTA, ATP and Ca <sup>2+</sup> .....	69
Figure III-9. Effect of 200 nM $\alpha$ -DTX application on whole-cell K <sup>+</sup> currents recorded in the presence of pipette EGTA, ATP and Ca <sup>2+</sup> .....	70

Figure III-10. Effect of 200 nM $\delta$ -DTX application on whole-cell $K^+$ currents recorded in the presence of pipette EGTA, ATP and $Ca^{2+}$ .....	71
Figure III-11. Effect of 200nM $\beta$ -DTX application on whole-cell $K^+$ currents recorded in the presence of pipette EGTA, ATP and $Ca^{2+}$ .....	72
Figure III-12. The corresponding I-V plots are shown for the representative traces in Figure III-11, revealing the dual effect of $\beta$ -DTX application.....	73
Figure III-13. Effect of 200 nM $\gamma$ -DTX application on whole-cell $K^+$ currents recorded in the presence of pipette EGTA, ATP and $Ca^{2+}$ .....	74
Figure III-14. The corresponding I-V plots are shown for the representative traces in Figure III-13, revealing the dual effect of $\gamma$ -DTX application.....	75
Figure III-15. Summary of the mean outward current at +20 mV (A) 5 minutes and (B) 10 minutes after drug application in the presence of pipette EGTA, ATP, and $Ca^{2+}$ .....	76
Figure III-16. Voltage protocols given, and the resultant $K^+$ currents showing recorded currents in the presence of pipette EGTA, and absence of ATP and $Ca^{2+}$ .....	77
Figure III-17. Effect of 2 $\mu$ M $\gamma$ -DTX application on whole-cell $K^+$ currents recorded in the presence of pipette EGTA, and absence of ATP and $Ca^{2+}$ .....	78
Figure III-18. Effect of 2 $\mu$ M $\gamma$ -DTX application on whole-cell $K^+$ currents recorded in the presence of pipette $Ca^{2+}$ and EGTA, and absence of ATP.....	79
Figure IV-1. Outside-out patches from undifferentiated N1E 115 cells exhibited 2 channel types active in the patch under the conditions used.....	88
Figure IV-2. Determination of single channel conductance based on linear regression of a current-voltage plot, and an all-points histogram from a recording of the larger channel are shown.....	89
Figure IV-3. The 63 pS channel exhibited a characteristic pattern of cycling through periods of burst openings followed by several seconds of silence.....	90
Figure IV-4. The 63 pS channel was found to be weakly voltage-dependent.....	91
Figure IV-5. The 187 pS channel exhibited a characteristic pattern of voltage-dependence.....	92
Figure IV-6. The 187 pS channel showed great variations in open probability.....	93

Figure IV-7. The 187 pS channel is very sensitive to Ca <sup>2+</sup> channel blockade by 1 μM nifedipine.....	94
Figure IV-8. The 63 pS channel is also sensitive to Ca <sup>2+</sup> channel blockade by 1 μM nifedipine.....	95
Figure IV-9. Effect of 10 nM ionomycin application on 63 pS channel open probability in patches held at positive potentials.....	96
Figure IV-10. Effect of 10 nM ionomycin application on 187 pS channel open probability in patches held at positive potentials.....	97
Figure IV-11. Neither the 63 pS channel, nor the 187 pS channel were sensitive to application of the Cl <sup>-</sup> channel blocker SITS (1 mM).....	98
Figure IV-12. The 63 pS channel is insensitive to application of the SK(Ca) channel blocker apamin (100 nM).....	99
Figure IV-13. Effect of 1 mM TEA application on 63 pS channel open probability in patches held at positive potentials.....	100
Figure IV-14. Effect of 1 mM TEA application on 187 pS channel open probability in patches held at positive potentials.....	101
Figure IV-15. Effect of 1 μM IbTX application on 63 pS channel open probability in patches held at positive potentials.....	102
Figure IV-16. Effect of 1 μM IbTX application on 187 pS channel open probability in patches held at positive potentials.....	103
Figure IV-17. Effect of 200 nM α-DTX application on 63 pS channel open probability in patches held at positive potentials.....	104
Figure IV-18. Effect of 200 nM α-DTX application on 187 pS channel open probability in patches held at various potentials.....	105
Figure IV-19. Effect of 200 nM β-DTX application on 63 pS channel open probability in patches held at positive potentials.....	106
Figure IV-20. Effect of 200 nM γ-DTX application on 63 pS channel open probability in patches held at positive potentials.....	107
Figure IV-21. Effect of 200 nM β-DTX application on 187 pS channel open probability in patches held at various potentials.....	108
Figure IV-22. Effect of 200 nM γDTX application on 187 pS channel open probability in	

patches held at various potentials.....	109
Figure IV-23. Effect of 20 nM $\gamma$ DTX application on 187 pS channel open probability in patches held at various potentials.....	110
Figure IV-24. Effect of 2 nM $\gamma$ DTX application on 187 pS channel open probability in patches held at various potentials.....	111
Figure IV-25. Graph of the effect of (A) 200 nM or (B) 20 nM $\gamma$ -DTX application on 187 pS channel open probability as a function of holding potential.....	112
Figure IV-26. Graph of the effect of 2 nM $\gamma$ -DTX application on 187 pS channel open probability as a function of holding potential.....	113



## List of Symbols and Abbreviations

$\alpha$	alpha
$\beta$	beta
$\delta$	delta
$\gamma$	gamma
$[\text{Ca}^{2+}]_{\text{free}}$	free calcium concentration
$[\text{K}^+]_i$	intracellular potassium concentration
$[\text{K}^+]_o$	extracellular potassium concentration
2TM	two transmembrane domains
4-AP	4-aminopyridine
6TM	six transmembrane domains
a.h.p.	afterhyperpolarization
ACh	acetylcholine
ATP	adenosine 5' triphosphate
$\text{Ba}^{2+}$	barium
BK(Ca)	large-conductance calcium-activated potassium channels
BPTI	bovine pancreatic trypsin inhibitor
$\text{Ca}^{2+}$	calcium
cAMP	cyclic monophosphate
$\text{Cd}^{2+}$	cadmium
ChBTX	charybdotoxin
$\text{Cl}^-$	chloride
CNG	cyclic nucleotide-gated channels
C-terminal	carboxy-terminal
DMEM	Dulbecco's Modified Eagle Medium
DMSO	dimethyl sulfoxide
<i>dslo</i>	<i>Drosophila</i> large-conductance calcium-activated potassium channel gene
DTX	dendrotoxin
eag	ether a go-go channel
EGTA	ethyleneglycol-bis-( $\beta$ -aminoethyl ether) N,N,N',N'-tetraacetic acid
$E_K$	equilibrium potential for potassium
ELI	external lock-in site
F	Faraday constant
FBS	fetal bovine serum
H5	potassium channel domain that is predicted to span half of the membrane
HBSS	Hank's Balanced Salt Solution
HEPES	N-2'-ethanesulfonic acid
<i>hslo</i>	human large-conductance calcium-activated potassium channel gene
IbTX	iberiotoxin

IK(Ca)	intermediate conductance calcium-activated potassium channels
I-V plot	current-voltage plot
K <sup>+</sup>	potassium
KQT	potassium channel implicated in long QT syndrome
KTX	kaliotoxin
MCDP	mast cell degranulating peptide
Mg <sup>2+</sup>	magnesium
MgTX	margatoxin
<i>mslo</i>	mouse large-conductance calcium-activated potassium channel gene
Na <sup>+</sup>	sodium
NAD(P)H	nicotinamide adenine dinucleotide phosphate, reduced form
N-terminal	amino-terminal
NTX	noxiustoxin
P-region	potassium channel pore-region
R	gas constant
S1-S6	putative potassium channel membrane-spanning domains
ScyTX	scyllatoxin (leiurotoxin I)
SITS	4-acetamino-4'-isothiocyano-2, 2'-disulfonic acid stilbene
SK(Ca)	small conductance calcium-activated potassium channels
StK	stichodactyla toxin
TEA	tetraethylammonium
TTX	tetrodotoxin
Zn <sup>2+</sup>	zinc

# Chapter I

## Introduction and Literature Review

### 1.1 Introduction

Potassium channels are among the most diverse channel types and are found in almost every eukaryotic cell. First characterized by Hodgkin and Huxley, potassium channels have been shown to play a role not exclusive to action potential repolarization, or even to excitable cells. Aside from regulation of excitability in nerve and muscle, ranging from interspike interval duration to bursting activity, potassium channels have been found to play a part in the regulation of volume in exocrine cells, of insulin release in endocrine pancreatic  $\beta$  cells (Jan, and Jan, 1989; Cook, 1988), and of transepithelial transport in kidney and colon (Schultz, 1984; Herbert, Friedman, and Andreoli, 1984; Winters, Reeves, and Andreoli, 1991; Dawson, 1991). Based on channel kinetics, there are four main groups of potassium channel type, loosely functionally organized into voltage-gated, calcium-activated, inward rectifiers, and ligand-gated (ligands include nucleotides, ATP (adenosine 5'-triphosphate), acetylcholine (ACh), and cations) channels. Within each of these groups there are significant functional and structural divisions, with new subtypes being discovered.

Structurally, potassium channels differ from other classes of voltage-gated channel (i.e. Na<sup>+</sup> and Ca<sup>2+</sup> voltage-gated channels) in that the channel pore is not formed from one contiguous unit, but from four separate subunits, coming together to form a homo- or heteromultimeric channel complex (Ruppersberg et al., 1990; Christie et al., 1990; Wang et al., 1993; Sheng et al., 1993; Dolly et al., 1994). Potassium channels are divided into three family classes based on the number of transmembrane domains per channel subunit: inward rectifiers, S4 superfamily members, and minK<sup>+</sup> channels. Subunits of potassium channel members of the S4 superfamily (which also include voltage-gated Na<sup>+</sup> and Ca<sup>2+</sup> channels) are thought to consist of six transmembrane (6TM) domains. In contrast, inwardly rectifying potassium channels (which are activated by hyperpolarizing potentials) have subunits with two transmembrane (2TM) domains (ATP- and pH-sensitive channels are members of this channel family; Christie, 1995), and minK<sup>+</sup> channels (a voltage-dependent, slowly activating K<sup>+</sup> channel) have a single transmembrane domain from hydrophathy profiles (Tagliatela and Brown, 1995; see Figure I-1). Genome sequencing of the nematode *Caenorhabditis elegans* revealed eight potassium channel types, discovered by using probes screening for the conserved pore-forming region of the potassium channel (Wei, Jegla, and Salkoff, 1996). Nearly all of the discovered channels are members of the 6TM subunit (or S4 family) class, and these include the voltage-gated (which are activated by depolarizing potentials, and include the *Shaker* (Kv1), *Shab* (Kv2), *Shaw* (Kv3), *Shal* (Kv4) subfamilies), large-conductance (*Slo*) calcium-activated, small-conductance calcium-activated, cyclic nucleotide-gated (CNG), KQT-like (implicated in long QT syndrome), and eag (nucleotide-activated ether a go-go)-like potassium channels (Wei, Jegla, and Salkoff, 1996). The eag channel is

permeable to  $K^+$  and  $Ca^{2+}$ , and is modulated by cAMP (cyclic monophosphate; Christie, 1995). Thus, to a certain extent, structural studies of the voltage-gated channels reveal basic structural elements that are conserved among a number of channel subfamilies.

Most functional studies use separate names, depending on cell type and species, which are unrelated to the genetic ones; in functional classification systems, the voltage-gated channels are designated as having characteristics similar to either delayed-rectifier (*Shab* (Kv2), or *Shaw* (Kv3)), or inactivating (*Shaker* (Kv1), or *Shal* (Kv4)) potassium currents. In case of multiple names for a single channel, the channel name will be correlated with the genetic counterpart where possible.

Although there is an absence of specific channel blockers, the majority of the structural and functional studies are predominantly based on sensitivity to various channel blockers, most notably organic cations, such as tetraethylammonium (TEA), and toxins (mainly from snake and scorpion venom), and more recently on manipulations of cloned potassium channels. Toxins have proven particularly useful as channel blockers and as tools in the study of potassium channel structural and functional diversity. One toxin family in particular, the dendrotoxins, derivatives of venom from the mamba (*Dendroaspis*) snakes, have been shown to selectively block potassium channels (Bentoit and Dubois, 1986; Penner et al., 1986; Benishin et al., 1988; Dolly et al., 1989), and have been used to characterize and isolate channels (Awan and Dolly, 1991; Muniz, Parcej, and Dolly, 1992; Hall et al., 1994; Scott et al., 1994). In a discussion of the effects of these toxins, it is important to document channel structure, and sites of action of channel blockers for both the voltage-gated and the calcium-activated potassium channels.

## 1.2 Voltage-Gated Potassium Channels

Depolarizing potentials activate voltage-gated potassium channels; there are two types of voltage-gated channel: delayed rectifiers (slowly inactivating), and transient (inactivating) “A” currents.

### 1.2.1 Channel Structure

Current models of potassium channel topology are based on work on voltage-gated potassium channels, which are, of all potassium channels, the best known and most well studied. Voltage-gated potassium channels fall into four main subfamilies, and are designated either *Shaker*, *Shab*, *Shaw* and *Shal*, from genetic work in mouse or fruit fly (Chandy, 1991), or Kv1, Kv2, Kv3, and Kv4 (nomenclature of Chandy, 1991), respectively, from work in humans.

All experimental data suggests that a functional voltage-gated potassium channel consists of four  $\alpha$ -subunits, each with six transmembrane domains (S1-S6), combining with four intracellular  $\beta$ -subunits (these are small, noncovalently linked, regulatory subunits; Dolly et al, 1994; Scott et al., 1994a). This very system of combining subunits allows for great diversity in potassium channel structure and function, as alternate splicing of channel genes provides endless variations of potassium channel primary structure, so the many combinations of these subunits results in further variety of tertiary structure. It is important to note, however, that while  $\alpha$ -subunit heteromultimers are possible within a subfamily, genes from different subfamilies have not been found to intermix (McCormack et al., 1990). The S1 region (the first transmembrane domain of the  $\alpha$ -subunit) is involved in the correct assembly of the  $\alpha$ -subunit tetramers (Keynes,

1994). Also, N- and C-terminal deletion mutants of mKv1.1 and mKv1.3 (mouse *Shaker*-like channels) revealed that a complete N-terminal is essential for correct assembly of functional channel homo- and heteromultimers (Hopkins, Demas, and Tempel, 1994). Li et al. (1992) have established that a 114 amino acid stretch in the N-terminal, which is conserved among the Kv1.1 (*Shaker*) subfamily, is necessary for binding a *ShakerB* N-terminal to a *ShakerB* polypeptide.

Hypothetical tertiary structure models indicate that the six transmembrane domains (S1 to S6) are oriented so that both the amino- and carboxy- termini are intracellular, and the region between the S5 and S6 domains forms a unique hairpin loop (the H5 or P-region) that spans half of the membrane (Kukuljan, Labarca and Latorre, 1995; see Figure I-1). The S4 domain is amphipathic, with up to 8 positively charged amino acids, and is similar to the voltage-sensors in the Na<sup>+</sup> and Ca<sup>2+</sup> voltage-gated channels (Kukuljan, Labarca, and Latorre, 1995). The structure of the S4 segment, as well as the hairpin loop of the H5 region is well conserved in the S4 superfamily of channels, which includes Na<sup>+</sup>, Ca<sup>2+</sup>, and K<sup>+</sup> voltage-gated channels, and also calcium-activated, cyclic-nucleotide-activated, and eag K<sup>+</sup> channels (Kukuljan, Labarca, and Latorre, 1995). In addition the H5 or pore-lining region is highly conserved among K<sup>+</sup> channel families (Wei, Jegla, and Salkoff, 1996; see Figure I-2).

Experiments using chimeric channels reveal that a stretch of amino acids between S5 and S6 (i.e. the P region) confer ion selectivity and TEA (a membrane impermeable, non-specific K<sup>+</sup> channel blocker, which blocks from either intracellular, or extracellular sites) sensitivity for delayed rectifier NGK2 (a channel of the *Shaw* subfamily, or Kv3.1a), and DRK1 (a channel of the *Shab* subfamily, or Kv2.1) (Hartmann et al., 1991).

Amino acid point mutations in the P region of *Shaker* K<sup>+</sup> channels dramatically affect conductance, gating and ionic selectivity (Yool and Schwarz, 1991). Pinpointing the amino acids in the P-region which when mutated affect either internal or external TEA block has led to the discovery of an 8 amino acid stretch that is not accessible to TEA, and, thus, are predicted to form the connection between the inner and outer vestibules of the channel (Yellen et al., 1991). Based on this information, to conform with biophysical predictions of pore size and conductance, the P-region needs to form a  $\beta$ -sheet and not an  $\alpha$ -helix, and this would provide a pore length of 2.7 nm (Guy and Conti, 1990). Furthermore, the sequence which acts as a K<sup>+</sup> channel “fingerprint” within the P-region is an 8 amino acid stretch of TXXTXGYG (X denotes any residue), and point mutations of this sequence indicate that it forms part of the selectivity filter (Heginbotham et al., 1994).

The search for K<sup>+</sup> channel pore structure is not limited to the H5 region and has been shown to include both the S4-S5 loop, and the S6 domain (Slesinger, Jan and Jan, 1993; Lopez, Jan and Jan, 1994). The site of internal TEA block has been found to be both in the P-region and the S6 domain, which is consistent with the charged head of the TEA molecule binding in the P-region, while the hydrophobic tail binds in the S6 domain (Choi et al., 1993). Internal TEA block has been shown by Choi et al. (1993) to be affected by point mutations of polar residues on the outer edge of the P-region. The binding site for 4-aminopyridine (4-AP), a membrane-permeant K<sup>+</sup> channel blocker is cytoplasmic (based on work with a membrane-impermeant analogue 4-AP methiodide; Kirsch and Drewe, 1993), and found in the S4-S5 segment, as well as the S6 domain (Kirsch et al., 1993). Interestingly, TEA and 4-AP have been found to compete for the



S6 domain binding site, which is thought to be the region for binding of the hydrophobic TEA tail (Kirsch et al., 1993). While the voltage-dependence of TEA block can be explained by the P-region binding site for the charged head, the 4-AP and TEA tail binding sites in the S6 domain are thought to be outside of the membrane electric field, explaining the voltage independence of 4-AP block and TEA tail binding (Kirsch et al., 1993).

### 1.2.2 Channel Kinetics

Voltage-gated  $K^+$  channels are activated by depolarizing potentials, and this activation was first described by Hodgkin and Huxley (1952) to follow a first-order kinetic variable of  $n^4$  (such that four “gating particles” are required for activation), and a sigmoidal time course. For delayed rectifiers, the time course of activation can vary between a msec to tens of msec; “A” current activation is faster than that of delayed rectifiers, but is dependent on hyperpolarizing potentials for maximal activation (Adams and Nonner, 1990). Once open, both types of voltage-gated channel share similar conductance ranges: delayed rectifiers have been reported to have a single channel conductance in the 2-60 pS range, and “A”-currents in the conductance range of 6-30 pS (Adams and Nonner, 1990).

It is a generally accepted theory that the S4 domain, which is conserved among voltage-gated channels, is the voltage sensor, and it is the movement of this domain (in each of the four channel subunits), in response to voltage, that forms Hodgkin and Huxley’s “gating particle” (Keynes, 1994). Mutation of charged amino acids in S4 has been found to alter both channel voltage sensitivity, and charge movement (Liman et al., 1991; Papazian et al., 1991; Logothetis et al., 1992). Movement of S4 segment amino

acid residues from within the membrane to the extracellular space has confirmed the theory that channels undergo conformational changes in response to voltage (Larsson et al., 1996; Mannuzzu, Maronne, and Isacoff, 1996). It should be noted, however, that while S4 segment movement is well established, a correlation of S4 segment charge with experimental determinations of the gating charge has not been made, so that the nature of S4 segment involvement in the a channel's transition from a closed to open state has not been established (Franciolini, 1994). Study of the movement of the S4 segment during channel activation (based on the interaction of substituted transmembrane cysteine residues with a membrane impermeable agent) has indicated that a stretch of at least 6 residues moves into the extracellular space following depolarization, and that these same residues could also be exposed to the extracellular space following hyperpolarizing pulses (Yusaf, Wray, and Sivaprasadarao, 1996). Current models of channel activation involve a transition through many closed states, before the channel opens (Taglialatela, and Brown, 1995). Helical movement of the positively charged S4 domain is thought to be the voltage-dependent step in gating, and is accompanied by the voltage-independent movement of leucine residues on the amphipathic S4-S5 loop (Guy and Durrell, 1994). Interaction of the positive residues on the S4-S5 loop with the negative charges on the S3 and S2 segments may play a role in opening the mouth of the pore (Keynes, 1994), and thus, allowing  $K^+$  ion movement.

### **1.2.3 Inactivation**

Inactivation kinetics distinguish delayed rectifiers from "A"-currents; while delayed rectifiers inactivate over seconds, transient "A"-currents spontaneously inactivate in milliseconds (Adams and Nonner, 1990). Inactivation of the voltage-gated potassium

channels can take one of two forms: fast, or N-type inactivation (common in “A”-type currents), or slower C-type inactivation (seen in either delayed rectifiers, or “A”-currents). There are two possible mechanisms for N-type inactivation, involving either the inactivation “ball”, which consists of the N-terminal domain of the channel itself, or the  $\beta$ -subunits. Both the inactivation ball and  $\beta$ -subunit compete for binding sites on the inner mouth of the channel. Work with *Shaker* deletion mutants showed that the N-terminal is involved in the fast inactivation of *ShakerB* channels. Deletion of the first 22 amino acids is similar to intracellular trypsin treatment, in that both dramatically slow inactivation, while deletion closer to the transmembrane domain S1 decreases mean open times proportionally to the length of deletion (Hoshi, Zagotta and Aldrich, 1990). On the basis of these results, Hoshi, Zagotta and Aldrich (1990) concluded that the 22 amino acid stretch forms the inactivation ball, which is tethered to the channel by the rest of the N-terminal. Deletion of the entire N-terminal of RCK4 (Kv1.4) results in a switch from an “A”-type current to a slowly inactivating current (Rettig et al., 1994); similarly, deletion of 25 amino acids from the N-terminal of mammalian cardiac fast-inactivating  $K^+$  channels significantly slows fast inactivation (Tseng-Crank et al., 1994a). Furthermore, channels that do not exhibit fast inactivation, such as  $Ca^{2+}$ -activated  $K^+$  channels and cyclic nucleotide-gated channels, can be blocked by intracellular application of the *ShakerB* inactivation ball peptide (Torro, Stefani, and Latorre, 1992; Kramer, Goulding and Siegelbaum, 1994).

The auxiliary  $\beta$ -subunits, which are tightly associated with  $K^+$  channel cytoplasmic domains, confer rapid inactivation on otherwise non-inactivating  $K^+$  channels (Rettig et al., 1994; Heinemann et al., 1996).  $K^+$  channel  $\beta$ -subunits belong to a

gene superfamily which resembles the NAD(P)H-dependent reductases (McCormack and McCormack, 1994), and the  $\beta$ -subunit inactivating domain shares similar structural features with the  $K^+$  channel  $\alpha$ -subunit N-terminal inactivation ball (Leicher et al., 1996). Based on studies with N-terminal deletion mutants of Kv1.4 (an “A” current channel), inactivation is more rapid when exerted by a  $\beta$ -subunit splice variant Kv $\beta$ 1.1, than with either the wild type channel, or coexpression of the wild type channel and the  $\beta$ -subunit (Leicher et al., 1996). Leicher et al. (1996) postulated that the intermediate inactivation time constant with coexpression of the wild type channel and the  $\beta$ -subunit could be explained by competition between the  $\alpha$ -subunit inactivation ball and the  $\beta$ -subunit for binding to the inactivating domain on the channel mouth.  $\beta$ -subunit splice variants exhibit differential expression in human brain slices, as well as variable potencies of conferring rapid inactivation on hKv1.5 (a non-inactivating  $K^+$  channel) when expressed in *Xenopus* oocytes (Leicher et al., 1996).  $\beta$ -subunit splice variants are not able to confer rapid inactivation on all Kv1 channels: Heinemann et al. (1996) found that Kv $\beta$ 1.1 potentiates rapid inactivation for Kv1.1, Kv1.2, Kv1.5 channels, but not Kv1.3 and Kv1.6.

The site of N-type channel inactivation is proposed to consist of both charged and hydrophobic binding sites (Kukuljan, Labarca, and Latorre, 1995). The inactivation ball itself consists of 11 uncharged amino acids followed by 8 highly polar amino acids; both of these regions are essential for inactivation (Hoshi, Zagotta, and Aldrich, 1990). Amino acid point mutations indicate both that the ball itself is positively charged and it exerts an electrostatic interaction with the negatively charged channel pore (Murrell-

Lagnado, and Aldrich, 1993), and that hydrophobic interactions between the inactivation ball and the pore stabilise channel inactivation kinetics (Isacoff, Jan and Jan, 1991; see Figure I-3). Similar to internal TEA blockade, the inactivation ball has been found to be an open channel blocker in *ShakerB*, since recovery from inactivation is accelerated both with increases in the extracellular  $K^+$  concentration and with hyperpolarization of the membrane (Demo and Yellen, 1991). The rate of fast inactivation is also affected by the number of inactivating balls per channel, so that channel variability may also be a function of the presence or absence of an inactivation ball on any of the four subunits which make up a functional channel. Experiments using *Shaker* subunits with or without the inactivation ball revealed that channels comprised of fewer than 4 inactivation ball segments exhibit slower inactivation rates in proportion to the number of inactivating balls per channel (MacKinnon, Aldrich and Lee, 1993).

Structurally the  $\beta$ -subunit N-terminal is similar to the  $\alpha$ -subunit N-terminal, and deletion of the  $\beta$ -subunit N-terminal also abolishes fast inactivation, which is recovered with the addition of the N-terminal peptide (Rettig et al., 1994).  $\beta$ -subunit induced fast inactivation responds to the same experimental manipulations that N-terminal induced inactivation does, in terms of the effect of external  $K^+$  concentration, and alterations of the charge of the  $\beta$ -subunit N-terminal. The  $\beta$ -subunit can mimic the effect of the N-terminal inactivation ball; both the  $\beta$ -subunit and the N-terminal inactivation ball are thought to interact with the same site on the channel pore, (Rettig et al., 1994). Oxidation of either the inactivation ball or the  $\beta$ -subunit dramatically hinders the entry into the inactivated state (Rettig et al., 1994).

A slower form of inactivation, C-type inactivation, is thought to be the domain of the pore itself (Kukuljan, Labarca, and Latorre, 1995). Contrary to N-type inactivation, all the evidence suggests that C-type inactivation involves a conformational change in the channel pore itself, rather than a ball-and-chain occlusion of the channel (Choi, Aldrich, and Yellen, 1991; see Figure I-3). C-type inactivation is thought to be related to a constriction in the external mouth of the pore, as mutations in the putative external mouth region, especially of amino acid threonine-449 in *ShakerB* channels, markedly alters the rate of inactivation (López-Barneo et al., 1993). External cations  $\text{Cd}^{2+}$  and  $\text{Zn}^{2+}$  slow the rate of recovery from inactivation, and increase the rate of entry into C-type inactivation (Yellen et al., 1994). Upon entry into C-type inactivation, the channel's affinity for  $\text{Cd}^{2+}$  increases by at least a thousand-fold, and  $\text{Cd}^{2+}$  binding is thought to stabilise the inactivation state (Yellen et al., 1994).

### **1.3 Calcium-Activated Potassium Channels**

There are three classes of  $\text{Ca}^{2+}$ -activated  $\text{K}^+$  channel: large, intermediate and small conductance channels. Of these channels, more is known about large conductance channels, while relatively little is known about the small and intermediate conductance  $\text{Ca}^{2+}$ -activated  $\text{K}^+$  channels. A wide range of channel kinetics and pharmacological sensitivities exists within each class, however, until more is known about channel structure, single channel conductance is the only criteria for classification of  $\text{Ca}^{2+}$ -activated channels. Several toxins have proven useful in studying  $\text{Ca}^{2+}$ -activated  $\text{K}^+$  channels, including charybdotoxin, iberiotoxin, and apamin (Hinrichsen, 1993). The role of  $\text{Ca}^{2+}$ -activated  $\text{K}^+$  channels has been found to vary from the control of neuronal

excitability, spike regeneration, transient hyperpolarizations, to regulation of the resting potential, fluid secretion, cell volume, and pacemaker activity (Reinhart, Chung, and Levitan, 1989).

### 1.3.1 Large Conductance $\text{Ca}^{2+}$ -Activated $\text{K}^+$ Channels

Large conductance  $\text{Ca}^{2+}$ -activated  $\text{K}^+$  channels (Maxi-K, or BK(Ca)) have a single channel conductance of 130-200 pS, which is near the maximum conductance for a membrane pore (Hinrichsen, 1993). Given the large conductance of these channels, the high selectivity for  $\text{K}^+$  is rather remarkable (Hinrichsen, 1993). BK(Ca) channels have been reported to be blocked by charybdotoxin (ChBTX), iberiotoxin (IbTX), noxiustoxin (NTX), and external TEA (Hinrichsen, 1993). Unlike ChBTX, NTX, and TEA, IbTX is a specific blocker of BK(Ca) channels: it has not been reported to block voltage-gated channels, or even other  $\text{Ca}^{2+}$ -activated  $\text{K}^+$  channel subtypes (Hinrichsen, 1993; Garcia et al., 1995; Miller, 1995).

Structurally, BK(Ca) channels are similar to the voltage-gated channels, except for the addition of a domain to the C-terminal which confers  $\text{Ca}^{2+}$ -dependent gating (Salkoff and Jegla, 1995); this added domain, which makes the primary sequence of BK(Ca) twice the length of voltage-gated channels, is highly conserved (Atkinson, Robertson, and Ganetzky, 1991; Butler et al., 1993; Wei et al., 1994; see Figure I-2). Unlike voltage-gated channels, BK(Ca) channels are insensitive to internal application of TEA (Hinrichsen, 1993), indicating that there are significant differences in the intracellular structure of these two channel types. A comparison of *Shaker* and *Drosophila* BK(Ca) (*dslo*) sequences reveals several similarities, especially in the H5 domain; also, mutation of equivalent sites affects the ion selectivity and TEA sensitivity of both *Shaker* and *dslo*

(Atkinson, Robertson, and Ganetzky, 1991). Chimera mutants created by switching the C-termini of mouse (*mslo*) and Drosophila (*dslo*) BK(Ca) variants indicated that the C-terminal tail confers calcium sensitivity, while having no effect on channel conductance and kinetics (Wei et al., 1994). Analysis of BK(Ca) channel genes from Drosophila (*dslo*) reveals that alternate splicing of the carboxy-terminal results in altered calcium sensitivity in the expressed channel (Lagutta et al., 1994). Sites for alternate splicing of the carboxy-terminal have also been found in mouse (*mslo*) and human (*hslo*) BK(Ca) channel genes (McCobb et al., 1995).

The  $\text{Ca}^{2+}$ -sensitive tail region was found to be necessary for channel function; experiments in which only the core region of the channel was expressed (without the C-terminal) indicated that the core alone does not form a functional channel (Wei et al., 1994). Furthermore, within one tissue, the calcium sensitivity of a channel may vary over a thousand-fold, providing evidence for several clusters of BK(Ca) subtypes, all of which are kinetically similar, but whose range of calcium sensitivity may be conferred by changes in the C-terminal tails (Wu, Shuttleworth, and Stampe, 1996). Also, depending on the tissue, the calcium sensitivity of BK(Ca) channels varies considerably, so that the concentration of calcium for a 50% open probability at 0 mV is lowest in secretory cells (0.001 to 3  $\mu\text{M}$ ), intermediate in smooth muscle (0.2 to 10  $\mu\text{M}$ ), and neurons (1 to 8  $\mu\text{M}$ ), and highest in skeletal muscles (4 to 100  $\mu\text{M}$ ; McMannus, 1991). The corresponding Hill coefficient (i.e. the slope from the relationship between calcium and channel open probability, which gives an estimate of the number of calcium binding sites) ranges from 4 to 6, in the presence of magnesium, indicating that there are 4 to 6 possible  $\text{Ca}^{2+}$  binding sites involved in channel opening (McMannus, 1991). Interestingly, high



concentrations of intracellular calcium decrease the open probability of BK(Ca) channels, especially at depolarized potentials (McMannus, 1991).

Similarities between the voltage-gated and large conductance  $\text{Ca}^{2+}$ -activated  $\text{K}^+$  channels extend to the structures involved in inactivation since, like the voltage-gated channels, some BK(Ca) channel variants have been found to have an inactivation ball, confirming that N-type inactivation is possible in some of these channels (Kukuljan, Labarca and Latorre, 1995). In the absence of a native inactivation ball, large conductance  $\text{Ca}^{2+}$ -activated  $\text{K}^+$  channels can be blocked by intracellular application of *ShakerB* inactivation ball peptides (Torro, Stefani, and Latorre, 1992). Also, membrane-spanning  $\beta$ -subunits unrelated to the  $\text{Kv}\beta 1$  or  $\text{Kv}\beta 2$  have been found to be associated with BK(Ca) channels (Christie, 1995).

Unlike voltage-gated channels, however, in BK(Ca) channels  $\beta$ -subunits have been found to confer calcium-sensitivity, and to affect calcium gating of the channel (Knaus et al., 1994). The well-documented order of magnitude increase in calcium sensitivity of smooth muscle BK(Ca) channels, over that of skeletal muscle or brain, has been suggested by McCobb et al. (1995) to be due to expression of accessory  $\beta$ -subunits. Coexpression of a cloned smooth muscle  $\beta$ -subunit with a cloned human vascular smooth muscle BK(Ca) channel, resulted in a dramatic (order of magnitude) shift in calcium sensitivity, accompanied by a concurrent shift in voltage-dependent activation to more negative potentials, when compared to expression of the channel alone (McCobb et al., 1995). Thus, in BK(Ca) channels, as in the *Shaker* and *Shaw* channels, channel diversity can be found to be a function of splice variants, and subunit expression.

Functional diversity of BK(Ca) is not limited to differences in  $Ca^{2+}$  sensitivity—variations in kinetics and pharmacological profiles have been reported. Studies of large conductance channels in rat brain revealed two noninactivating  $Ca^{2+}$ -activated  $K^+$  channels with similar conductance and vastly different kinetics and pharmacology: a ChBTX-sensitive slow gating channel with short open and closed times, and a ChBTX-insensitive fast gating channel with long open and closed times, and decreased (2- to 5-fold) calcium sensitivity (Reinhart, Chung, and Levitan, 1989). Reinhart, Chung and Levitan (1989) postulate that variations in ChBTX sensitivity are indicative of structural differences in the channel mouth since ChBTX has been found to physically occlude the BK(Ca) channel's external mouth (MacKinnon and Miller, 1988). Interestingly, despite the variation in channel properties, all large conductance channels in this rat brain preparation (whole brain vesicles in a planar lipid bilayer) were blocked by external TEA at  $\mu$ M concentrations, indicating some structural similarities (Reinhart, Chung and Levitan, 1989).

The possibility of variations within a family of channels was confirmed by the discovery of multiple splice exons within the *Drosophila* BK(Ca) channel *dslo* (or slowpoke; Adelman et al., 1992). Dworetzky, Trojnacki, and Gribkoff (1994) subsequently isolated a human BK(Ca) gene (*hslo*) based on the use of a probe generated from the cloning of a mouse BK(Ca) (*mslo*) channel. The *hslo* sequence has been found to share 92% sequence identity with *mslo* and 67% identity with *dslo* sequences; most of the differences are localised to the N- and C- termini (Tseng-Crank et al., 1994b). Both Dworetzky, Trojnacki, and Gribkoff (1994) and Tseng-Crank et al. (1994b) have reported the presence of multiple isoforms of *hslo*, and differential expression of these isoforms in

the CNS and periphery. Multiple splice sites were found in the putative *hslo* C-terminal domain, and at least 9 separate isoforms were identified; four *hslo* mRNA transcripts (with alternatively spliced variants present) were found to be differentially expressed throughout the human CNS and periphery, with variable tissue-dependent levels of expression (Tseng-Crank et al., 1994b). Alternative splice sites have also been found in *dslo* and *mslo*, all of which are located on the C-terminal domain, and one splice site in particular is shared amongst *hslo*, *mslo*, and *dslo* genes (Atkinson, Robertson, and Ganetzky, 1991; Adelman et al. 1992; Butler et al., 1993).

Variations have also been reported to be inherent to the gating kinetics, open probability and conductance level of *dslo* channels expressed in *Xenopus* oocytes (Bowlby and Levitan, 1996). A wide variety of subconductance levels were found which ranged from 74% to 31% of the main conductance level. Furthermore, *dslo* channels have been found to exhibit variable gating kinetics and open probability, independent of the free  $\text{Ca}^{2+}$  concentration and voltage (Bowlby and Levitan, 1996; Silberberg et al., 1996). Such variability in *dslo* channel behaviour has been termed “wanderlust” kinetics by Silberberg et al. (1996).

Studies of BK(Ca) channel gating indicate that, like *Shaker* channels, a “gating site” is present in the pore, and the occupancy of this site makes the closed state unstable, thus increasing open probability (Demo and Yellen, 1992). Neyton and Miller (1988a) have reported that BK(Ca) channels have a minimum of four ion binding sites in the pore. Preference for one ion binding site over another is probably dependent on the energy profile of the ion in question (i.e. the relationship between an ion’s binding site and the membrane electric field, and this is used to explain the kinetics of channel blockade by

various ions; Demo and Yellen, 1992). The “gating site” itself is considered by Demo and Yellen (1992) to be deep within the channel pore, since internal  $\text{Cs}^+$  and external TEA, which bind superficially to the pore, are unable to affect gating. Alternately, Neyton and Pelleschi (1991) propose the presence of an external lock-in site (ELI), which would be similar to the “gating site,” but located in the external pore region. According to their model, the presence of external ions which occupy the ELI reduces the removal rate of blocking ions, such as  $\text{Ba}^{2+}$  (Neyton and Miller, 1988b), which would render the closed-blocked state unstable (Neyton and Pelleschi, 1991). As Demo and Yellen (1992) note, both the “gating site” and ELI model are similar in that an ion has the potential to destabilize channel closing, depending on the binding location.

BK(Ca) channels are implicated in a range of physiological roles in several different cell types. In neurons BK(Ca) channels play a role in action potential repolarization, and the fast phase of afterhyperpolarization (Haylett and Jenkinson, 1990; Sah, 1996). Also, BK(Ca) channels are involved in the establishment of electrical excitability in developing neurons (Ribera and Spitzer, 1992). BK(Ca) channels are implicated in mitogen-induced hyperpolarization, and thus, mitogenesis and activation of lymphocytes (Lewis and Calahan, 1990). In exocrine gland cells BK(Ca) channels are linked to ion secretion, such as, for example, the release of isotonic solution from salivary gland cells (Haylett and Jenkinson, 1990; McManus, 1991; Sah, 1996). In pancreatic  $\beta$ -cells BK(Ca) channels play a role in the regulation of bursting patterns of action potentials which leads to pulsatile insulin release (Haylett and Jenkinson, 1990). In smooth muscle BK(Ca) channels are involved in the regulation of contractile tone (McManus, 1991); in vascular smooth muscle cells BK(Ca) channels regulate intrinsic

vascular tone and dilation in response to endogenous dilators like adenosine and nitric oxide (Brayden, 1996).

### **1.3.2 Small Conductance $\text{Ca}^{2+}$ -Activated $\text{K}^+$ Channels**

Compared to the Maxi- $\text{K}^+$  channels, the structure and function of the small conductance  $\text{Ca}^{2+}$ -activated  $\text{K}^+$  channels (SK(Ca)) is less well known, however it is known that these channels, while in the same genetic subclass as the voltage-gated and Maxi- $\text{K}^+$  channels, do exhibit some structural differences. Small conductance  $\text{Ca}^{2+}$ -activated  $\text{K}^+$  channels have a single channel conductance less than 20 pS, are more responsive to low concentrations of  $\text{Ca}^{2+}$  and less voltage-dependent than BK(Ca) (Hinrichsen, 1993). For SK(Ca) channels the concentration of intracellular calcium which results in a 50% open probability at 0 mV ranges from 0.2 to 1  $\mu\text{M}$  in neurons, red blood cells, lymphocytes, secretory cells, and skeletal muscle (McMannus, 1991). SK(Ca) channels have been found to be largely TEA-insensitive (Hinrichsen, 1993). The bee venom toxin apamin has proved to be a specific blocker of the SK(Ca) channels, with no effect on either the BK(Ca) or IK(Ca) channels (Hinrichsen, 1993). The scorpion toxin leiurotoxin I (scyllatoxin (ScyTX)) also blocks SK(Ca) channels by binding to the same site as apamin on the external side of the channel (Hinrichsen, 1993).

In terms of the function of SK(Ca) channels, their high calcium sensitivity, compared to BK(Ca) channels in the same tissue, at negative membrane potentials indicates that they may be involved in maintaining the resting potential (McMannus, 1991). Also, SK(Ca) channels are known to play a role in slow afterhyperpolarization following an action potential in neurons,  $\text{GH}_3$  cells and skeletal muscle cells (McMannus, 1991). In differentiated neuroblastoma cells, treatment with apamin completely

suppresses afterhyperpolarization following action potentials (Hugues et al., 1982).

Apamin-induced block of TEA-insensitive  $\text{Ca}^{2+}$ -activated  $\text{K}^+$  currents has revealed that SK(Ca) channels play a crucial role in mediating afterhyperpolarization in many neurons (Harvey et al., 1994).

### **1.3.3 Intermediate Conductance $\text{Ca}^{2+}$ -Activated $\text{K}^+$ Channels**

Structurally and functionally, little is known about this class of  $\text{Ca}^{2+}$ -activated  $\text{K}^+$  channel (IK(Ca)). The IK(Ca) channels have a single channel conductance of 25-135 pS (Hinrichsen, 1993). IK(Ca) channels are about equally as sensitive to intracellular calcium as SK(Ca) channels: the concentration of calcium required for a 50% open probability at 0 mV is 0.5 to 1  $\mu\text{M}$  in neurons, cardiac myocytes, and veins (McMannus, 1991). This group of channels has the widest range of voltage sensitivities of any other channel class, a marked variation in response to the channel blockers TEA, ChBTX, and quinidine, even within the same cell type, and share an insensitivity to apamin (Hinrichsen, 1993).

In the absence of a molecular structure for the IK(Ca) channels, structural questions are the domain of pharmacological studies. The Gardos channel in human and rabbit erythrocytes is blocked by ChBTX, stichodactyla toxin (StK, a sea anemone toxin), and margatoxin (MgTX), and is markedly less sensitive to kaliotoxin (KTX, a scorpion toxin), and iberiotoxin (IbTX, a scorpion toxin; Brugnara et al., 1995). Such a toxin profile places the Gardos channel in a unique class since the rank order of toxin potency is ChBTX > StK > MgTX > KTX > IbTX = 0 (Brugnara et al., 1995); while the rank order suggested from studies of smooth and skeletal muscle BK(Ca) channels is IbTX > ChBTX > KTX > NTX > MgTX, which reflects an increasing specificity for voltage-

gated channels as the specificity for  $\text{Ca}^{2+}$ -activated  $\text{K}^+$  channels decreases (Romi et al., 1993). The reported sensitivity of human and rabbit erythrocyte Gardos channels to StK (Brugnara et al., 1995) is interesting since StK was described by Kem et al. (1989) to be a blocker of DTX- sensitive  $\text{K}^+$  channels. MgTX, another reportedly selective inhibitor of voltage-gated  $\text{K}^+$  channels (Garcia-Calvo et al., 1993), has no effect on human T-lymphocyte IK(Ca) channels (Bednarek et al., 1994), or on tracheal smooth muscle BK(Ca) channels (Garcia-Calvo et al., 1993), but has been reported to block human and rabbit erythrocyte Gardos channels (Brugnara et al., 1995). KTX, which has been reported to block SK(Ca) and BK(Ca) channels (Crest et al., 1992), had little effect on IK(Ca) channels in rabbit and human erythrocytes (Brugnara et al., 1995). It is also interesting to note that the SK(Ca) channel blockers apamin and scyllatoxin (ScyTX, or leurotoxin I) had no effect, nor did the voltage-gated  $\text{K}^+$  channel blocker DTX-I (Brugnara et al., 1995). ChBTX point mutants were found to have an inverse potency of block on red blood cell IK(Ca) compared to skeletal muscle BK(Ca): of the point mutations which affected toxin potency, several showed a 2- to 3-fold increase in red cell IK(Ca) blocking potential, and a corresponding 2- to 3- fold decrease in skeletal muscle BK(Ca) block potency (Brugnara et al., 1995). Thus, the different classes of  $\text{Ca}^{2+}$ -activated  $\text{K}^+$  channel show differential requirements for binding to and block of the channel.

The potassium channel in red blood cells described by Gardos (1959), and subsequently termed the Gardos channel is an intermediate conductance  $\text{Ca}^{2+}$ -activated  $\text{K}^+$  channel (Latorre et al., 1989; Christopherson, 1991). The functions of IK(Ca) channels cover a wide spectrum: in immune tissues they have been found to play a

protective role to prevent swelling and lysis following complement activation in erythrocytes (Halperin, Brugnara, and Nicholson-Weller, 1989), to play a role in mitogen- or antigen-stimulated lymphocyte activation (Lewis and Calahan, 1990; Lewis and Calahan 1995), but not to be involved in regulatory volume decreases in lymphocytes (voltage-gated  $K^+$  and  $Cl^-$  channels are involved in volume regulation in lymphocytes; Lewis and Calahan, 1990). While  $IK(Ca)$  channels have been characterized extensively in the immune system—where the  $IK(Ca)$  channels are largely voltage-independent (Haylett and Jenkinson, 1990)—they have also been found in the nervous system where they are voltage-dependent and contribute to spike repolarization and frequency dependent firing in snail neurons (McMannus, 1991), and in vertebrate sympathetic neurons (Adams et al., 1982). In bullfrog sympathetic neurons a 100 pS TEA-sensitive  $Ca^{2+}$ -activated  $K^+$  channel was found to contribute to cell repolarization and spike afterhyperpolarization (Adams et al., 1982). Two noninactivating, ChBTX-, and TEA-sensitive  $IK(Ca)$  channels were found in rat brain, one of which was found to exhibit short open and closed times, while the other exhibited predominantly long open and closed times (Reinhart, Chung and Levitan, 1989).

In an interesting twist, Meinville and Baker (1996) have identified calcium-activated channels in undifferentiated embryonic rat neuroepithelium with a decreased conductance (on par with that of  $IK(Ca)$  channels) which they classify as an “immature” form of  $BK(Ca)$  channels. Upon limited proteolysis of the intracellular membrane the conductance and gating of these channels resembles that of  $BK(Ca)$  channels in the patch (Meinville and Baker, 1996). These “immature”  $BK(Ca)$  channels are insensitive to ChBTX and less sensitive to voltage than the “normal”  $BK(Ca)$  channels also found in



the patch (Meinville and Baker, 1996). The conclusion that mild intracellular proteolysis causes a transformation of the “immature” BK(Ca) channels into mature or “normal” BK(Ca) channels is based on a dramatic increase in “normal” BK(Ca) channel opening following the brief exposure to trypsin (Meinville and Baker, 1996). An alternative explanation could be that the observed changes are a function of trypsin affecting BK(Ca) channel modulators, since IK(Ca)-like openings are seen pre- and post-trypsin treatment, and especially since post-trypsin treatment BK(Ca)-like channel opening is seen in  $\text{Ca}^{2+}$ -free conditions (Meinville and Baker, 1996). It is possible that the “immature” BK(Ca) channels are, in fact, IK(Ca) channels, and that trypsin treatment is affecting the BK(Ca) channels in the patches, rather than causing a conversion of the IK(Ca)-like channels to BK(Ca) channels. The absence of IK(Ca)-like channels in differentiated rat neuroepithelium, and the prevalence of that type of channel in early embryogenesis (Meinville, 1994) suggests that IK(Ca) channels may play a role in differentiation, or in early development.

#### **1.4 $\text{K}^+$ Channel Blockers from Venoms**

A wide range of scorpion, snake, sea anemone, and bee toxins have proved useful as  $\text{K}^+$  channel blockers, and are, to a large extent, more specific blockers of the various types of  $\text{K}^+$  channels than other non-toxin blockers (Hinrichsen, 1993). Many of the toxins studied differentiate between various  $\text{K}^+$  channel subtypes, and, while there is some overlap in the specificity for one channel type over another, toxin-induced blockade does reveal insights into the structural similarities between the channel types. The scorpion toxins charybdotoxin and the structurally related noxiustoxin, in particular, have

been found to have overlapping specificity for voltage-gated and  $\text{Ca}^{2+}$ -activated  $\text{K}^+$  channels (Hinrichsen, 1993). ChBTX and DTX, two toxins which are well documented  $\text{K}^+$  channel blockers have proven useful as  $\text{K}^+$  channel probes (Awan and Dolly, 1991; Muniz, Parcej and Dolly, 1992; Hall et al., 1994; Scott et al., 1994; Garcia et al., 1995; Miller, 1995).

#### 1.4.1 Charybdotoxin

One of the most studied toxins with respect to interacting with  $\text{K}^+$  channels, and  $\text{Ca}^{2+}$ -activated  $\text{K}^+$  channels in particular, is the scorpion toxin charybdotoxin (ChBTX) from the venom of the Israeli scorpion *Leiurus quinquestriatus hebraeus*. While initially described as a specific blocker of  $\text{Ca}^{2+}$ -activated  $\text{K}^+$  channels, subsequent studies have revealed an overlapping blockade of voltage-gated  $\text{K}^+$  channels (Hinrichsen, 1993).

ChBTX block of voltage-gated channels has been shown to be restricted to the *Shaker* family Kv1.3 and Kv1.2 subtypes (MacKinnon, Reinhart, and White, 1988; Grissmer et al., 1994). While ChBTX has been reported to block some SK(Ca), and IK(Ca) channels, and many BK(Ca) channels (Leonard et al., 1992; Hinrichsen, 1993), it does not block all (Reinhart, Chung and Levitan, 1989; Goh et al., 1992). However, similarities in the site and manifestation of block have been noted for both BK(Ca) and *Shaker* family subtypes: in both cases ChBTX binding sites are localised to the pore (P) region and block is voltage-dependent and increased by channel activation (MacKinnon, Reinhart and White, 1988; Hinrichsen, 1993; Spruger, Stewig and O'Grady, 1996).

Toxin binding studies have shown that charybdotoxin (ChBTX) blocks BK(Ca) channels by binding to a receptor located in the external mouth of the channel (Miller, 1988) and physically occluding the pore in both voltage-gated and  $\text{Ca}^{2+}$ -activated  $\text{K}^+$

channels (Goldstein and Miller, 1993). The toxin binding site has been found to be near a region of negative charge density by two related lines of evidence: decreases in ionic strength enhance ChBTX block, and point mutations in the P-region on the external mouth of the channel affect ChBTX binding in an electrostatic manner (Anderson et al., 1988; MacKinnon and Miller, 1989). Also, ChBTX binding affinity has been shown to be affected by point mutations of the S5-S6 linker, which lines the outer mouth of the channel, and toxin binding is sensitive to the number of negative residues lining the external vestibule (MacKinnon and Miller, 1989; MacKinnon, Heginbotham, and Abramson, 1990). In the same way, positively charged residues on the ChBTX peptide have been identified by Park and Miller (1992) to be crucial for toxin binding and activity. ChBTX binding and block of voltage-gated and  $\text{Ca}^{2+}$ -activated  $\text{K}^+$  channels is not irreversible:  $\text{K}^+$  ion movement through the pore destabilises toxin binding (Miller, 1988; Park and Miller, 1992; Garcia et al., 1995; Miller, 1995; Naini et al., 1996). That ChBTX can block voltage-gated "A" currents is indicative of a similar toxin binding site in the mouth of the pore (Reinhart, Chung, and Levitan, 1989), reinforcing the structural similarities between the voltage-gated and  $\text{Ca}^{2+}$ -activated channels.

Purification of BK(Ca) channels from bovine smooth muscle using radiolabelled [ $^{125}\text{I}$ ]ChBTX led to the discovery of the accessory  $\beta$ -subunit which is non-covalently linked to the channel forming  $\alpha$ -subunit (Garcia-Calvo et al., 1994). Cloning of the  $\beta$ -subunit has enabled the discovery of its putative structure: this subunit is predicted to have two membrane-spanning domains, and a large extracellular loop (Knaus et al., 1994). Cross-linking of [ $^{125}\text{I}$ ]ChBTX with the BK(Ca) channel covalently linked the  $\beta$ -subunit to the radiolabelled toxin (Garcia-Calvo et al., 1991). Subsequent studies have

isolated the residues on both the  $\beta$ -subunit (Lys<sub>69</sub>; Knaus et al., 1994), and ChBTX (Lys<sub>32</sub>; Munujos et al., 1995) which are involved in the cross-linking. Based on this work Munujos et al. (1995) postulate that the  $\beta$ -subunit is very closely associated with the  $\alpha$ -subunit, at a maximum of 11 Å from the pore itself, and that this subunit may participate in toxin binding. While the  $\beta$ -subunit has been documented to profoundly affect K<sup>+</sup> channel gating and pharmacology (McManus et al., 1995), Gribkoff et al. (1996) report that in the absence of  $\beta$ -subunit expression *mSlo* and *hSlo* BK(Ca) channels expressed in *Xenopus* oocytes are blocked by ChBTX. Thus,  $\beta$ -subunit expression is not a prerequisite for ChBTX binding or block of K<sup>+</sup> channels (Gribkoff et al., 1996), although it does add another level of possible variability in channel characteristics.

#### 1.4.2 Dendrotoxins

Dendrotoxins are neurotoxins derived from the venom of the mamba (*Dendroaspis*) snakes: dendrotoxins from eastern green mamba (*Dendroaspis angusticeps*), and black mamba (*Dendroaspis polylepis*) venom were found by Harvey and Karlsson (1982) to dramatically increase acetylcholine release from motor nerve terminals, and bind to prejunctional nerve membranes. DTXs are short peptides, the green mamba DTXs are of 58 to 59 amino acids in length, with a molecular weight of approximately 7000 (Benishin et al, 1988). The neurotoxic effect of the DTXs is not exclusive to peripheral neurons, black mamba toxin-I, and green mamba  $\alpha$ -DTX have been found to increase noradrenaline release (Ennis and Minchin. 1993). and produce seizures, brain damage, and neuronal loss (Bagetta, Nistico, and Dolly, 1992; Bagetta et al., 1994) in rat brain. Subsequent studies have shown that the homologous black (DTX-I, and DTX-K) and

green mamba ( $\alpha$ -,  $\beta$ -,  $\delta$ -, and  $\gamma$ -DTX) dendrotoxins, as well as the related DTXs in the western green mamba (*Dendroaspis viridis*) venom are potent and specific blockers of  $K^+$  channels (Benishin et al., 1988; Blaustein et al., 1988; reviewed by Harvey, 1997). DTXs have also proven useful tools for the classification and purification of  $K^+$  channels (Awan and Dolly, 1991; Muniz, Parcej, and Dolly, 1992; Hall et al., 1994; Scott et al., 1994).

DTXs are related to the Kunitz class of peptides—peptides with serine protease inhibitor activity (such as bovine pancreatic trypsin inhibitor)—the structural similarities (33-35% sequence homology between BPTI and DTX-I and  $\alpha$ -DTX, respectively) have led to the hypothesis that DTXs are derived from an ancestral Kunitz-like protease inhibitor (Foray et al., 1993). Interestingly,  $K^+$  channel-blocking potency is inversely related to protease inhibition: DTXs are weak protease inhibitors, and protease inhibitors are poor  $K^+$  channel blockers (Harvey and Karlsson, 1982). While structurally similar to protease inhibitors, X-ray crystallography of  $\alpha$ -DTX has shown it to differ significantly from the homologous bovine pancreatic trypsin inhibitor (BPTI) in the “antiprotease site” (Skarzynski, 1992); in fact it is in this markedly different region that a site essential for  $K^+$  channel blockade is found in DTXs (Hollecker, Marshall and Harvey, 1993).

Swaminathan et al. (1996) have found that the black mamba DTX-I and DTX-K were also structurally similar to BPTI. All the DTXs share common conformational motifs, and fold in such a way as to expose sites rich in positively charged amino acid residues to the anionic residues of the  $K^+$  channel itself (Swaminathan et al., 1996).  $K^+$  channel binding affinity has been reported by Hollecker, Marshall and Harvey (1993) to involve two of the three disulphide bonds, and much of the secondary structure of the DTXs—a secondary structure which, while similar to the serine proteases, does exhibit significant

alterations in protein folding (Skarzynski, 1992; Swaminathan et al., 1996). Both the serine protease inhibitors and the DTXs share sequence similarity with another  $K^+$  channel blocker  $\beta$ -bungarotoxin, although neither have the phospholipase  $A_2$  subunit that  $\beta$ -bungarotoxin does (Skarzynski, 1992; Harvey et al., 1994).

In addition to the structural similarities between DTX and serine proteases several other classes of peptides have been noted to have similar pharmacological binding profiles. The scorpion toxins ChBTX and noxiustoxin (NTX) have been found to displace DTX binding from voltage-gated  $K^+$  channels (Harvey, Marshall, and Possani, 1992; Werkman et al., 1992; Sprunger, Stewig and O'Grady, 1996). In addition, both ChBTX, and mast cell degranulating peptide (MCDP) were found to have similar blocking profiles to DTX when applied to cloned Kv1.2 channels (Werkman et al., 1992). ChBTX and DTX-I were found to bind to the same region of the channel at distinct, but allosterically related sites; ChBTX, like DTX, physically occludes the channel by binding in the pore region (Schweitz et al., 1989). Finally, the snake toxin  $\beta$ -bungarotoxin has been noted by Awan and Dolly (1991) to discriminate between subtypes of  $\alpha$ -DTX-sensitive  $K^+$  channels, indicating some overlap of blocking potential.

While generally  $\alpha$ -DTX (or the homologous black mamba toxin I) targets "A" currents (Benoit and Dubois, 1986; Halliwell et al., 1986), and  $\beta$ -DTX (or black mamba toxin-K) targets delayed rectifiers (Smith et al., 1993; Ren, Karpinski, and Benishin, 1994), such a generalisation does not hold for every cell or channel type (Tygat et al., 1995). One source of variability lies in the finding that for a high affinity DTX binding site all four  $K^+$  channel  $\alpha$ -subunits must interact with the toxin (Tygat et al., 1995).

Mutation of a Kv1.1 channel in the H5 loop between S5 and S6 (a region crucial for DTX binding) resulted in a significant decrease in sensitivity to  $\alpha$ -DTX, which is reversed as the concentration of wild type  $\alpha$ -subunits increases (Tygat et al., 1995). Use of  $\alpha$ -DTX as a probe has revealed that, in bovine brain,  $\alpha$ -DTX-sensitive channels are tightly associated with accessory channel  $\beta$ -subunits in a 4:4 ratio (i.e.  $\alpha$ -DTX-sensitive channels are composed of 4  $\alpha$ -subunits to 4  $\beta$ -subunits), thus accounting for some of the variability in DTX specificity (Parcej, Scott and Dolly, 1992).

In a DTX-sensitive cell preparation, such as rat CNS, several  $K^+$  channel subtypes, with variable conductances, have been found to be blocked by DTX (Pelchen-Matthews and Dolly, 1989; Awan and Dolly, 1991). Monoclonal antibodies directed against  $\alpha$ -DTX-sensitive  $K^+$  channels purified from bovine brain have been used to isolate multiple isoforms (Kv1.1, 1.2, 1.4, and 1.6) of the channel  $\alpha$ -subunit, and to show that native  $K^+$  channels are hetero-oligomeric complexes of  $\alpha$ -, and  $\beta$ -subunits (Muniz, Parcej, and Dolly, 1993; Scott et al., 1994b).  $K^+$  channel  $\alpha$ -subunits, identified by monoclonal antibody, were differentially expressed throughout the CNS and periphery, with some subunits (Kv1.2) found to be exclusively expressed in mammalian brain (Muniz, Parcej, and Dolly, 1993; Scott et al., 1994b). Smith et al. (1993) have cloned black mamba DTX-K to provide a source of toxin mutants to isolate and structurally characterise  $K^+$  channel subtypes and their interaction with DTXs.

There is also variation among the DTXs in terms of blocking potency and specificity for one  $K^+$  channel subtype over another.  $\delta$ -DTX has been found to discriminate between certain subtypes of  $\alpha$ -DTX-sensitive  $K^+$  channels in rat brain, while the structurally

related  $\beta$ -, and  $\gamma$ -DTX were largely ineffective in either binding to  $\alpha$ -DTX-sensitive channels, or in competing with  $\delta$ -DTX for binding sites (Awan and Dolly, 1991). In neonatal rat sensory neurons all the DTX homologues ( $\alpha$ -,  $\beta$ -,  $\delta$ -, and  $\gamma$ -DTX, and DTX-I and DTX-K; 10 nM) were found to block outward  $K^+$  currents by 30-40% (Hall et al., 1994). Of all the DTXs, only  $\alpha$ -, and  $\delta$ -DTX showed blocking specificity:  $\alpha$ -DTX preferentially blocked the inactivating current, and  $\delta$ -DTX (the most potent of the blockers) preferentially blocked the non-inactivating component (Hall et al., 1994). Black mamba toxins also exhibit preferential blockade of  $K^+$  channels in some preparations: cloned rat or human Kv1 channels Kv1.1, Kv1.2, and Kv1.6 expressed in *Xenopus* oocytes were all blocked by DTX-I, while DTX-K selectively blocked Kv1.1 (Robertson et al., 1996). Cloned mouse voltage-gated  $K^+$  channel Kv1.1 (MK-1) expressed in Chinese hamster ovary cells was found to be sensitive to a range of DTXs, with a potency profile of: DTX-K >  $\gamma$ -DTX >  $\delta$ -DTX > DTX-I =  $\alpha$ -DTX >  $\beta$ -DTX (Owen et al., 1997).

There is some debate as to the nature of DTX-induced voltage-gated  $K^+$  channel block—in some preparations block has been found to be voltage-independent (Werkman et al, 1992; Owen et al., 1997), and in others it was concluded to be voltage-dependent (Robertson et al., 1996). DTX block of fibroblast cells transfected with mouse neuroblastoma Kv1.2 was not relieved by increasing external  $K^+$ , and block decreased with increased voltage (Werkman et al., 1992). Furthermore, the toxin was concluded to have no effect on activation kinetics, as toxin dissociation from the channel was voltage-dependent (Werkman et al., 1992). DTX block of mouse Kv1.1 channels expressed in



Chinese hamster ovary cells was found to be independent of voltage, and the toxins had no effect on channel activation kinetics (Owen et al., 1997). In contrast, DTX block of rat or human Kv1 channels Kv1.1, 1.2, and 1.6 expressed in *Xenopus* oocytes was found to slow activation and inactivation kinetics, and while decreases in activation were voltage-independent over the range of  $-30$  to  $+30$  mV, block was concluded to be voltage-dependent (Robertson et al., 1996).

In  $\text{Ca}^{2+}$ -activated  $\text{K}^+$  channels, in contrast with voltage-gated  $\text{K}^+$  channels, DTXs have been found to block BK(Ca) channels when applied to the intracellular side of the channel (Lucchesi and Moczydlowski, 1991), but not when exposed to the external face (Tauc, Gastineau, and Poujeol, 1993). DTX has no effect on voltage-gated channels when applied to the intracellular side of the channel (Werkman et al., 1992). Application of DTX-I, or the structurally similar BPTI to the intracellular face of BK(Ca) channels has been found to increase subconductance events (Lucchesi and Moczydlowski, 1991). Such a finding is consistent with the hypothesis forwarded by Moss et al. (1996) that a serine protease inhibitor binding site is conserved in BK(Ca) since Kunitz proteinase inhibitor BPTI, and chicken ovomucin inhibitor (a member of the Kazal family of proteinase inhibitors) induce subconductance events when exposed to internal channel face.

### **1.5 Neuroblastoma N1E 115 Cell Line**

The N1E 115 cell line is an adrenergic clone of the mouse sympathetic tumour line CL-100. The majority of the experiments in the literature involve the use of N1E 115 cells treated with 2% DMSO. This cell line is known to differentiate spontaneously, but at a much slower rate compared to cells treated with DMSO (Quandt, 1994). Treatment

with DMSO has been found to increase the proportion of cells producing neurites, while inhibiting cell growth (Quandt, 1994). Cells not differentiated by DMSO exhibit a distinct channel profile, in terms of the proportions of channels exhibited, from those that are differentiated (Quandt, 1994). The ionic currents in these mouse neuroblastoma cells were first studied under patch clamp by Moolenaar and Spector (1978) who identified sodium, potassium and calcium currents in DMSO-differentiated N1E 115 cells.

Subsequently, DMSO-differentiated N1E 115 cells have been reported to possess four different types of potassium channel, and two types of calcium channel (Narahashi, Tsunoo, and Yoshii, 1987). The two voltage-gated  $\text{Ca}^{2+}$  channels are classed as transient (T), which is active at potentials more positive than  $-50$  mV, and reaches peak channel activity at  $-20$  mV, and long-lasting (L), active at potentials more positive than  $-20$  mV, and reaches peak channel activity at  $+10$  mV (Narahashi, Tsunoo, and Yoshi, 1987).

The four types of potassium channel present in differentiated N1E 115 cells fall into the following general categories: a delayed rectifier channel (SK), an "A"-current-like channel (FK), and a large and small conductance calcium-activated potassium channel (Quandt, 1988; Leinders and Vijverberg, 1992; Disbero, Antonny, and Verdeti, 1994). Quandt (1988) has termed the two voltage-gated channels SK (35 pS conductance), and FK (14 pS conductance), respectively, based on their single channel kinetics; SK channels have a lower probability of opening compared to FK channels, and a slower inactivation time constant (7.14 sec at  $+20$  mV) compared to that of the FK channels (1.27 sec at  $+20$  mV). Also, the FK channels are more sensitive to 4-AP block ( $100\mu\text{M}$ ), while both channels are TEA ( $10$  mM) sensitive (Quandt, 1988). 4-AP was found to

preferentially block FK channels in the open state, and to have an internal site of action (Hirsh and Quandt, 1993).

In DMSO differentiated N1E 115 cells, the BK(Ca) channel has a conductance of 180- 200 pS, is blocked by 100nM charybdotoxin, and external TEA (1 mM), and is insensitive to apamin (100 nM; Disbero, Antonny, and Verdetti, 1994). This BK(Ca) channel is voltage-sensitive; the probability of opening shifts to more negative potentials as the intracellular calcium concentration increases, with a dramatic increase in open probability at 0mV under physiological calcium concentrations of 0.5 to 1  $\mu$ M (Disbero, Antonny, and Verdetti, 1994). However, with intracellular calcium concentrations above 1  $\mu$ M, the BK(Ca) channel in these cells exhibits long periods of closure at high voltage (greater than +30 mV; Diserbo, Antonny and Verdetti, 1994). In DMSO-differentiated N1E 115 cells, the resting concentration of intracellular calcium is 0.20 to 0.25  $\mu$ M, and increases to 1.2 to 1.3  $\mu$ M (via mobilization of intracellular stores and entry through voltage-gated channels) upon histamine stimulation (Oakes et al., 1990). Interestingly, Leinders and Vijverberg (1992) report the presence of a 98 pS  $Ca^{2+}$ -activated  $K^+$  channel, which is more in the range of an intermediate conductance channel, although they term it a large-conductance channel. This channel has a half-maximal opening probability and opening frequency at a ten-fold higher internal calcium concentration of 7.5 to 21  $\mu$ M; it is sensitive to mM concentrations of TEA, and apamin-insensitive (Leinders and Vijverberg, 1992). The small conductance SK(Ca) channel has a single channel conductance of 5.4 pS, is blocked by 3 nM apamin, and insensitive to 20 mM TEA (Leinders and Vijverberg, 1992). This channel is largely voltage-independent between –

16 to +40 mV, but is active over a similar range of calcium concentrations (0.5 to 1  $\mu$ M) to the BK(Ca) channel (Leinders and Vijverberg, 1992).

DMSO-differentiated channels exhibit both L- and T-type voltage-gated  $\text{Ca}^{2+}$  channels, while the T-type is predominant in cells not treated with DMSO (Wang, 1991). Also, the potassium currents differ in that both the delayed rectifier and "A"-current are present in DMSO differentiated cells, while the "A"-current is largely absent in cells not exposed to DMSO (Quandt, 1994). In DMSO-differentiated N1E 115 cells, the density of  $\text{Ca}^{2+}$ -activated  $\text{K}^+$  channels is fairly low; Leinders and Vijverberg (1992) found that only 1% of the patches studied contained small conductance (SK(Ca)) channels, while 5% contained large-conductance (BK(Ca)) channels). Hugues et al. (1982) reported that only 20% of DMSO-differentiated N1E 115 cells exhibit afterhyperpolarization (a.h.p.) when bathed in a solution with 25 mM  $\text{Ca}^{2+}$ ; this a.h.p. is attributable to an apamin-sensitive, TEA-insensitive channel (the SK(Ca) channel), and is completely absent in the presence of sub- $\mu$ M concentrations of apamin.

Neuroblastoma N1E 115 cells treated with 2% DMSO, while exhibiting electrical excitability and morphological differentiation, were found to show a decrease in tyrosine hydrolase and acetylcholinesterase activity, as well as a drop in cAMP concentrations (Kimhi et al., 1976). Alternately, untreated N1E 115 cells at confluency are found to show both morphological differentiation, and neurotransmitter enzyme induction (Amano, Richelson, and Nirenberg, 1972). It is true, however that DMSO treated N1E 115 cells are more electrically excitable than control (untreated) cells at confluency (Kimhi et al., 1976).

## 1.6 Objectives

The main objective of this study is to determine the effect of the eastern green mamba venom peptides  $\alpha$ -,  $\beta$ -,  $\delta$ -, and  $\gamma$ -dendrotoxin (DTX) on potassium currents in N1E 115 neuroblastoma cells. These toxins are known to affect voltage-gated potassium channels in various cell types, although the channel blocking effect of the dendrotoxins is not consistent for every cell type (in some cell types they have no effect on the potassium channels studied). Generally,  $\alpha$ -DTX has been reported to block “A” currents, while  $\beta$ -DTX blocks delayed rectifiers;  $\delta$ -DTX, and  $\gamma$ -DTX have not been widely studied. Thus, one aim of this study is to focus on the effect of the lesser studied  $\delta$ -DTX, and  $\gamma$ -DTX. More specifically the aims of the study are as follows:

1. to characterise the whole-cell potassium currents in the undifferentiated N1E 115 cell line, both in terms of kinetics (activation and deactivation parameters) and pharmacology (response to the non-specific  $K^+$  channel blockers TEA and 4-AP);
2. to determine the effect of  $\alpha$ -,  $\beta$ -,  $\delta$ -, and  $\gamma$ -DTX on the kinetics of the whole-cell potassium currents, with special emphasis on the  $Ca^{2+}$ -activated component of the whole-cell  $K^+$  currents;
3. to characterise the  $Ca^{2+}$ -activated  $K^+$  channels affected by  $\beta$ - and  $\gamma$ -DTX in outside-out patches, again in terms of kinetics (probability of opening) and pharmacology (response to known  $Ca^{2+}$ -activated  $K^+$  channel blockers IbTX, TEA, and apamin).

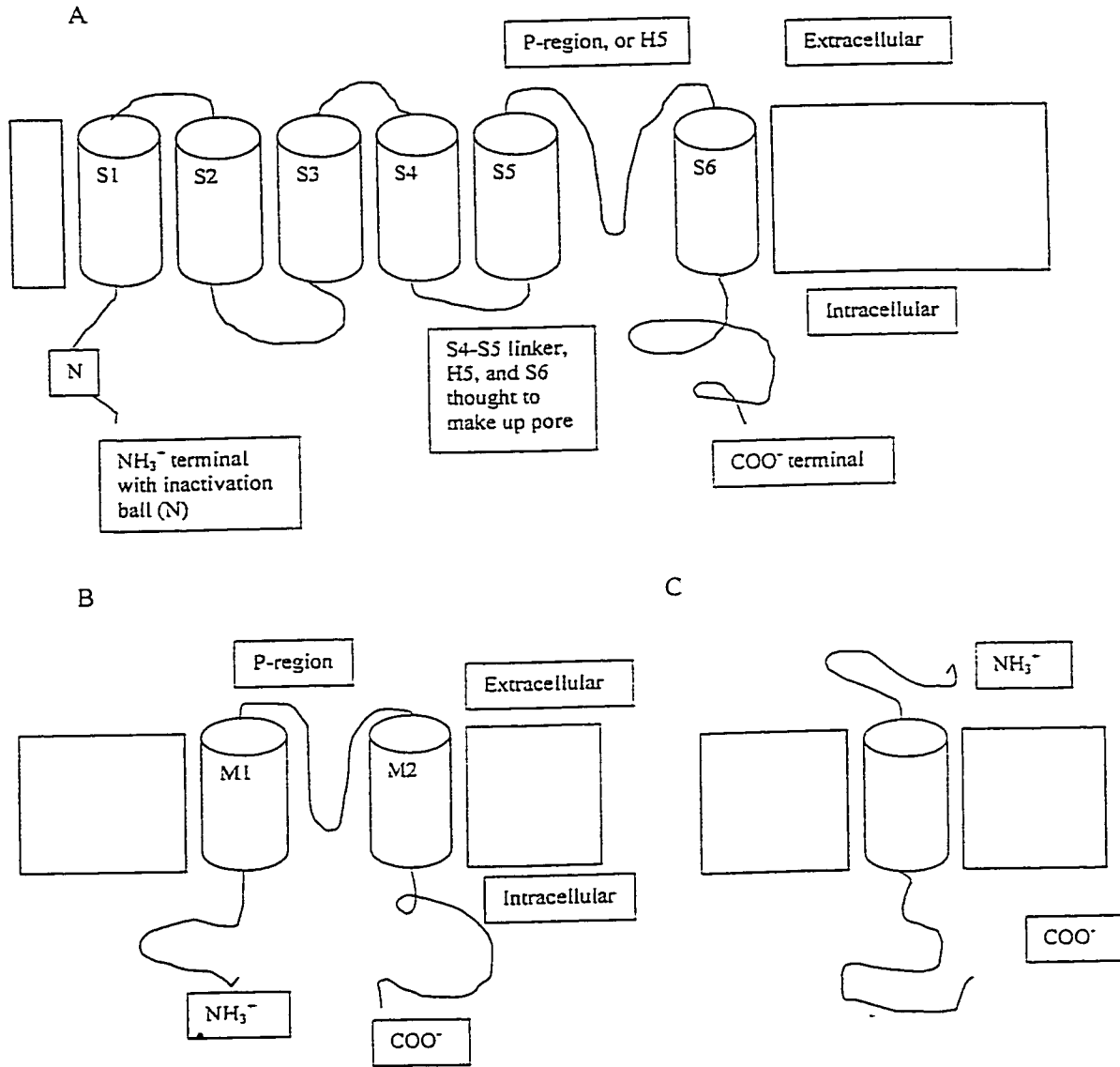
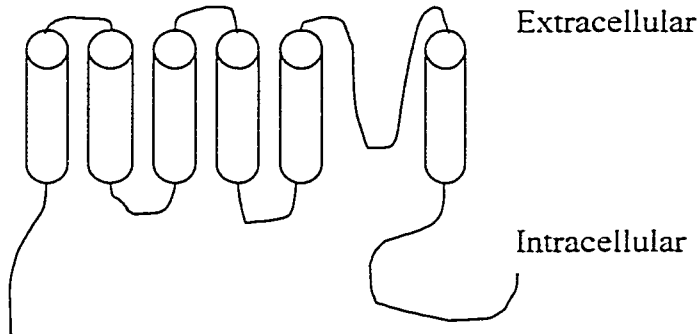


Figure I-1. Hypothetical arrangement of the  $K^+$  channel subunit for (A) voltage-gated, (B) inward rectifier, and (C) minimal  $K^+$  (minK<sup>+</sup>) channels. Four subunits are thought to come together to form the ion channel. The pore (P)-region is highly conserved and contains a  $K^+$  channel "fingerprint," which enables identification of  $K^+$  channel genes. (adapted from Kukuljan, Labarca, and Latorre, 1995)

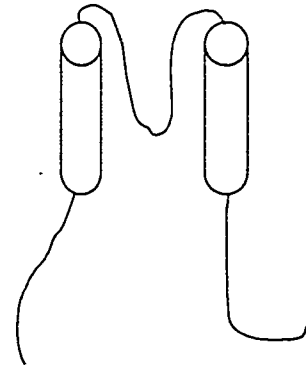
## K<sup>+</sup> Channels

Structural class:

**6TM subunits**

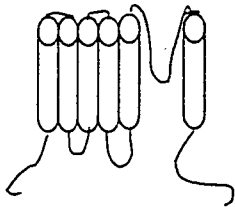


**2TM subunits**



Family:

**Voltage-gated**



Subfamily:  
Shaker (Kv1)  
Shab (Kv2)  
Shaw (Kv3)  
Shal (Kv4)

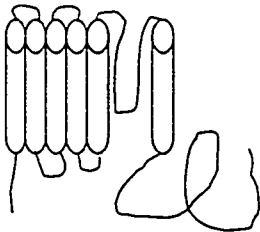
Family:

**Inward Rectifier**

Subfamily:  
Kir1, Kir2, Kir3, Kir4  
Kir5, Kir6, nIRK

Family:

**Large conductance Ca<sup>2+</sup>-activated**



Subfamily:  
Slo  
nSlo2

Calcium regulatory sites in long  
carboxy-terminal tail

Figure I-2. A scheme showing the classification of K<sup>+</sup> channels, showing the six transmembrane (6TM), and two transmembrane (2TM) subunit structural classes and their division into K<sup>+</sup> channel families and subfamilies. Subunits forming the highly conserved pore region are shaded. 6TM structural class members are part of the S4 superfamily of ion channels that include the voltage-gated Na<sup>+</sup> and Ca<sup>2+</sup> channels; this structural class is the most conserved. Members of the 6TM K<sup>+</sup> channel family include: voltage-gated, cyclic nucleotide-gated, large and small conductance Ca<sup>2+</sup>-activated, KQT-like, and eag-like channels. Only the voltage-gated, large conductance Ca<sup>2+</sup>-activated, and inward rectifier K<sup>+</sup> channel families and subfamilies are shown here. (adapted from Wei, Jegla, and Salkoff, 1996)

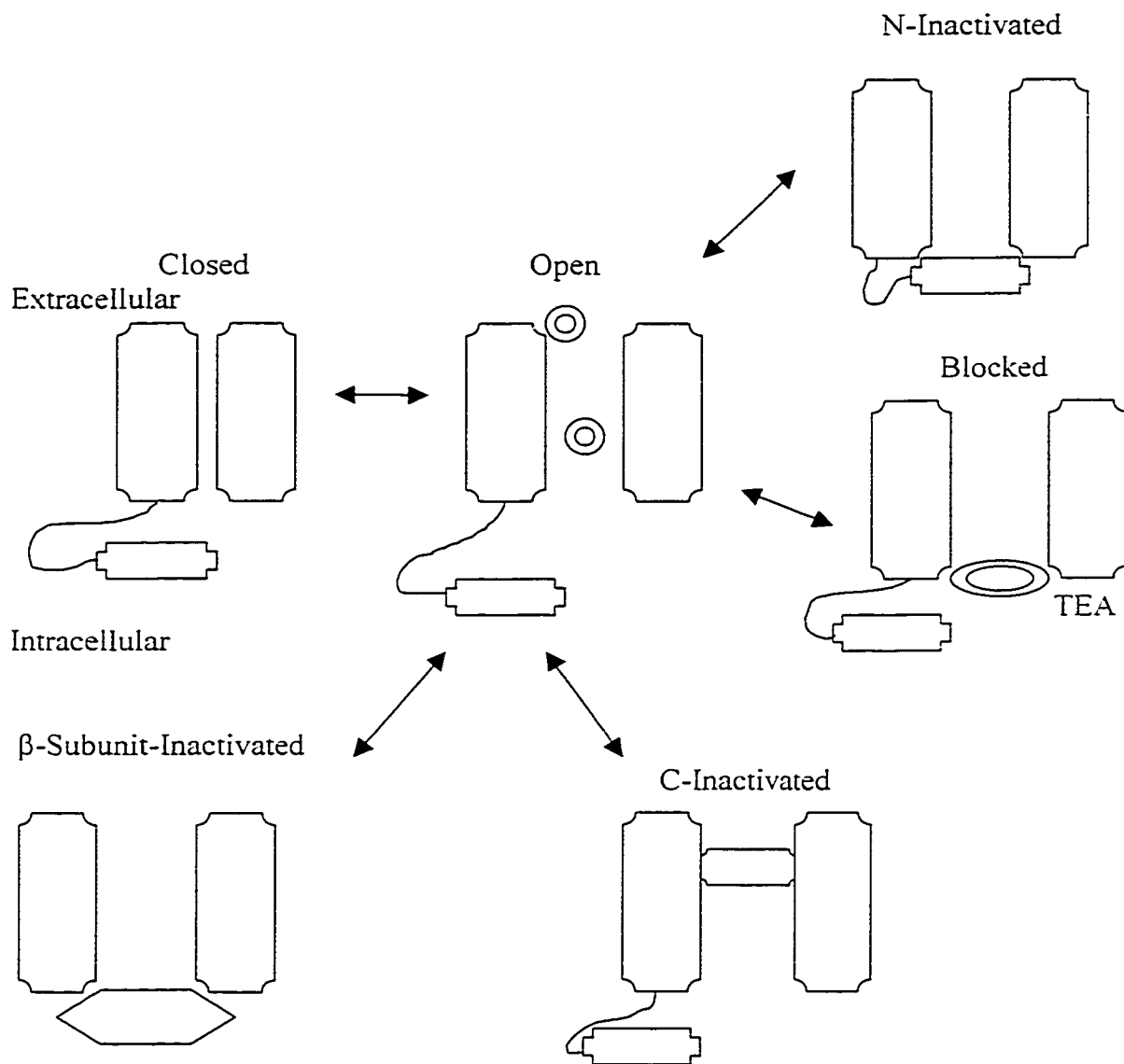


Figure I-3. Models of channel N-type and C-type, and  $\beta$ -subunit inactivation in voltage-gated  $K^+$  channels. A conformational change within the pore enables the transformation from the open to the closed state. Following channel opening, N-type (fast) inactivation takes place when the amino-terminal inactivation-ball electrostatically interacts with the inner vestibule of the pore; intracellular TEA competes with the inactivation ball for a binding site to the inner mouth of the channel. The channel can also undergo C-type (slow) inactivation, which involves a conformational change within the pore to occlude ion movement. Finally,  $\beta$ -subunits can mimic N-type inactivation by blocking the inner mouth, and competing with the inactivation ball for binding sites, or by occluding the pore in channels that lack the inactivation ball. (adapted from Kukuljan, Labarca, and Latorre, 1995)



## Chapter II

### Materials and Methods

#### 2.1 Cell Culture of Neuroblastoma (N1E 115) Cells

Mouse neuroblastoma N1E 115 cells, an adrenergic clone of mouse sympathetic tumour cells, were cultured from passage 25 to 55, and maintained at 37.5<sup>0</sup>C and 5% CO<sub>2</sub> in Dulbecco's Modified Eagle Medium (DMEM) supplemented with NaHCO<sub>3</sub> (3.7g/L), and 10% fetal bovine serum (FBS). Cells were subcultured once they reached confluency by washing twice with Hank's Balanced Salt Solution (HBSS), supplemented with 0.35 g/L NaHCO<sub>3</sub>, then adding DMEM supplemented with FBS, and removing the cells from the bottom of the dish by mechanical agitation. These cells are easily dissociated by agitation and do not require treatment with trypsin. Cells were then plated onto 35 mm culture dishes, at approximately 1x10<sup>4</sup> cells per dish, for patch clamp studies, and onto 100 mm culture dishes for cell growth and maintenance. Cells for patch clamp studies were kept in the incubator for half an hour to attach to the bottom of the dish, and then used within 8 hours after passing.

To maintain cell stocks, cells were frozen in liquid nitrogen. Cells at confluency in 100 mm dishes were subcultured as usual by washing twice with HBSS, and then cells suspended in FBS-supplemented DMEM were transferred to centrifuge tubes and spun at 1000 r.p.m. for 10 minutes. The pellet was resuspended in a 90% FBS, 10% DMSO (dimethylsulphoxide) solution and transferred to cryovials at a volume of 1.0 to 1.5 mL,

cooled on ice for 1 hour, then on dry ice for another hour before being placed in liquid nitrogen. This method of slowly freezing the cells resulted in a higher yield of cells when thawed.

Cells were not used beyond passage 55; after p55 cells begin to lose uniformity, and channel characteristics change (Wang, 1991). New cells were then quickly thawed to 37<sup>0</sup>C in a water bath and then suspended in centrifuge tubes in a volume of DMEM that was at least 10 times that of the cryovial (to quickly dilute the DMSO and prevent cell damage). Cells were spun at 1000 r.p.m. for 10 minutes, the supernatant was removed and the pellet resuspended in DMEM and plated onto 100 mm dishes. Cells were not treated with DMSO to induce differentiation. The use of DMSO as a cryoprotectant does not induce cell differentiation (Quandt, 1994).

## **2.2 Whole-Cell Version of the Patch Clamp Technique**

The whole-cell version of the patch clamp technique was used, as per Hamill et al. (1981), and outward potassium currents were measured under voltage clamp conditions. All experiments were performed at room temperature (20-22<sup>0</sup>C).

### **2.2.1 Electrodes**

The patch pipettes were pulled from borosilicate capillary tubing (1.2 mm outer diameter, 0.9 mm inner diameter, FHS, USA) on a two stage puller (Narishige Scientific Instruments, PP-83, Japan), and fire polished by a microforge (Narishige Scientific Instruments, MF-83, Japan). Pipette resistance was in the 4-8 M $\Omega$  range when filled with solution.

### 2.2.2 Solutions

The composition of the solutions was designed to study potassium channels. The bath (outside) solution consisted of NaCl 140 mM, KCl 5.4 mM, MgCl<sub>2</sub> 1.2 mM, CaCl<sub>2</sub> 1.8 mM, HEPES 10 mM, glucose 10 mM, tetrodotoxin (TTX) 1 μM, and was adjusted to a pH of 7.4 using NaOH. TTX is a known Na<sup>+</sup> channel blocker, and was used to eliminate Na<sup>+</sup> transients. The pipette (inside) solution, unless otherwise stated, was composed of K-Aspartate 130 mM, NaCl 10 mM, CaCl<sub>2</sub> 1 mM, MgCl<sub>2</sub> 2 mM, EGTA 11 mM, ATP 4 mM, HEPES 10 mM, glucose 5 mM. A high concentration of EGTA was used to chelate intracellular Ca<sup>2+</sup>, and thus study the voltage-gated potassium channels alone. The addition of Ca<sup>2+</sup> and ATP to the pipette solution was found to promote cell viability under voltage clamp; Ca<sup>2+</sup> and ATP are more commonly used to prevent Ca<sup>2+</sup> channel run-down; the consequences of using this solution will be described in Chapter 3. For some experiments a low Ca<sup>2+</sup> solution was used, and in this case the CaCl<sub>2</sub> and ATP were excluded from the pipette solution (to be discussed in the text). The inside solution was adjusted to a pH of 7.25 using KOH. Both inside and outside solutions were adjusted to within the 320-330 mOsm range using sucrose. All solutions were filtered through a filter with a pore size of 0.45 μM before use.

### 2.2.3 Experimental Procedures

Cells used had a diameter of 30-40 μm, were isolated, round, without neurites and attached to the dish. Cells were washed three times with outside solution. 3 mL of outside solution was added, and then the dish was mounted on an inverted phase-contrast microscope (Nikon, Diaphot, Japan). A hydraulic three-dimensional micromanipulator (Narishige Scientific Instruments, MO-102, Japan) was used to guide the pipettes.

Electrodes were chloride-coated silver wire, and the ground electrode was connected to the bath via a 1% NaCl agar bridge.

Currents were monitored using a digital oscilloscope (Nicolet Instrument Company, model 310, USA). Currents were recorded using an Axopatch-1C patch clamp amplifier, filtered via a Bessel filter (Axon Instruments, USA), and saved onto disk using a personal computer (Zenith 486, Canada). Pulse protocols were generated by pClamp software (Axon Instruments, version 5.5.1, USA) through a digital-to-analog converter (TL-1 DMA Interface, Axon Instruments, USA). Resistance measurements were made by pulsing from a potential of 0 mV to +10 mV, increasing the gain to 100, and measuring the potential difference from the oscilloscope, comparing before and after the pulse. The resistance was then calculated using the following equation:  $R = V/I$ , with  $V = 1 \times 10^{-2}$  V, and  $I = (\text{potential difference/gain}) \times 10^{-12}$  pA.

Liquid junction potentials, the potential difference between the bath and inside solutions were zeroed manually once the electrode was in the bath solution. Seal resistance was in the 2-5 G $\Omega$  range, and leakage subtraction was made on-line using a P/2N protocol, from a holding potential of -80 mV, with two hyperpolarizing subpulses to -110 mV given prior to the depolarizing pulse. Neither the subpulses nor the holding potential are in the activation range for any of the potassium channels studied, thus, only passive leakage currents are subtracted. Whole-cell recordings were made using a gain of 5 and filtered at 2 KHz. Seal resistance was monitored throughout the experiment to detect seal degradation, and if the seal was deteriorating, then the experiment was terminated.

Two voltage protocols were used, one to generate a current-voltage relationship, which gave a series of depolarizing pulses, and another which gave a single depolarizing pulse. The first protocol depolarized the cell from a holding potential of  $-80$  mV in  $10$  mV increments to potentials of  $+40$  mV,  $60$  mV, or  $80$  mV. The second voltage protocol went from a holding potential of  $-80$  mV to  $+20$  mV in a single depolarizing pulse. Pulses were given at a frequency of  $0.1$  Hz and were of a  $280$  msec duration.

A whole-cell recording mode was achieved by rupturing the membrane, using suction, after suction had been used to generate a seal in the appropriate  $G\Omega$  range. Once a stable recording was made following a depolarizing pulse to  $+20$  mV, then control currents from a single cell were recorded. Due to considerable cell-to-cell variability in mean current (from  $200$  to  $2000$  pA), each cell acted as its own control, and control recordings, made after membrane rupture, were considered to be  $100\%$  to normalize data. All drugs tested were added to the bath solution and the point of addition of the drug was considered time zero. Currents were recorded at  $5$ ,  $10$  and  $15$  min. following the application of the drug. The currents recorded did not exhibit run-down, and a control recording (that is the addition of outside solution rather than a test solution) revealed no change in the mean currents over the time course used. Solvents (DMSO, dilute acetic acid, ethanol and deionized, distilled  $H_2O$ ) used had no effect on the currents observed.

#### **2.2.4 Data Analysis**

Recordings were analyzed using the pClamp 5.5.1, and pClamp 6.0 software (Axon Instruments, USA). The stable section of the current recording was used for analysis (i.e.  $200$ - $250$  msec after the depolarizing pulse). Normalized results were compared to control recordings and each other via non-parametric ANOVA, and results

are considered significant with a p value of 0.05 or less. Whole-cell current data is given as mean  $\pm$  standard error, as is given as a % of control recordings, with each cell acting as its own control. Tail currents were analyzed using the pClamp software by fitting the current decay to an exponential curve fit protocol. The equation used to fit the data is:  $y = A_n e^{-(t-K/\tau)^n} + C$ , with  $\tau$  (msec) = time constant for each component (n), A (pA) = amplitude of the tail current for each component, t (msec) = time of decay, K = start time of analysis (msec), C (pA) = steady-state asymptote. An instantaneous current-voltage relationship was generated by plotting the tail current amplitude (pA) for each voltage point, and fitting this plot by linear regression to find the reversal potential (at which no current flows). The reversal potential was compared to the equilibrium potential for  $K^+$  determined using the Nernst equation:  $E_K = RT/F \ln([K]_o/[K]_i)$ , with R = gas constant, T = absolute temperature, F = Faraday constant,  $[K]_o$  = extracellular  $K^+$  concentration,  $[K]_i$  = intracellular  $K^+$  concentration.

## 2.3 Single Channel Recording

The single channel version of the patch clamp technique was used (Hamill et al., 1981); all single channel recordings involved the preparation of outside-out patches. Calcium-activated potassium channel currents were measured in response to voltage clamp. All experiments were performed at room temperature.

### 2.3.1 Electrodes

The pipettes used were prepared as described in section 2.2.1, using the same capillary tubing, except that those used for single channel studies have a higher resistance (7-9 M $\Omega$ ; to decrease capacitance at the tip of the pipette) when filled with solution, and

were coated with Polystyrene Q-Dope (GC Electronics, USA) after being fire-polished to reduce capacitance and background noise.

### **2.3.2 Solutions**

The bath (outside) solutions used were composed of NaCl 140 mM, KCl 5.4 mM, MgCl<sub>2</sub> 1.2 mM, CaCl<sub>2</sub> 2.0 mM, or 4.0mM (as noted in the text), HEPES 10 mM, glucose 10 mM, TTX 1μM, and the pH was adjusted to 7.4 using NaOH. The pipette (inside) solutions were composed of K-Aspartate 130 mM, Mg Cl<sub>2</sub> 2 mM, NaCl 10 mM, CaCl<sub>2</sub> 81 μM, or CaCl<sub>2</sub> 160 μM, EGTA 200μM, HEPES 10 mM, glucose 5 mM, and the pH was adjusted to 7.25 using KOH. The changes in CaCl<sub>2</sub> composition and the consequences of these changes will be discussed in Chapters 3 and 4. Both solutions were adjusted to within the 320-330 mOsm range using sucrose. The composition of the solutions used was designed to study the calcium-activated potassium channels. The combination of EGTA and CaCl<sub>2</sub> resulted in a free calcium concentration of 500 nM to 5μM, see section 2.4 for the procedure for measuring free calcium.

### **2.3.3 Experimental Procedures**

Cells used for single channel recordings were round, and isolated, and were washed five times with 1 mL outside solution per wash, and 1 mL outside solution was added to the dish before recording (rather than the 3 mL added for whole cell recordings, to reduce noise). Unlike whole cell recordings, the procedure used for single channel recordings involved seals of at least 10 GΩ. Outside-out patches were used to generate single channel data: once a good seal was made, suction was used to break the membrane, and the pipette was quickly moved away from the cell, creating a patch which seals with the outside of the membrane facing the bath solution (see Figure 2.1). pClamp

5.5.1 was used to generate the voltage protocols used: patches were taken from a holding potential of  $-40$  mV (a potential at which no channel openings were observed) to potentials of  $-20$  mV,  $0$  mV,  $+20$  mV, and  $+40$  mV for  $1000$  msec at a frequency of  $0.1$  Hz. Alternately patches were held at potentials of  $-20$  mV,  $0$  mV,  $+20$  mV, or  $+40$  mV for  $6$  seconds at a time. For single channel recordings the filter frequency was  $500$  Hz, and the gain was  $100$ . Patches were monitored throughout the course of the experiment, and experiments were terminated when the patch deteriorated.

### **2.3.4 Data Analysis**

Analysis of the single channel data was carried out using pClamp 6.0 software to determine the probability of opening. Single channel conductance was determined by fitting a plot of single channel current versus voltage by linear regression. All points histograms were fitted using an exponential fit protocol (see section 2.2.4 for the exponential fit equation). Probability of opening calculations were done by hand for the patches that were pulsed to varying potentials, and the duration of opening was measured by hand for each  $1000$  msec pulse. Open probability calculations, made using the pClamp software, for the patches held at positive potentials were checked by hand. Calculation of the open probability was based on the equation:  $P(\text{open}) = \text{duration of channel opening per section} / (\text{duration of section measured} * \text{number of channels per patch})$ . Open probability results were compared to each other via non-parametric ANOVA, and results were considered significant with a  $p$  value of  $0.05$  or less. Open probabilities are presented as a % change from control  $\pm$  standard error, with control standardised to  $100\%$ . Single channel records were not long enough for calculations of mean open or closed times to be statistically relevant.



## 2.4 Measurement of Free Calcium

The concentration of free calcium in the inside (pipette) solutions was calculated using the method of Grynkiewicz, Poenie and Tsien (1985). The  $\text{Ca}^{2+}$  indicator Fura-2 was used to measure free  $\text{Ca}^{2+}$  concentrations: Fura-2, at a final concentration of 2  $\mu\text{M}$ , was added to the pipette solution in the dark at room temperature, and then the  $\text{Ca}^{2+}$  concentration was measured by spectrophotometer. To measure the  $\text{Ca}^{2+}$  concentration the solutions were mounted on the stage of an inverted phase microscope (Diaphot TMD, Nikon, Japan), a Spex excitation spectrophotometer was used to measure the intensity of Fura-2 fluorescence, and data was collected by a 386 IBM computer with CM3000DM software. The solution was alternately irradiated with excitation wavelengths of 340 nm or 380 nm, and fluorescence was measured at a wavelength of 510 nm. As the  $[\text{Ca}^{2+}]$  increases, fluorescence increases in response to the 340 nm excitation wavelength and decreases in response to the 380 nm wavelength. Free  $[\text{Ca}^{2+}]$  is then determined using the following formula:  $[\text{Ca}^{2+}]_{\text{free}} = K_d (R - R_{\text{min}}) / (R_{\text{max}} - R) * b$ , with  $K_d$  = the Fura-2 dissociation constant (assumed to be 135 nM),  $R$  = the ratio of fluorescent intensity measured at 340 nm and 380 nm,  $R_{\text{max}}$  = the value of the intensity ratio when the indicator is saturated with  $\text{Ca}^{2+}$ ,  $R_{\text{min}}$  = the value of the intensity ratio when the indicator is  $\text{Ca}^{2+}$ -free, and  $b$  = the ratio of fluorescence intensities measured at 380 nm under low, and saturating  $\text{Ca}^{2+}$  conditions.  $R_{\text{max}}$  and  $R_{\text{min}}$  were determined by applying 10 mM  $\text{CaCl}_2$ , or 10 mM EGTA, respectively, to the solutions tested.

## 2.5 Chemicals and Their Preparation

The dendrotoxins used ( $\alpha$ -,  $\beta$ -,  $\delta$ -, and  $\gamma$ -DTX) were prepared in the lab by Dr. Benishin, and were separated from crude *Dendroaspis angusticeps* venom (Sigma, Sigma Chemical Company, USA) using high performance liquid chromatography, following the method outlined by Benishin et al. (1988). The following chemicals were purchased from Sigma (Sigma Chemical Company, USA): 4-aminopyridine (4-AP), 4-acetamino-4'-isothiocyano-2, 2'-disulfonic acid stilbene (SITS), adenosine 5'-triphosphate (ATP), ethyleneglycol-bis- ( $\beta$ -aminoethyl ether) N, N, N', N'-tetraacetic acid (EGTA), N-2'-ethanesulfonic acid (HEPES), L-aspartic acid monopotassium salt (K-Aspartate), dimethyl sulfoxide (DMSO), tetraethyl ammonium chloride (TEA), apamin, tetrodotoxin (TTX), nifedipine,  $\text{CoCl}_2$ , and  $\text{NaCl}$ .  $\text{KOH}$ ,  $\text{CaCl}_2$ ,  $\text{MgCl}_2$ ,  $\text{KCl}$ , and glacial acetic acid were purchased from Fisher (Fisher Scientific, USA). Sucrose, D-glucose,  $\text{NaHCO}_3$ , and  $\text{NaOH}$  were purchased from BDH (BDH Inc., Canada). Dulbecco's Modified Eagle Medium (DMEM), and Hank's Balanced Salt Solution (HBSS) were purchased from Gibco (Gibco BRL Life Technologies, USA). Fetal bovine serum was purchased from HyClone (HyClone Laboratories, USA). Iberiotoxin was purchased from RBI (Research Biochemicals International, USA). Fura-2 pentapotassium salt was purchased from Molecular Probes (Eugene, USA). Nifedipine, and Fura-2 were dissolved in 50% DMSO. Apamin and iberiotoxin were dissolved in dilute (0.05M) acetic acid. All other chemicals were dissolved in deionized, distilled  $\text{H}_2\text{O}$ .

## 2.6 Statistics

Unless original traces or single experiments are shown, all data is expressed as mean  $\pm$  standard error. Data from whole-cell studies are expressed as percentage change in current from pre-drug controls (normalised to 100%) at 20 mV. Single channel data are expressed as percent change in probability of opening from pre-drug controls (normalised to 100%) at 20 mV. The paired Student's t-test (paired or grouped) was used to compare control values with those recorded after drug administration. Analysis of variance in conjunction with the Newman-Keul's test was used for multiple group comparisons. P values less than 0.05 were considered statistically significant (in the figures \* denotes p values less than 0.05 and \* \* denotes p values less than 0.01). An exponential curve-fitting program was used to determine deactivation time constants for whole cell tail current decay. A linear regression curve (set at a 95% confidence interval, with  $R^2 = 0.99$ ) was fitted to the whole cell instantaneous tail current-voltage relationship data and the single channel current-voltage data to determine the current reversal potential and  $\text{Ca}^{2+}$ -activated  $\text{K}^+$  channel conductances, respectively.

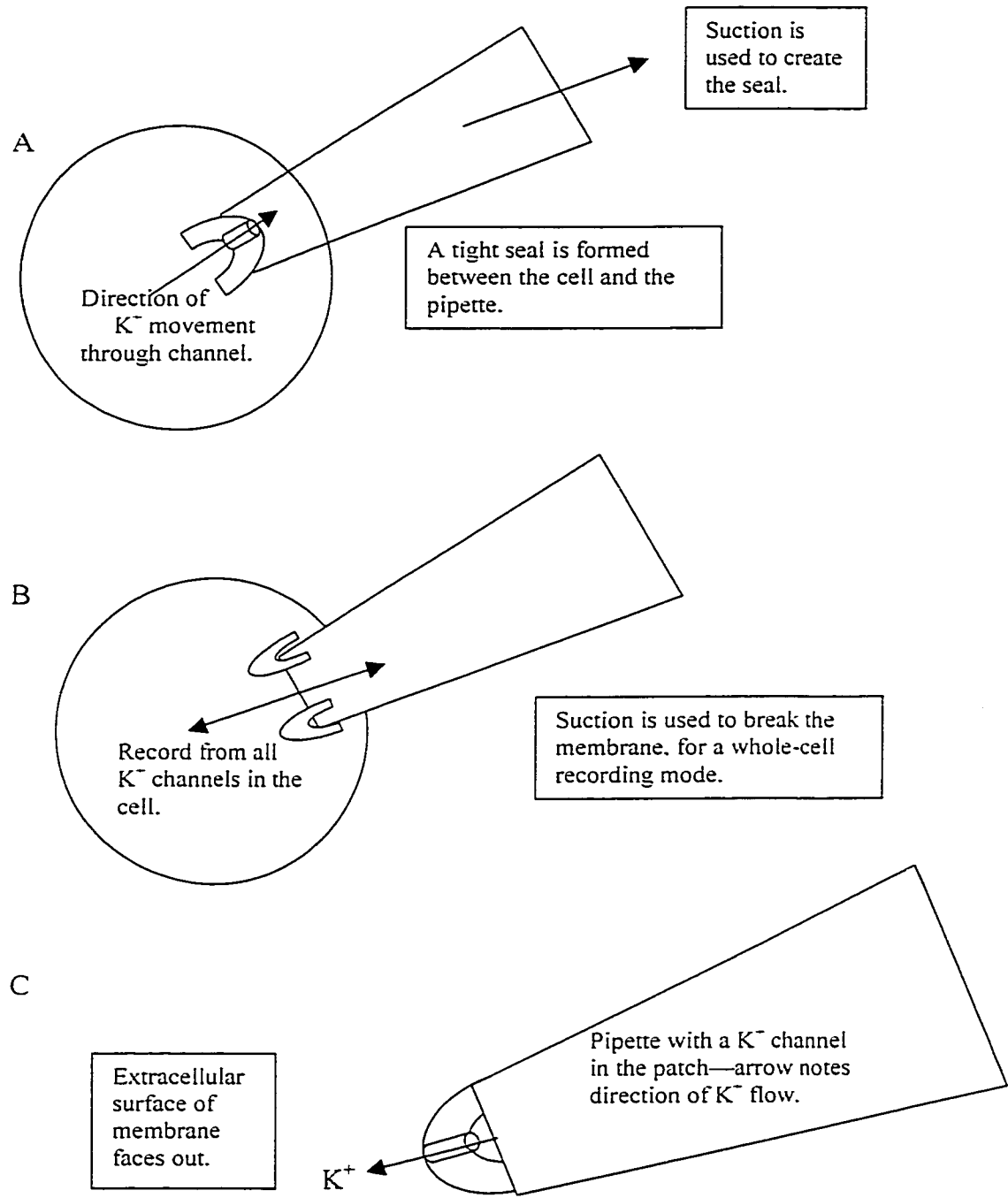


Figure II-1. A diagram showing how outside-out patches are prepared. In (A) a strong ( $G\Omega$ ) seal is made to the cell, (B) the cell membrane is ruptured, establishing a whole-cell recording mode, and (C) the pipette is ripped from the cell, the patch reseals, and an outside-out patch is formed. (adapted from Hamill et al., 1981)

## Chapter III

### Whole-Cell Results

#### 3.1 Introduction

Potassium currents in the undifferentiated neuroblastoma N1E 115 cells have not been extensively studied, however, in DMSO-differentiated cells, the presence of voltage-gated, and calcium-activated potassium channels has been established (see Section 1.5 for review; Quandt, 1988; Leinders and Vijverberg, 1992; Disbero, Antony, and Verdeti, 1994). Undifferentiated N1E 115 cells were used in this study, and by studying the nature and pharmacological interactions of  $K^+$  channels in undifferentiated cells it is possible to gain a greater understanding of the role  $K^+$  channels play in immature neurons, and, potentially, in the differentiation process.

#### 3.2 Experimental Design

##### 3.2.1 Characterization of Outward Currents

Using the whole-cell version of the patch clamp technique, outward currents measured in undifferentiated neuroblastoma N1E 115 cell line were studied. The pipette and bath solutions used were designed to elicit potassium currents (see Section 2.2.2) in response to changes in voltage from a holding potential of  $-80$  mV, increasing in  $10$  mV steps to  $+40$  mV, or  $+80$  mV. Once the whole-cell recording mode was established, and current recordings were stable, tail currents generated by incremental increases in voltage

steps were studied to determine the reversal potential. Also, tail current decay time constants were used to determine the potential for maximal activation of the channels.

### **3.2.2 Pharmacology of Potassium Currents**

The non-specific potassium channel blockers tetraethylammonium (TEA), and 4-aminopyridine (4-AP) were used to further characterise these outward potassium currents. Following stable current recordings (with each cell acting as its own control), using a voltage protocol from a holding potential of  $-80$  mV, increasing incrementally to  $+40$  mV, each channel blocker was added to the bath, and current recordings were made at 5 and 10 minutes after drug application, without washout of the test solution. TEA at 20 mM and 1 mM and 4-AP at 1 mM and 50  $\mu$ M were used. Currents recorded at the  $+20$  mV voltage step were used, to ensure maximal channel activation, as the basis for comparison pre- and post-application of TEA or 4-AP. All recordings were made in the presence of pipette EGTA,  $\text{Ca}^{2+}$  and ATP (see Section 2.2.2).

### **3.2.3 Effect of Dendrotoxins on Potassium Currents**

Each of the four green mamba venom peptides  $\alpha$ -,  $\beta$ -,  $\delta$ -, and  $\gamma$ -dendrotoxin (DTX) at a concentration of 200 nM were added to the bath solution, and whole-cell currents were recorded, in the presence of pipette  $\text{Ca}^{2+}$  and ATP, using a voltage protocol increasing incrementally from a holding potential of  $-80$  mV to  $+40$  mV, before, and at 5 and 10 minutes following application of each toxin. To further establish and identify the potassium channels involved, the effect of  $\gamma$ -DTX (200 nM and 2  $\mu$ M) in the absence of either pipette ATP, or calcium, was studied, using a voltage protocol increasing incrementally from a holding potential of  $-80$  mV to  $+80$  mV. Currents recorded at the  $+20$  mV voltage step were used to ensure maximal channel activation, as the basis for

comparison pre- and post-DTX application. Currents recorded for the  $\alpha$ -,  $\beta$ -, and  $\gamma$ -DTX experiments were recorded in the presence of pipette EGTA,  $\text{Ca}^{2+}$  and ATP. Pipette composition for the  $\gamma$ -DTX studied varied, and changes in  $\text{Ca}^{2+}$ , EGTA, and ATP are noted in the text.

### 3.3 Results

#### 3.3.1 Characterization of Outward Currents

Once a whole-cell recording mode was established, outward currents were generated in response to changes in voltage from a holding potential of  $-80$  mV, as shown in Figure III-1A and 1B; of the cells tested ( $n = 53$ ), 86% exhibited a saturation of the current generated following increasing voltage pulses in the range of  $+10$  to  $+40$  mV (see Figure III-1B). Saturating currents, seen under conditions of high pipette  $\text{Ca}^{2+}$ , and ATP (most commonly used to prevent  $\text{Ca}^{2+}$  channel run-down), are indicative of the activation of  $\text{Ca}^{2+}$ -activated  $\text{K}^+$  channels (O'Dowd, Ribera and Spitzer) in the cells studied—saturating currents are not seen in the absence of pipette  $\text{Ca}^{2+}$  and ATP (see Section 3.3.3). Also, as shown in Figure III-1B, in some cells no saturation is seen even in the presence of pipette  $\text{Ca}^{2+}$  and ATP. Furthermore, as can be seen in Figure III-1, the current amplitude varied widely, from 100 to 1500 pA at  $+80$  mV, from cell to cell in response to the same train of voltage pulses, and under the same pipette conditions. Maturing voltage-gated and  $\text{Ca}^{2+}$ -activated  $\text{K}^+$  currents show a similar variability in current amplitude (O'Dowd, Ribera and Spitzer, 1988).

Tail currents represent the passive current decay following the end of a voltage pulse, and the return to holding potential (see Figure III-2A); the decay can be fitted by

an exponential curve fitting program to give a time constant of decay. In these cells, tail current decay could be fitted by either a single exponential (see Figure III-2B, or, in a small percentage of cells, by two exponentials (see Figure III-2C). The time constant for tail current decay varied considerably, in most (93%) cells the rate of tail current decay is described by a single exponential and falls into one of three main groupings: fast (1 to 3 msec), medium (5 to 7 msec), or slow (8 to 16 msec). The representation of each grouping depended on the conditions—the presence of pipette EGTA,  $\text{Ca}^{2+}$ , and/or ATP (see Table III-1). With EGTA,  $\text{Ca}^{2+}$  and ATP in the pipette solution, the deactivation time constants ranged from fast  $2.5 \pm 0.2$  msec, to medium  $5.8 \pm 0.4$  msec, or slow  $9.2 \pm 1.1$  msec, with the majority of the time constants (69% of 29 cells) falling into the fast category. In the absence of ATP, but in the presence of pipette  $\text{Ca}^{2+}$  and EGTA, the majority (57%) of the deactivation time constants shifted toward the medium category, for an average value of  $5.4 \pm 0.2$  msec. Of the 7 cells studied under these conditions, two cells were found to have a deactivation time constant of 2.1 msec, while one had a time constant of 16.5 msec. Similarly, in the absence of pipette  $\text{Ca}^{2+}$  and ATP, but in the presence of EGTA, the majority of time constants (66%) again fell in the middle category, with a deactivation time constant of  $6.1 \pm 0.6$  msec. Of the 6 cells studied without  $\text{Ca}^{2+}$  or ATP, one had a fast time constant of 2.4 msec, and one had a slow time constant of 10.1 msec. In two cells (7% of the total number studied), both in the presence of EGTA, ATP and  $\text{Ca}^{2+}$ , the tail current decay was best represented by two exponentials, in these cases the deactivation time constants fell into the fast and slow groupings exclusively (for a mean  $\tau_1$  of 1.5 msec, and a mean  $\tau_2$  of 11.4 msec).



Plotting tail current amplitude versus voltage gives an instantaneous current-voltage (I-V) plot. This instantaneous I-V plot is useful for determining the potential at which the majority of the K<sup>+</sup> channels are active. Since the tail current decay reflects channel deactivation, the potential at which most of the K<sup>+</sup> channel population is active is seen in the saturating phase of the current-voltage plot, which in these cells is in the 0 to +10 mV range (see Figure III-3A). The voltage at which the channels are maximally active can be confirmed by a plot of tail current time constant amplitude versus voltage, which, like tail current amplitude reaches a peak at the point where most channels are active. In these cells tail current time constants also are at maximum in the 0 to +10 mV range (see Figure III-3B).

The reversal potential for these currents was within the range estimated, based on the Nernst equation, for potassium channel reversal: given the concentration of potassium in the pipette solution versus that in the bath solution, the estimated reversal potential is –78.9 mV. Tail current amplitudes from the decay of a pulse to +20 mV, followed by a range of voltage steps from -20 to –110 mV were used as the basis for the determination of the reversal potential (see Figure III-4A). The potential at which outward current reverses was determined based on linear regression of an instantaneous current-voltage plot to be  $-81.2 \pm 1.0$  mV (n = 9; see Figure III-4B).

The differences seen in current amplitude, saturation and time constant of tail current decay are indicative of a wide variance in potassium channel expression and composition in this population of cells, perhaps attributable to cell cycle or spontaneous cell differentiation—which is known to occur in a small percentage of any given population of N1E 115 neuroblastoma cells (Quandt, 1994).

### 3.3.2 Pharmacology of Whole-Cell Potassium Currents

The non-specific K<sup>+</sup> channel blockers TEA, and 4-AP were found to block the whole-cell current, to varying degrees, regardless of whether the currents recorded exhibited saturation at positive potentials. Application of 20 mM TEA to the bath solution resulted in a complete block of whole-cell currents within 5 minutes (n = 3, see Figure III-5), confirming that the currents recorded were K<sup>+</sup> currents. A lower concentration of TEA (1 mM), was found to have a slower onset of block: after 5 minutes the whole-cell current was reduced to  $59.9 \pm 14.1\%$  of control at +20 mV, and at 10 minutes the current was reduced to  $41.3 \pm 1.6\%$  of control (at +20 mV; n = 4, see Figure III-6). The slowest onset of current inhibition was apparent with 4-AP: 1 mM 4-AP decreased the current recorded to only  $85.9 \pm 1.6\%$  of control, which was further reduced to  $53.4 \pm 12.8\%$  of control after 10 minutes (at +20 mV; n = 3, see Figure III-7). Both the TEA and the 1 mM 4-AP results are significant at 10 minutes (p < 0.01). A lower concentration of 4-AP of 50  $\mu$ M caused a reduction in the outward current to  $92.2 \pm 2.8\%$  of control at 5 minutes, and  $69.4 \pm 3.8\%$  of control at 10 minutes (at +20 mV; n = 4, see Figure III-8). At the lower concentration, only the results after 10 minutes are significantly different from control, with a p value of 0.05. The 4-AP data indicates that only a percentage of the outward current is 4-AP sensitive.

### 3.3.3 Effect of Dendrotoxins on Whole-Cell Potassium Currents

Of the DTXs studied, only  $\beta$ - and  $\gamma$ -DTX were found to have any effect on the K<sup>+</sup> currents in the N1E 115 cells, and this effect was found to be dependent upon saturation of the outward current. Neither  $\alpha$ -DTX, nor  $\delta$ -DTX had any measurable effect on

whole-cell currents, regardless of whether the currents recorded saturated at positive potentials. Application of 200 nM  $\alpha$ -DTX resulted in a negligible decrease in  $K^+$  currents ( $95 \pm 3.7\%$  of control within 10 minutes, at +20 mV;  $n = 5$ , seen in Figure III-9), as did the application of 200nM  $\delta$ -DTX ( $95.0 \pm 4.1\%$  of control after 10 minutes, at +20 mV,  $n = 4$ , seen in Figure III-10).

In contrast, application of 200 nM  $\beta$ -DTX ( $n = 6$ ) had a widely varying effect on  $K^+$  currents recorded, ranging from an increase to 130% of control, to a decrease to 41.4% of control, for an average of  $88.8 \pm 17.5\%$  of control (all measured at +20 mV). The effect of  $\beta$ -DTX was dependent on current saturation—in cells showing saturation of the outward current ( $n = 5$ ), prior to the application of toxin, it caused a change in the currents measured, and, again, the direction of this change depended upon continued current saturation following toxin application (see Table III-2). In one cell in which the outward currents did not saturate at positive potentials, no change was seen in overall outward currents after toxin application. As shown in Figure III-11, and Table III-2, if saturating currents are present after application of  $\beta$ -DTX, a decrease in total current was seen ( $n = 3$ ; see Figure III-11A and 12A), if, however, application of the toxin resulted in absence of saturating currents, an increase in total current was seen ( $n = 2$ ; see Figure III-11B and 12B). Yet, despite these trends in the effect of  $\beta$ -DTX, and a large spread in data, actual changes in current were found to be so variable that overall they were not statistically significant.

Similarly, the effect of the  $\gamma$ -DTX was found to have a dependence on the presence of current saturation prior to toxin application (see Table III-2). In cells

exhibiting current saturation after toxin application,  $\gamma$ -DTX (200nM) was found to decrease current recordings to  $74.7 \pm 2.0\%$  of control after 5 minutes, and to maintain current inhibition for 10 minutes ( $74.0 \pm 1.9\%$  of control, at +20 mV, n = 3; see Figure III-13A, 14A, and Table III-2). Like the structurally similar  $\beta$ -DTX,  $\gamma$ -DTX was also found, in two cells, to increase current amplitude by 29%, and, like  $\beta$ -DTX, in cells where there was an increase in total current, these currents do not exhibit saturation following toxin application (see Figure III-13B, 14B, and Table III-2). Unlike  $\beta$ -DTX, however,  $\gamma$ -DTX was found to alter overall current in a consistent and statistically significant manner ( $p < 0.05$ ).

A summary of the results discussed so far, that is the response to TEA, 4-AP, and the DTXs 5 and 10 minutes after application, compared to control (each cell acts as its own control) is shown in Figure III-15.

Both the changing representation of the time constant populations and the presence or absence of saturating currents indicated that different subtypes of  $K^+$  channel are being activated, depending on the conditions used. Also the variation of time constants within each set of pipette conditions listed in Table III-1 indicates that the channel population itself varies from cell to cell. Since activation of  $Ca^{2+}$ -activated  $K^+$  channels is known to cause a saturation of outward currents at positive potentials, and since ATP is commonly used in studies of  $Ca^{2+}$  channels to prevent channel run-down, the role of  $Ca^{2+}$  and ATP in the pipette solution was examined. In the absence of pipette  $Ca^{2+}$  and ATP, none of the cells recorded exhibited a similar degree of saturation at positive potentials (any saturation seen was relatively minor, and was lost as the cell was

dialyzed with intracellular solution), as shown Figure III-16, despite the use of an extended voltage range (to +80 mV). In the absence of pipette  $\text{Ca}^{2+}$  and ATP,  $\gamma$ -DTX had no significant effect on these currents at 200 nM ( $n = 3$ ), or 2  $\mu\text{M}$  ( $n = 3$ ), even 15 minutes after application of the DTX (see Figure III-17); also no current run-down was observed over 15 minutes. Returning  $\text{Ca}^{2+}$ , but not ATP (or returning ATP, but not  $\text{Ca}^{2+}$ ) to the pipette solution, did not result in a significant change in outward currents after application of 2  $\mu\text{M}$   $\gamma$ -DTX ( $n = 3$ , see Figure III-18); again no current run-down was observed over 15 minutes, although minor current saturation was lost by 5 minutes, when compared to control. Given that  $\gamma$ -DTX did not significantly effect outward currents in the absence of pipette ATP, and/or  $\text{Ca}^{2+}$ , and that 11 mM EGTA was present in the pipette solution, regardless of the presence or absence of  $\text{Ca}^{2+}$  and ATP, it is unlikely that  $\gamma$ -DTX blocks purely voltage-gated  $\text{K}^+$  channels in these cells. Furthermore, given that outward current block by  $\beta$ - or  $\gamma$ -DTX is dependent upon the presence of saturating currents, and pipette  $\text{Ca}^{2+}$  and ATP, it is likely that these DTXs are affecting  $\text{Ca}^{2+}$ -activated  $\text{K}^+$  channels. Since the effect of  $\gamma$ -DTX is dependent on the presence of pipette ATP, it is also possible that the toxin was acting on purinergic receptors, or even affecting the  $\text{Ca}^{2+}$ -activated  $\text{K}^+$  current indirectly via voltage-gated  $\text{Ca}^{2+}$  channels. In order to confirm that a  $\text{K}^+$  channel is directly involved and to clarify the nature of this effect, single-channel experiments were necessary.

Pipette Conditions	Tail Current Time Constant( $\tau$ ) Populations		
	A Fast	B Medium	C Slow
EGTA, ATP, and $\text{Ca}^{2+}$ (n = 29)	2.5 $\pm$ 0.2 (69%)	5.8 $\pm$ 0.4 (24%)	9.2 $\pm$ 1.1 (7%)
EGTA, $\text{Ca}^{2+}$ , no ATP (n = 7)	2.1 (29%)	5.4 $\pm$ 0.2 (57%)	16.5 (14%)
EGTA, no ATP, no $\text{Ca}^{2+}$ (n = 6)	2.4 (17%)	6.1 $\pm$ 0.6 (66%)	10.1 (17%)

Table III-1. Tail current decay from +20 mV to the holding potential of -80 mV, the population of deactivation time constants fitted by one exponential can be divided into three main groups: fast (A), medium (B) and slow (C). All time constants are given in msec as mean  $\pm$  standard error, with the % representation of total cells in brackets.

Effect of $\beta$ -, and $\gamma$ -DTX on Whole-Cell Outward Currents				
Toxin	No saturation in control currents		Saturation in control currents	
	No saturation of currents following toxin application	Saturation of currents following toxin application	No saturation of currents following toxin application	Saturation of currents following toxin application
$\beta$ -DTX	No effect N = 1	N/A	Increase N = 2	Decrease N = 3
$\gamma$ -DTX	No effect N = 9	N/A	Increase N = 2	Decrease N = 3

Table III-2. The effect of  $\beta$ - and  $\gamma$ -DTX on whole cell  $K^+$  currents is dependent on the presence of saturating currents in control recordings. The direction of the effect on overall  $K^+$  currents also depends on whether saturating currents are seen following toxin application. Overall current increases following toxin application correlated with the loss of saturating currents, while overall current decrease correlated with the maintenance of saturating currents.

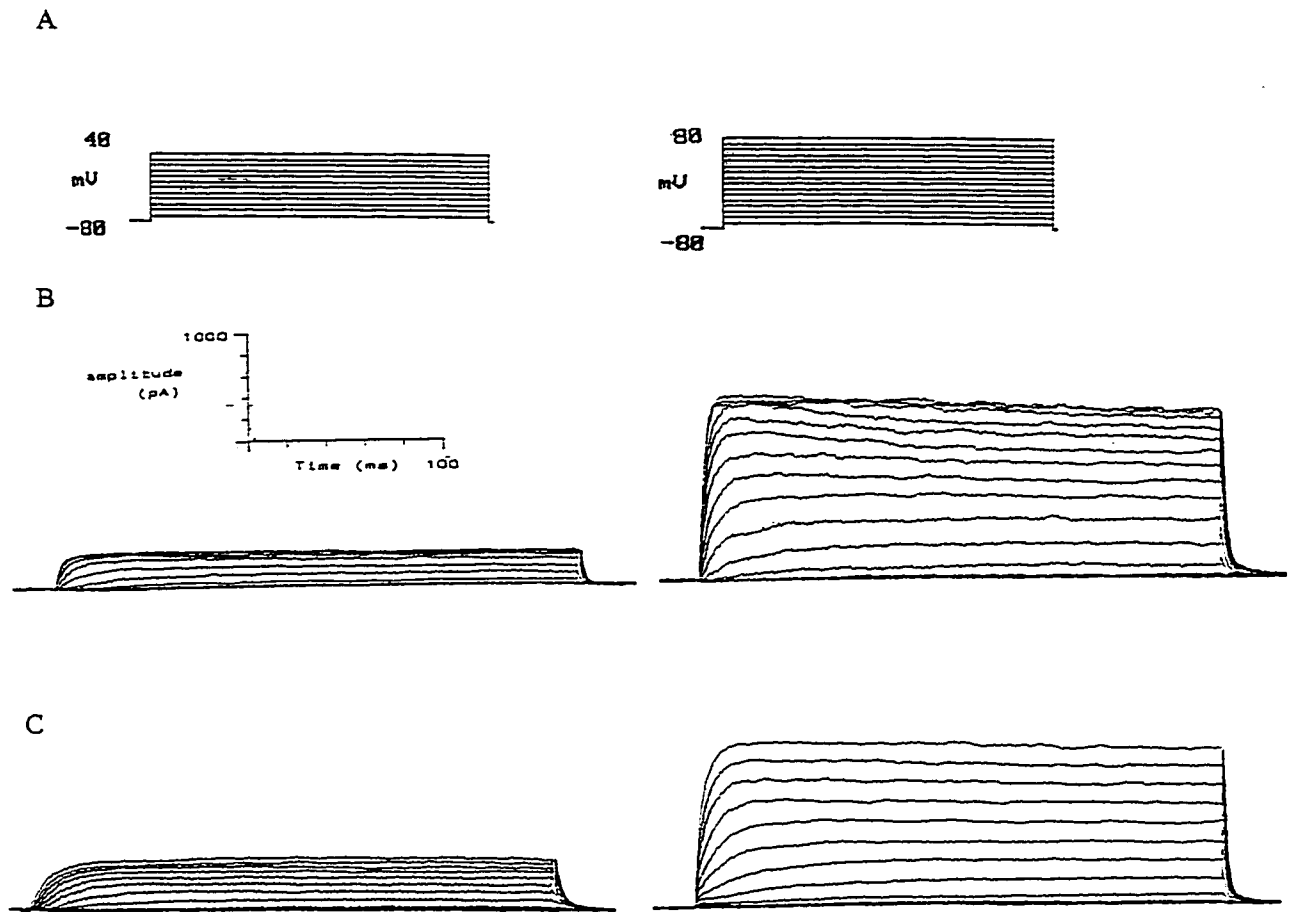


Figure III-1. Voltage protocols given, and the resultant outward currents showing cell-to-cell variation among recorded currents in the presence of EGTA, ATP, and  $Ca^{2+}$ . Traces are from 4 different cells. In (A) voltage protocols with trains of voltage pulses lasting for 280 msec from a holding potential of -80 mV to potentials of +40 mV, or +80 mV are shown. The resultant outward current traces are shown in (B) and (C), with examples of both large (right) and small (left) current recordings in each. Traces in (B) show a saturation of the current recorded at positive potentials, despite increases in voltage potentials; the current traces shown in (C) do not exhibit saturation, as would be expected for purely voltage-dependent  $K^+$  currents. See Section 3.3.1 for discussion.



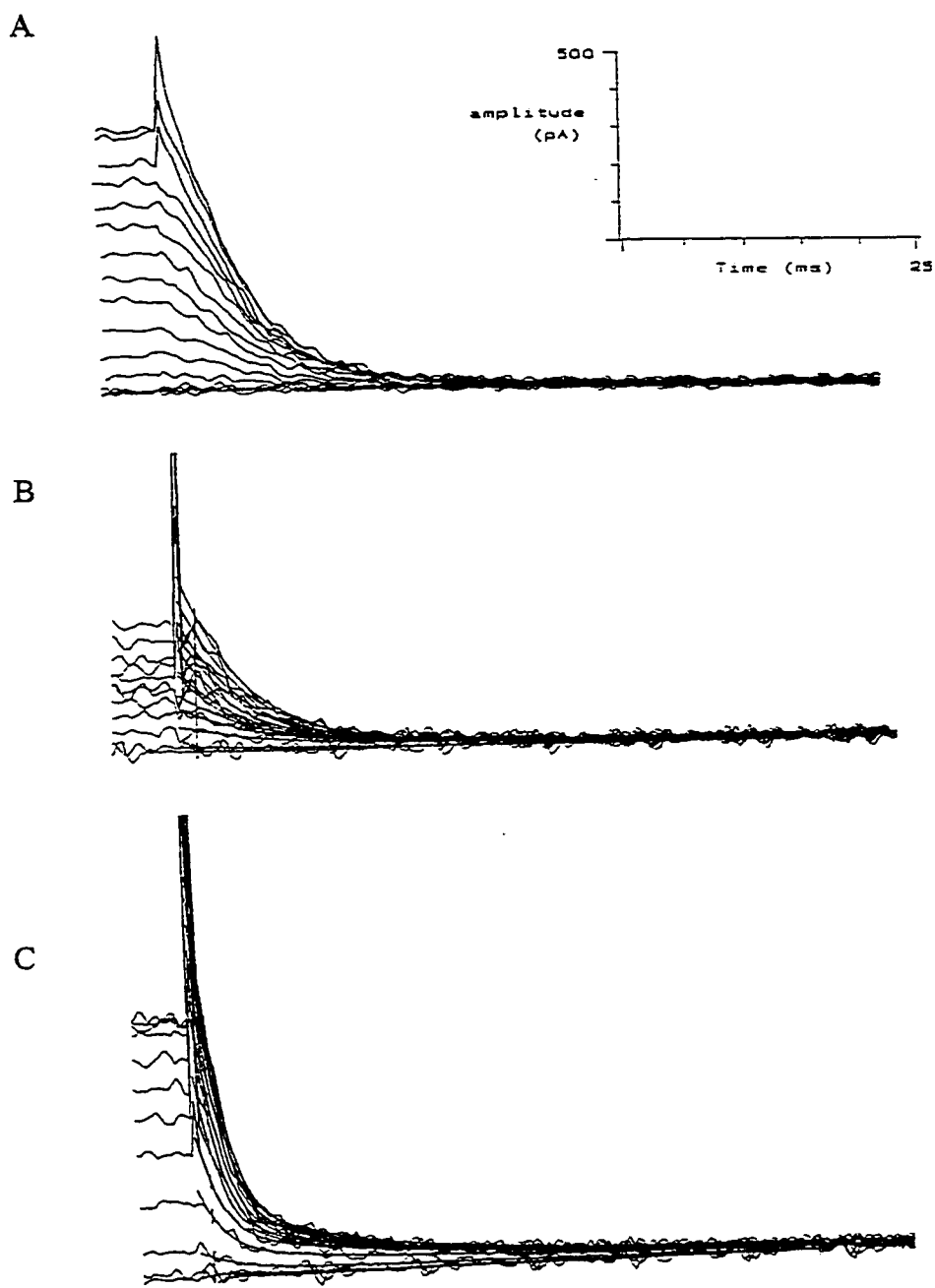
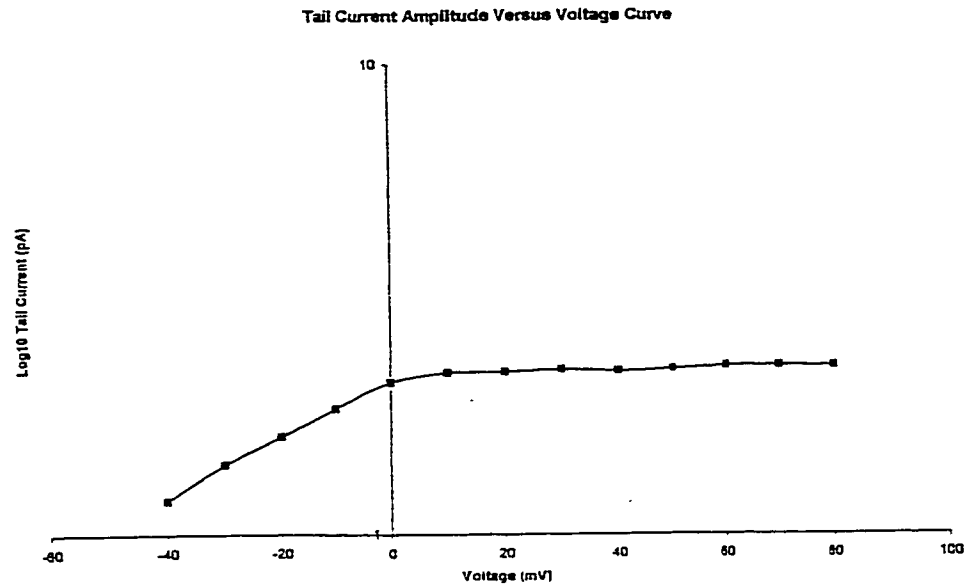


Figure III-2. Tail current decay and calculation of deactivation time constants by exponential curve fitting are shown. Traces are from 3 different cells. An enlarged segment of an original current trace is shown in (A), with the return to the holding potential and the resultant current decay. This decay represents channel deactivation, and fitting the current decay by one (B), or two (C) exponentials gives the deactivation time constant ( $\tau$ , in msec), and amplitude of the decay (in pA). See Table III-1, and Section 3.3.1 for values and discussion.

A



B

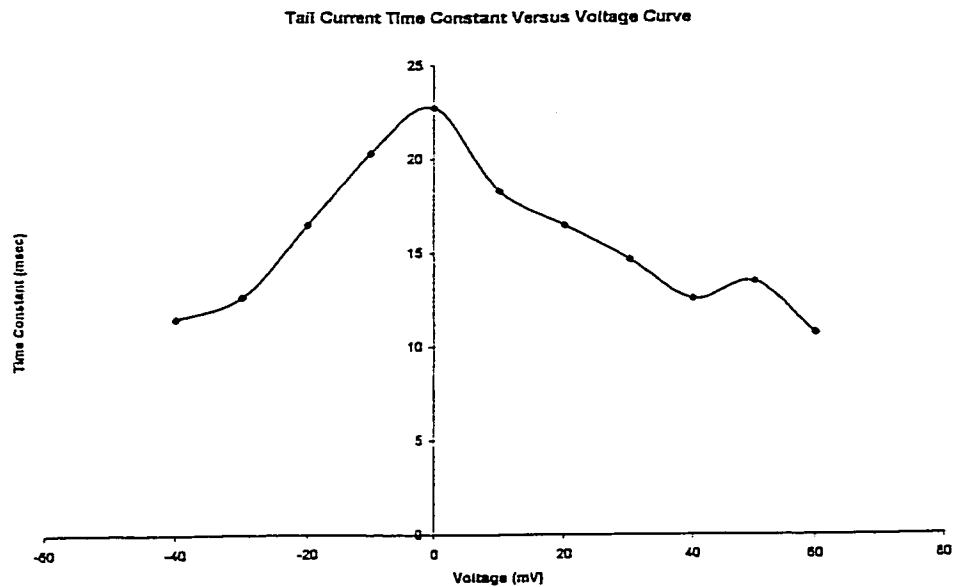
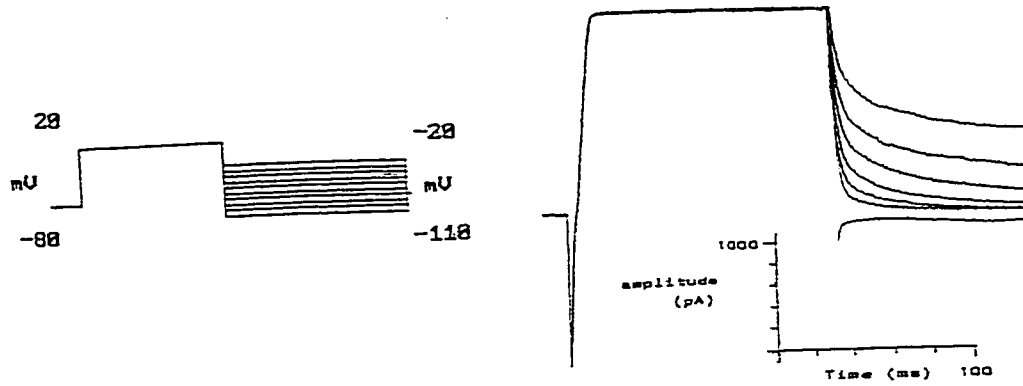


Figure III-3. Plots of tail current decay versus voltage and tail current deactivation time constants versus voltage are used to determine the potential at which all the  $K^+$  channels are active. The logarithmic amplitude of tail current decay versus voltage gives a plot (A); as the majority of the channels are activated, the amplitude of the deactivating current no longer follows an exponential rate of increase, and this occurs in the 0 to +10 mV range. In (B) the time constants for tail current decay are plotted versus voltage--the time constant amplitude reaches a peak (at 0 mV) as the majority of the channel population is activated. The data for these graphs is from a single, representative cell, measured in the presence of pipette EGTA,  $Ca^{2+}$ , and ATP. See Section 3.3.1 for discussion.

A



B

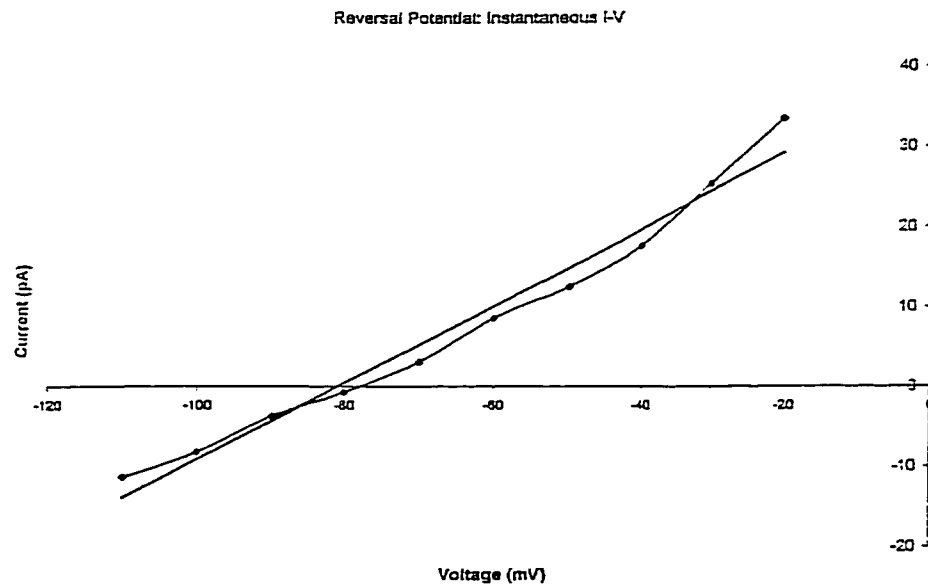
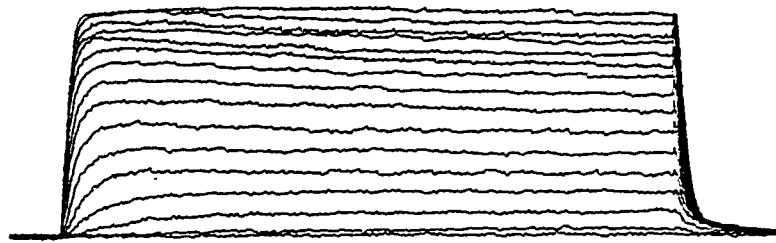
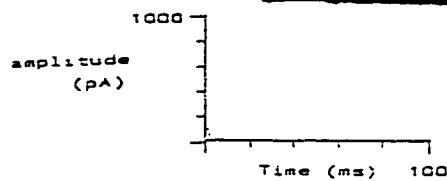


Figure III-4. The reversal potential of whole cell  $K^+$  currents recorded in the presence of EGTA, ATP, and  $Ca^{2+}$ . In (A) the traces from one representative cell shown on the right are the result of a train of voltage pulses (shown on the left) from a holding potential of  $-80$  mV to  $+20$  mV, then stepped to a range of potentials between  $-20$  and  $-110$  mV. In (B) the relationship between tail current amplitude and step membrane potential is shown fitted by a linear regression line to determine the reversal potential—for this cell regression analysis gives a reversal potential of  $-82.0$  mV. Outward currents were found to have a mean reversal potential of  $-81.2 \pm 1.0$  mV ( $n = 9$ ); see Section 3.3.1 for discussion.

A  
Control



5 minutes



B

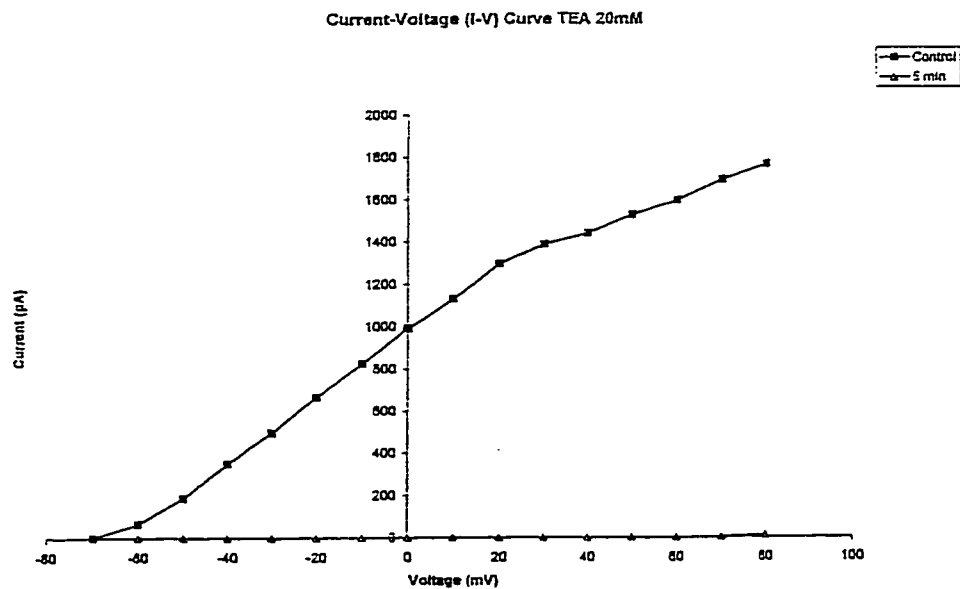


Figure III-5. Effect of 20 mM TEA application on whole-cell  $K^+$  currents recorded in the presence of pipette EGTA, ATP, and  $Ca^{2+}$ . The original current traces from a single, representative, cell (A) showing the response to a series of voltage pulses before, and 5 minutes after the application of TEA, and the corresponding current-voltage (I-V) plot (B) for this cell. Note the complete block of current flow after 5 minutes (significant,  $p < 0.01$ ), without washout.

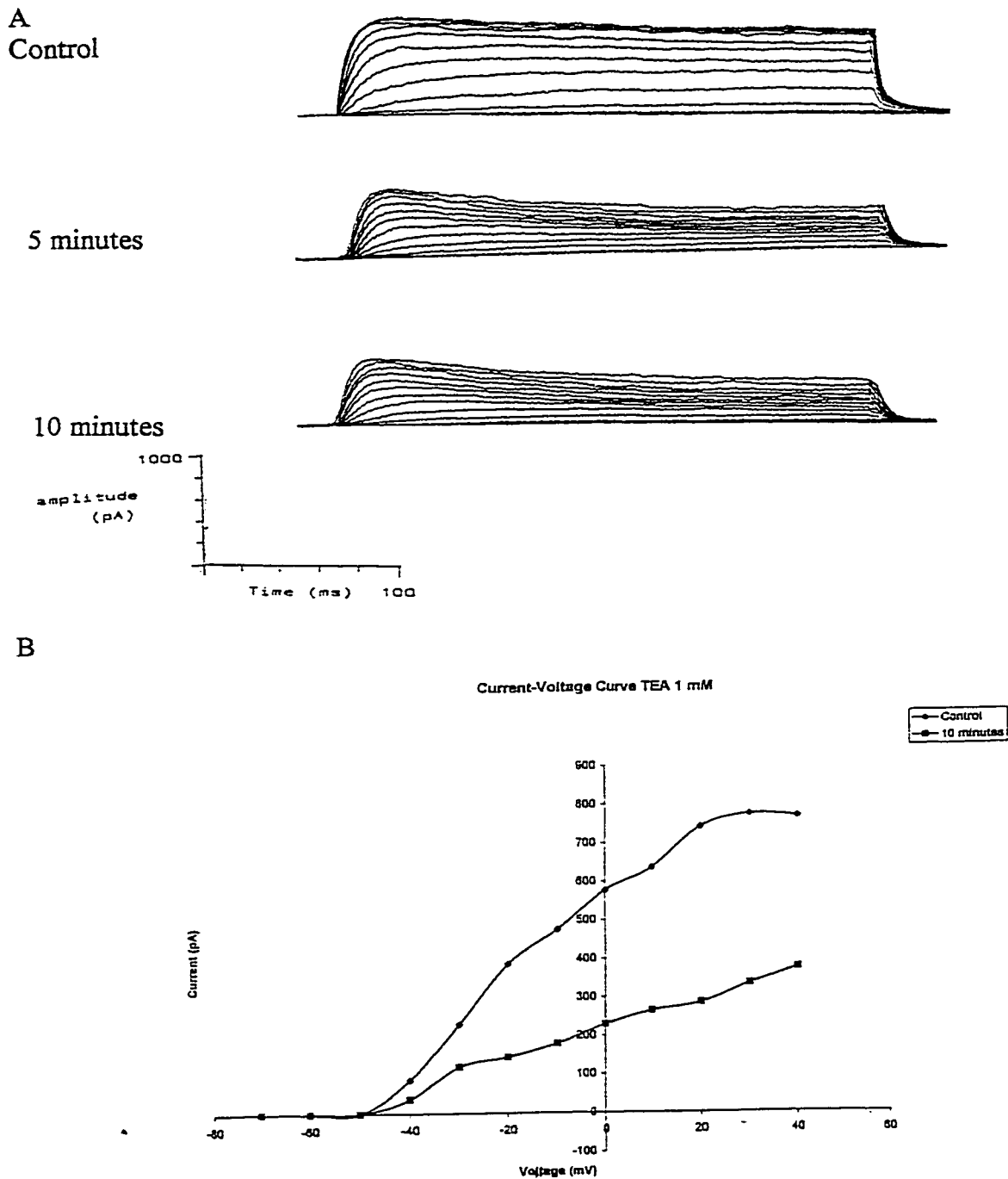


Figure III-6. Effect of 1 mM TEA application on whole-cell  $K^+$  currents recorded in the presence of pipette EGTA, ATP, and  $Ca^{2+}$ . A representative original current trace from a single cell (A) showing the response to a series of voltage pulses before and 5 and 10 minutes after the application of TEA, and the corresponding I-V plot (B). Note the decrease in overall current after 5 minutes (significant,  $p < 0.05$ ) without washout.

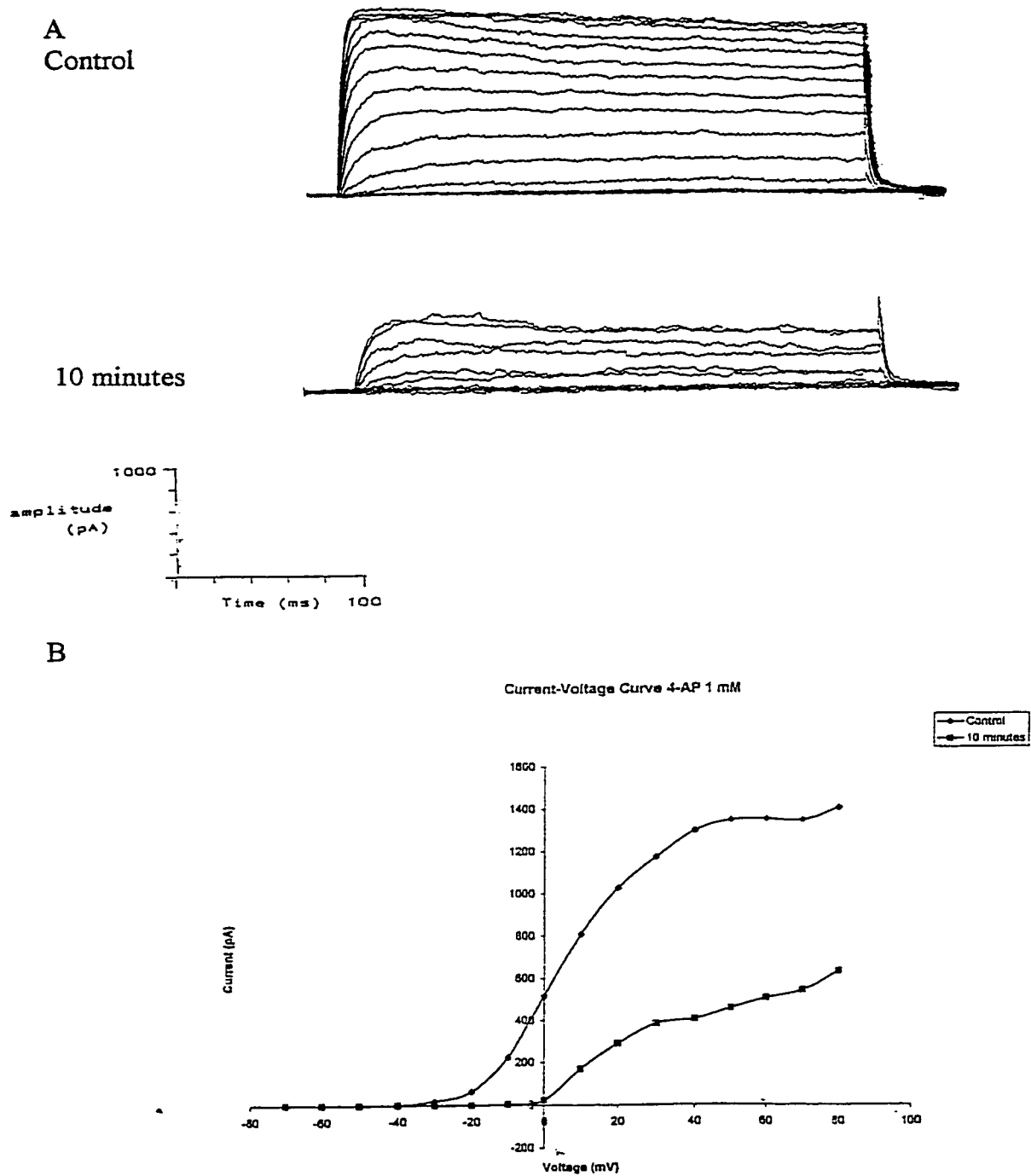
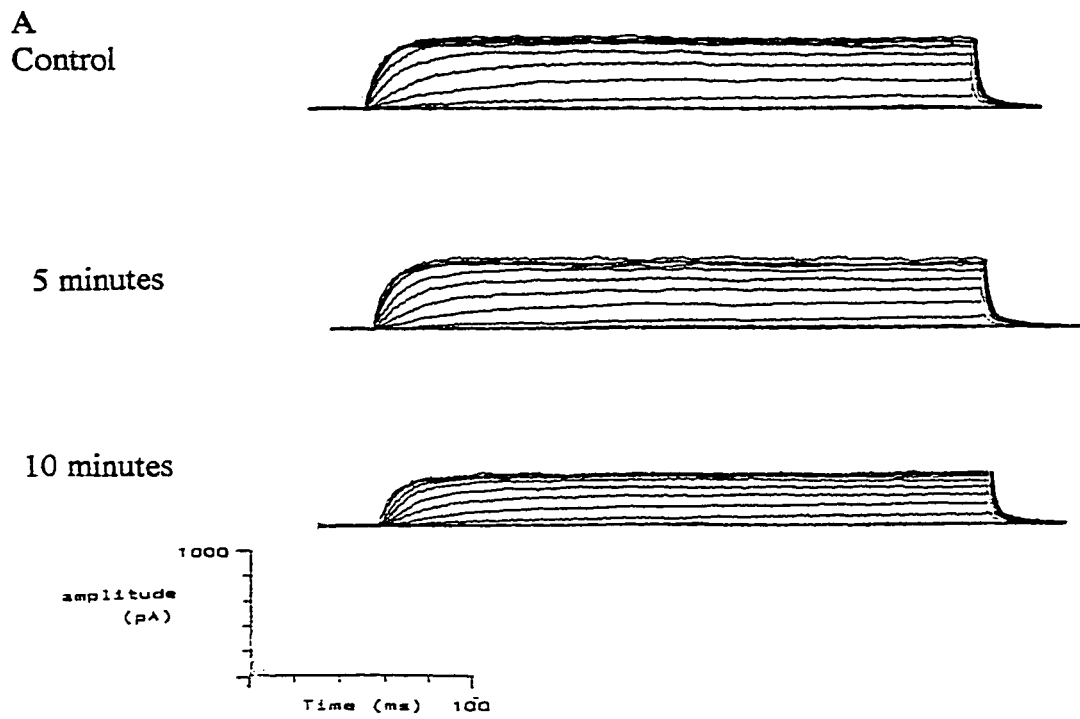


Figure III-7. Effect of 1 mM 4-AP application on whole-cell  $K^+$  currents recorded in the presence of pipette EGTA, ATP, and  $Ca^{2+}$ . A representative original current trace from a single cell (A) in response to a series of voltage pulses before and 10 minutes after the application of 4-AP, and the corresponding I-V plot (B) is shown. Note the decreased current at 10 minutes (significant  $p < 0.01$ ), without washout.



B

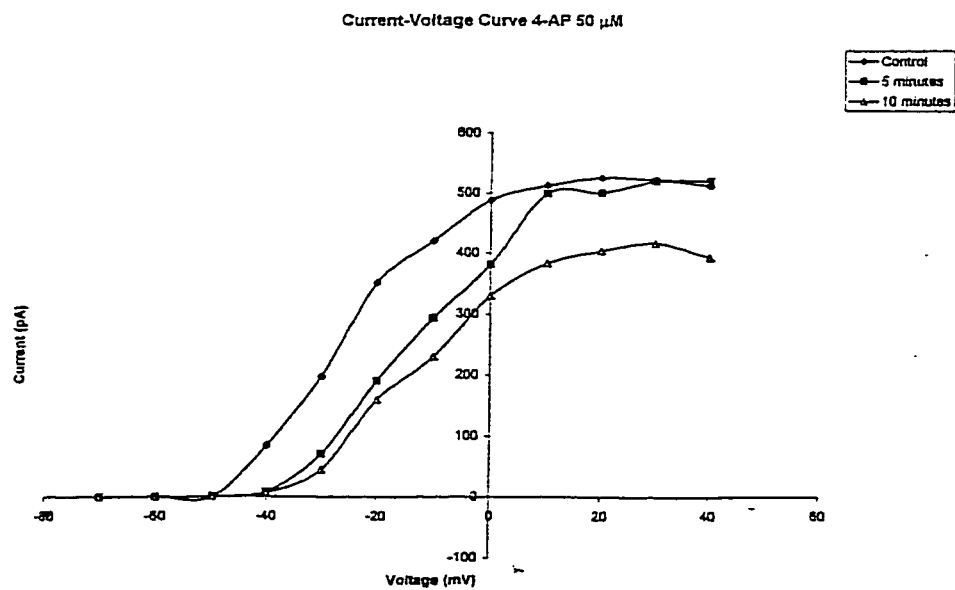


Figure III-8. Effect of 50  $\mu$ M 4-AP application on whole-cell  $K^+$  currents recorded in the presence of pipette EGTA, ATP, and  $Ca^{2+}$ . A representative original current trace from a single cell (A) showing the response to a series of voltage pulses before and 5 and 10 minutes after the application of 4-AP, and the corresponding I-V plot (B). Note the decrease in outward current at 10 minutes (significant,  $p < 0.05$ ) without washout.

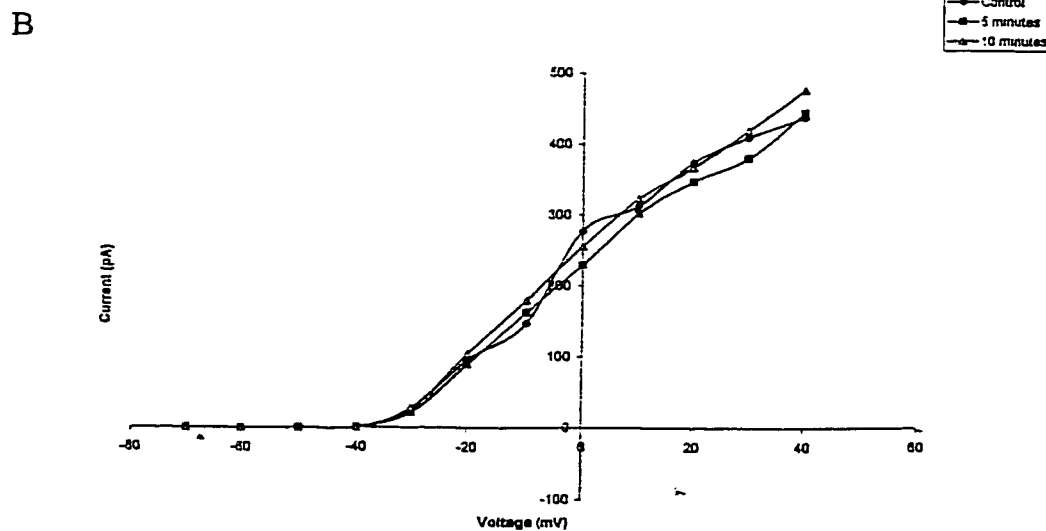
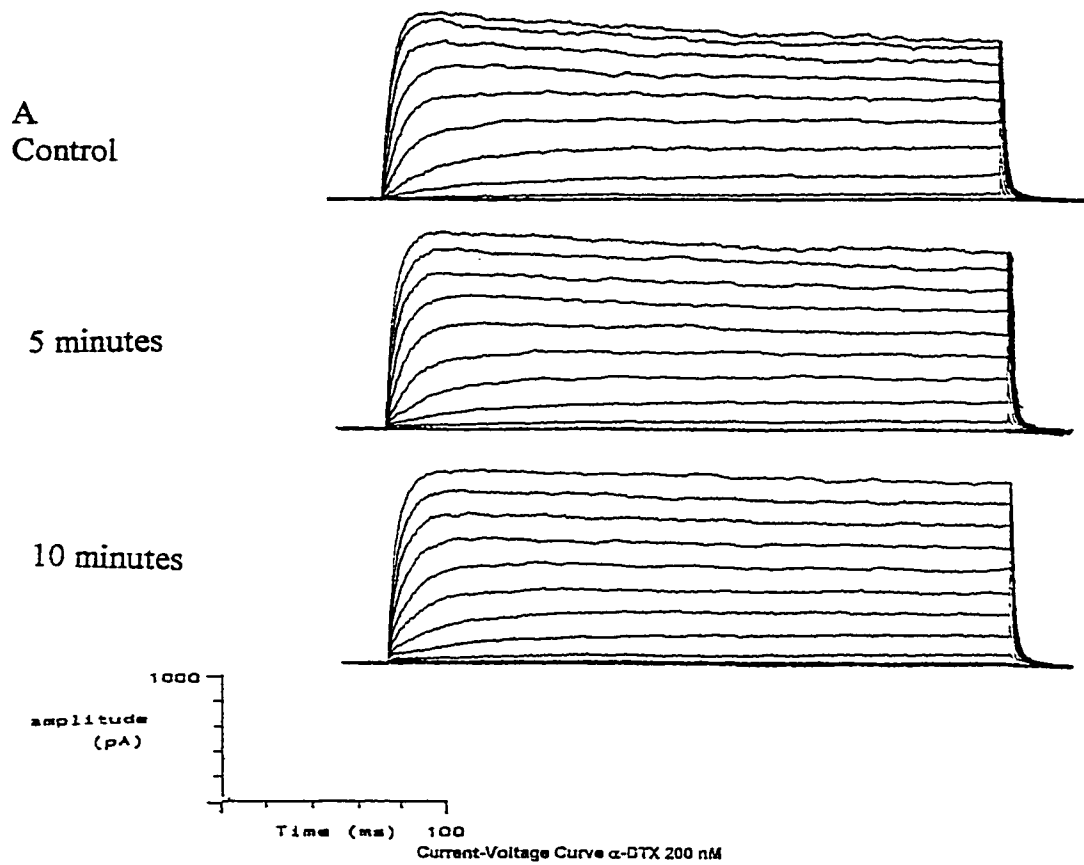


Figure III-9. Effect of 200 nM  $\alpha$ -DTX application on whole-cell  $K^+$  currents recorded in the presence of pipette EGTA, ATP, and  $Ca^{2+}$ . A representative original current trace from a single cell (A) showing the response to a series of voltage pulses before and 5 and 10 minutes after the application of  $\alpha$ -DTX, and the corresponding I-V plot (B). Note that there is no significant change after 5 or 10 minutes.



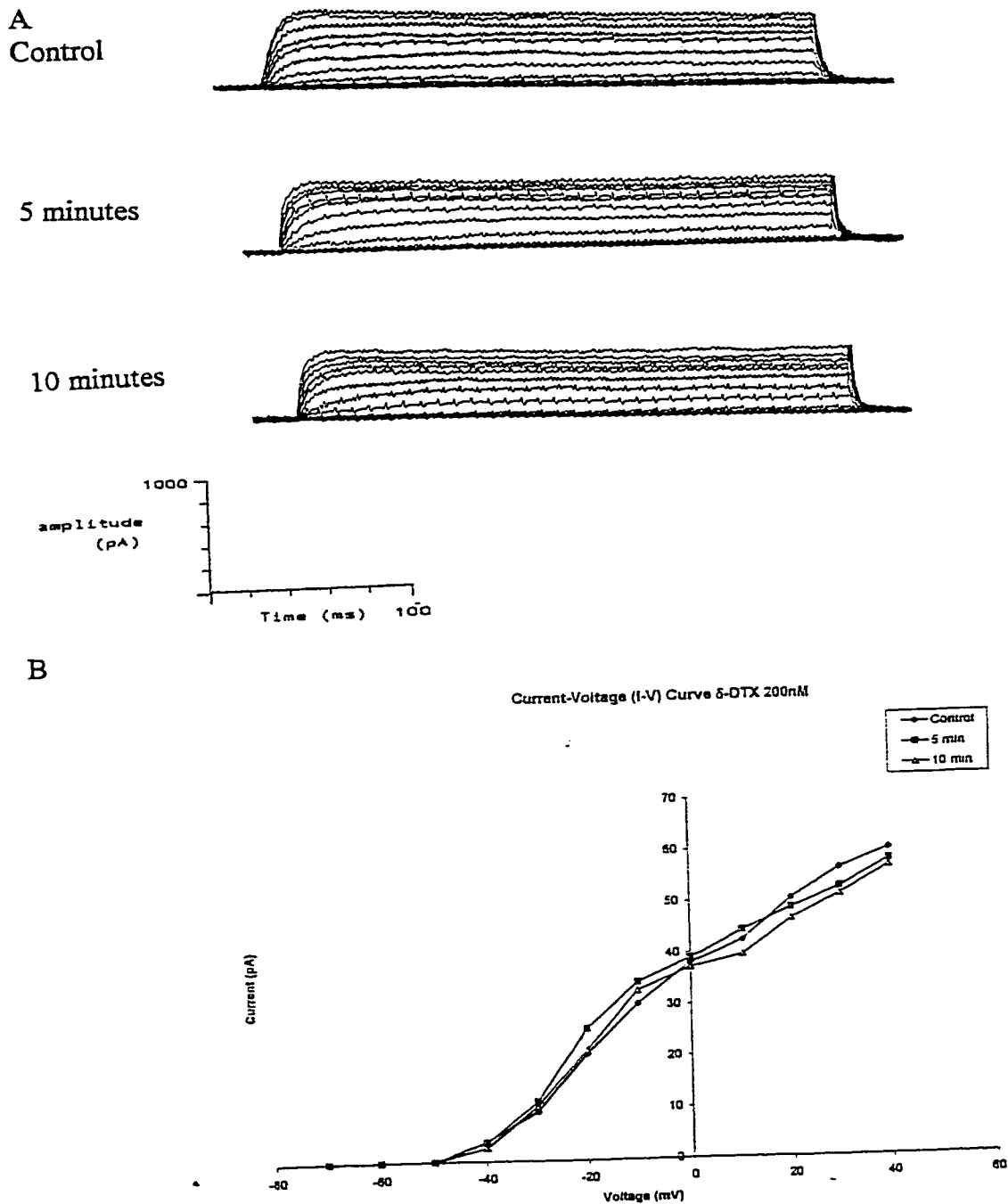


Figure III-10. Effect of 200 nM  $\delta$ -DTX application on whole-cell  $K^+$  currents recorded in the presence of pipette EGTA, ATP, and  $Ca^{2+}$ . A representative original current trace from a single cell (A) showing the response to a series of voltage pulses before and 5 and 10 minutes after the application of  $\delta$ -DTX, and the corresponding I-V plot. Note that there is no significant change after 5 or 10 minutes.

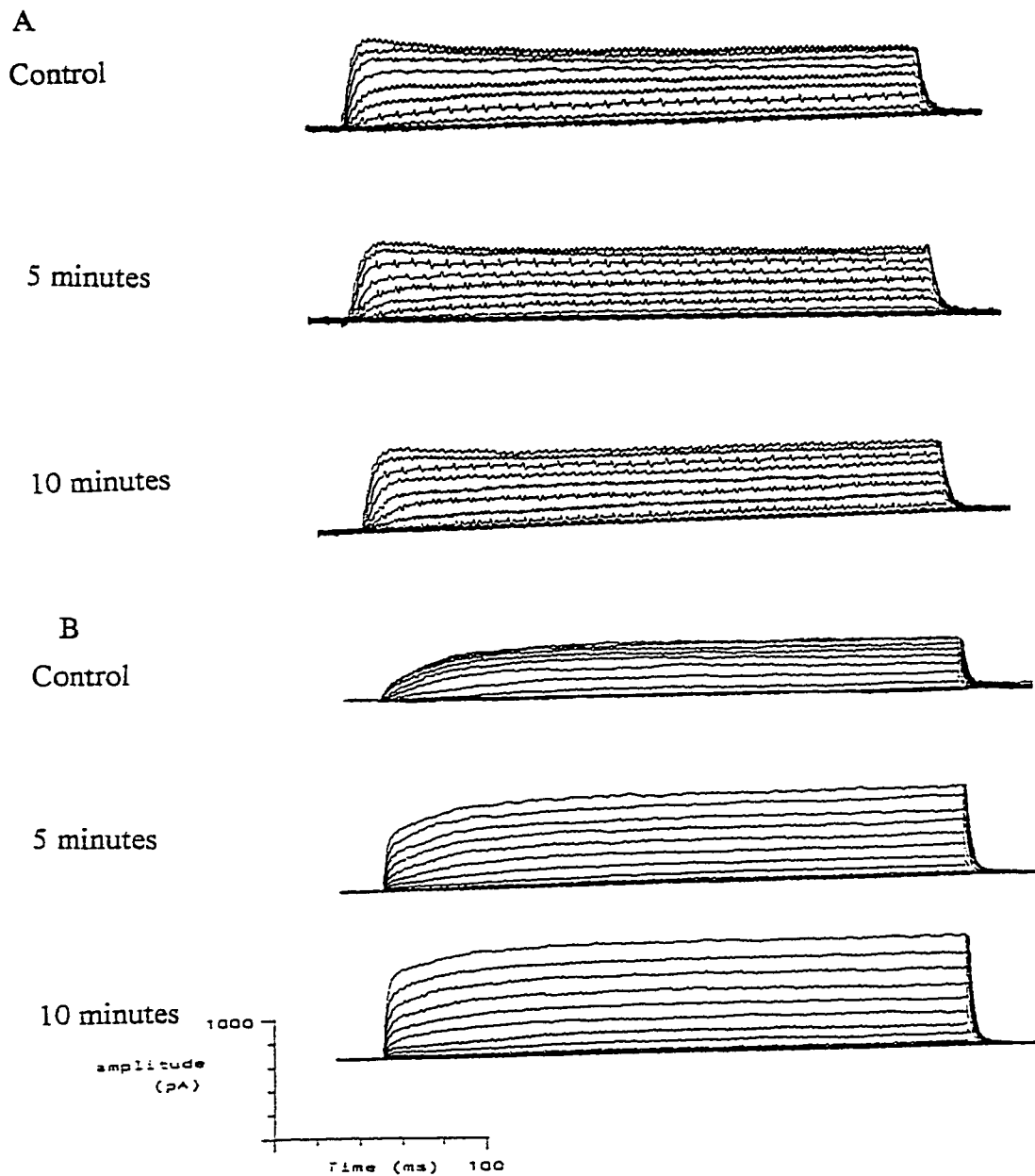
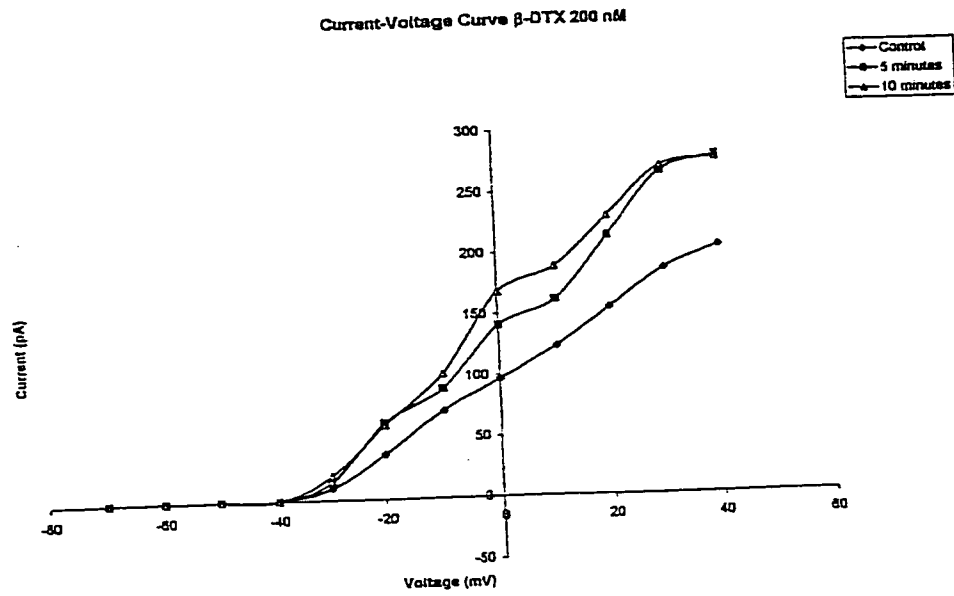


Figure III-11. Effect of 200 nM  $\beta$ -DTX application on whole-cell  $K^+$  currents recorded in the presence of pipette EGTA, ATP, and  $Ca^{2+}$ . A series of original single cell current traces showing the response to a series of voltage pulses before and 5 and 10 minutes after the application of  $\beta$ -DTX. Note that the response to  $\beta$ -DTX is dependent upon the presence of saturating outward currents, and the direction of the change in overall current recorded depends on whether current saturation is still present following application of  $\beta$ -DTX. In (A) a decrease in total current is seen, while in (B) an increase in total current is seen, following the application of  $\beta$ -DTX.

A



B

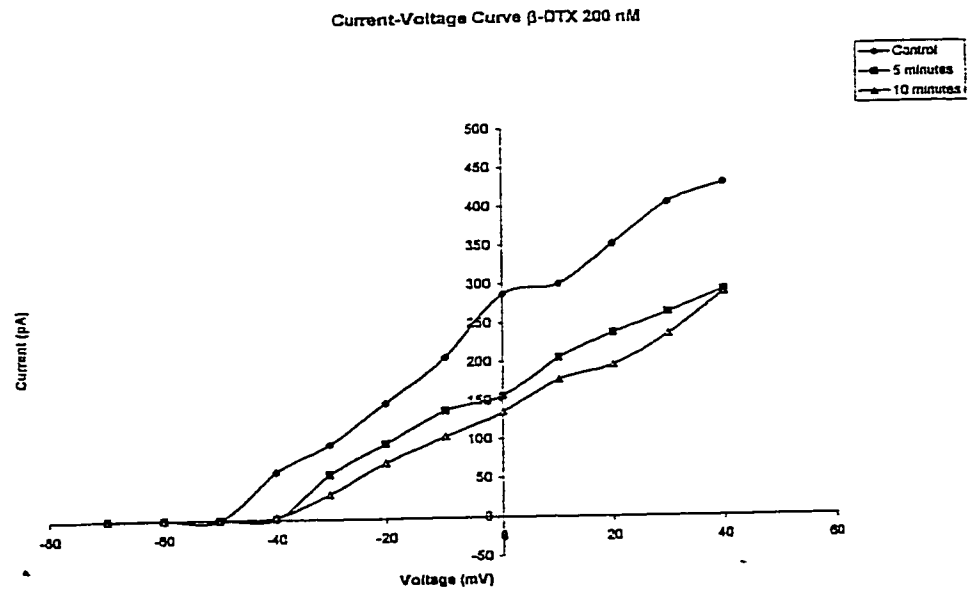


Figure III-12. The corresponding I-V plots are shown for the traces in Figure III-11 revealing the dual effect of  $\beta$ -DTX application. The I-V curve, illustrating the overall decrease in outward current, for the traces shown in Figure III-11A is shown in (A), and the curve, illustrating the increase in outward current, for Figure III-11B is shown in (B).

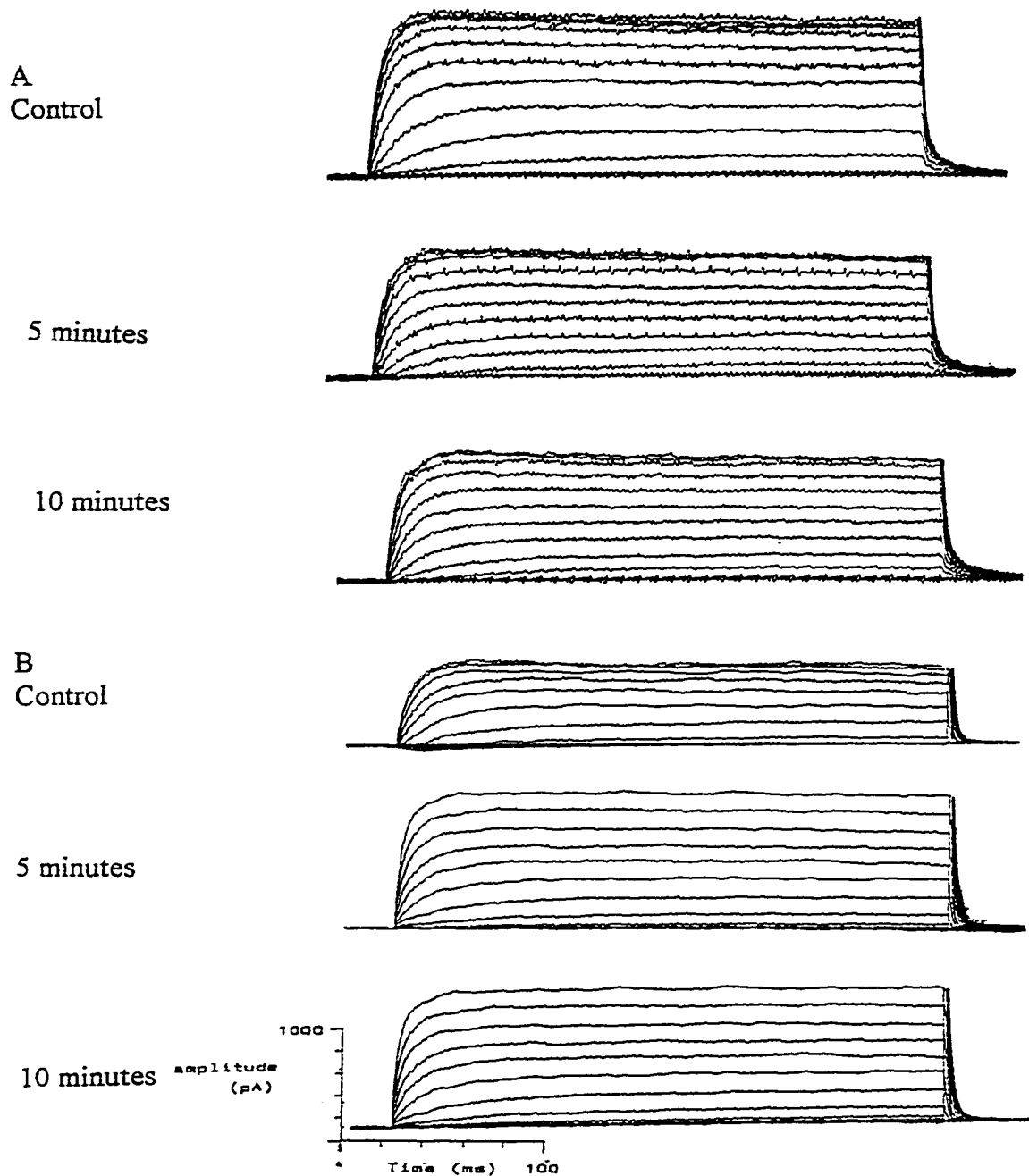
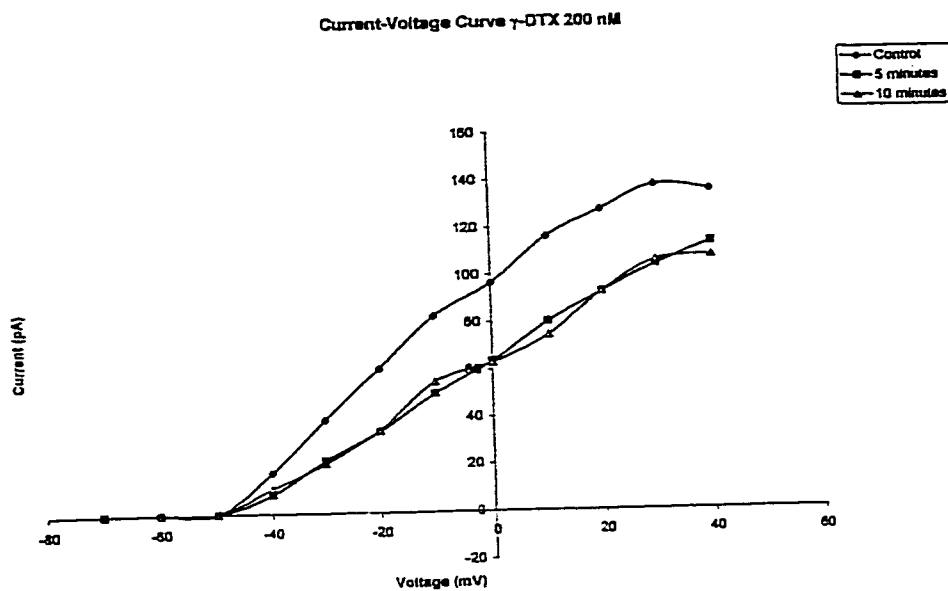


Figure III-13. Effect of 200 nM  $\gamma$ -DTX application on whole-cell  $K^+$  currents recorded in the presence of pipette EGTA, ATP, and  $Ca^{2+}$ . A series of original traces from single cell current recordings showing the response to a series of voltage pulses before, and 5 and 10 minutes after the application of  $\gamma$ -DTX. Note that the response to  $\gamma$ -DTX is dependent on the presence of saturating currents. In (A) application of  $\gamma$ -DTX did not remove saturation, and the overall effect was a decrease in total current, yet in (B) current saturation is not seen after the application of  $\gamma$ -DTX, and an overall increase in total current occurred. Overall, a significant change occurs 10 minutes after toxin application ( $p < 0.05$ ).

A



B

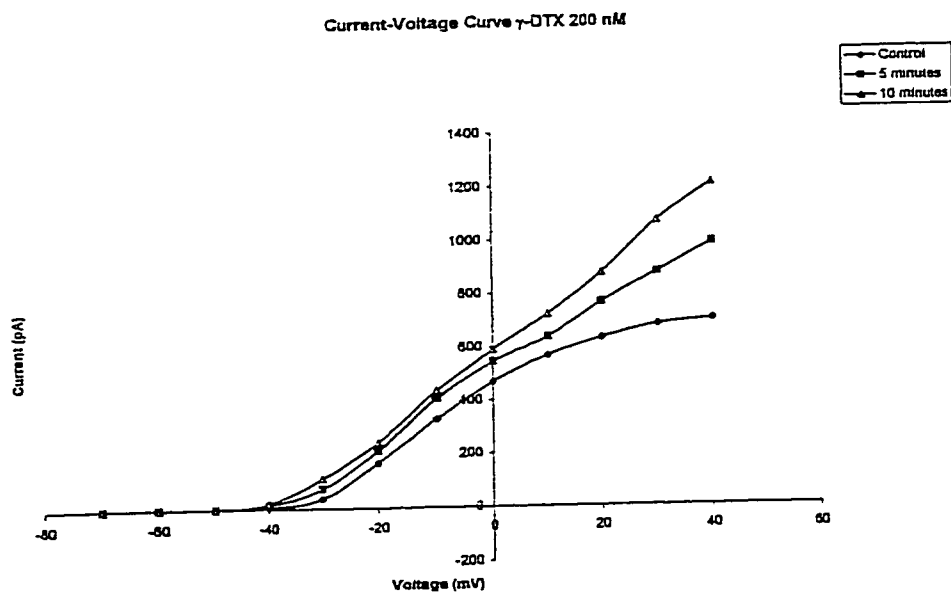
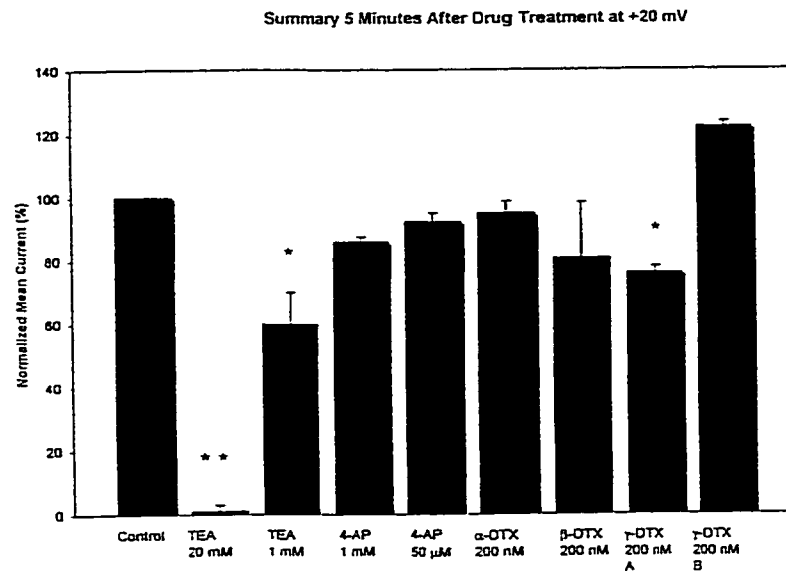


Figure III-14. The corresponding I-V plots are shown for the representative traces in Figure III-13 revealing the dual effect of  $\gamma$ -DTX. In (A) application of  $\gamma$ -DTX resulted in a decrease in total current, with continued current saturation, while in (B) application of  $\gamma$ -DTX resulted in an increase in total current, in the absence of current saturation; both were significant ( $p < 0.05$ ) at 10 minutes.

A



B

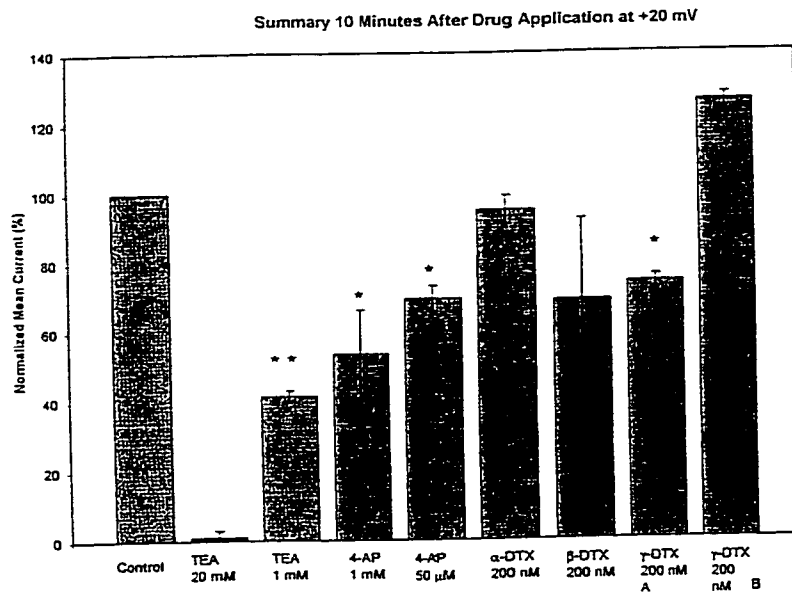
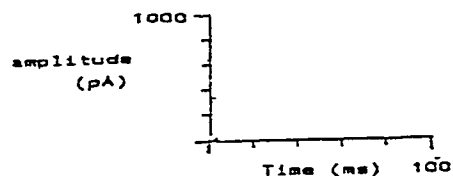


Figure III-15. Summary of the mean outward current, at +20 mV (within the range for maximal channel activation), (A) 5 minutes, and (B) 10 minutes after drug application in the presence of pipette EGTA, ATP, and  $Ca^{2+}$ . All values are presented as a % of control (defined as 100% to standardize data), and represent the mean of 2 to 5 cells (as noted in the text). For  $\gamma$ -DTX, increases in outward current (seen with non-saturating currents after toxin application; denoted (B) in the chart, given as a range since  $n = 2$ ) are separated from measured decreases (seen with saturating currents after toxin application; denoted (A) in the chart). All statistically significant results are indicated (\* denotes  $p < 0.05$ ; \*\* denotes  $p < 0.01$ ).

A



B

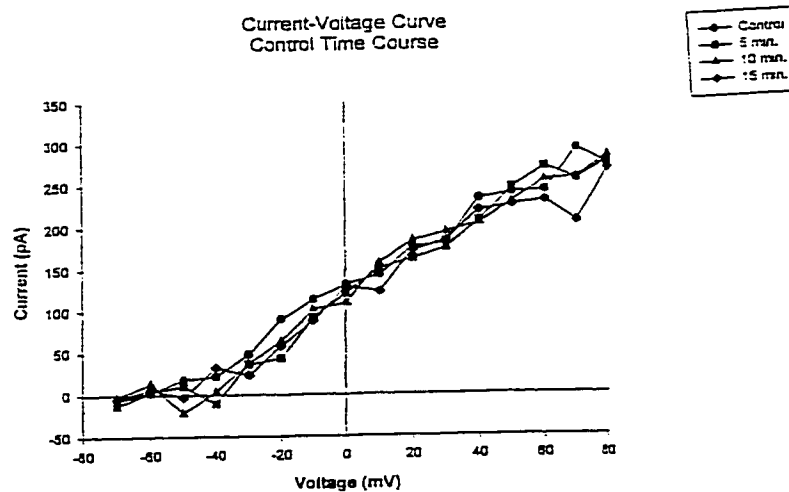


Figure III-16. Voltage protocols given, and the resultant  $K^+$  currents recorded in the presence of pipette EGTA, and absence of  $Ca^{2+}$  and ATP. A representative original current trace (A) from a single cell in response to a series of voltage pulses from a holding potential of  $-80$  mV to  $+80$  mV. Under these conditions the currents recorded are expected to represent purely voltage-gated  $K^+$  channels. Note the absence of saturating currents at positive potentials. A corresponding I-V plot is given, in the form of a time-course (B), showing no change in outward current over the course of 15 minutes.

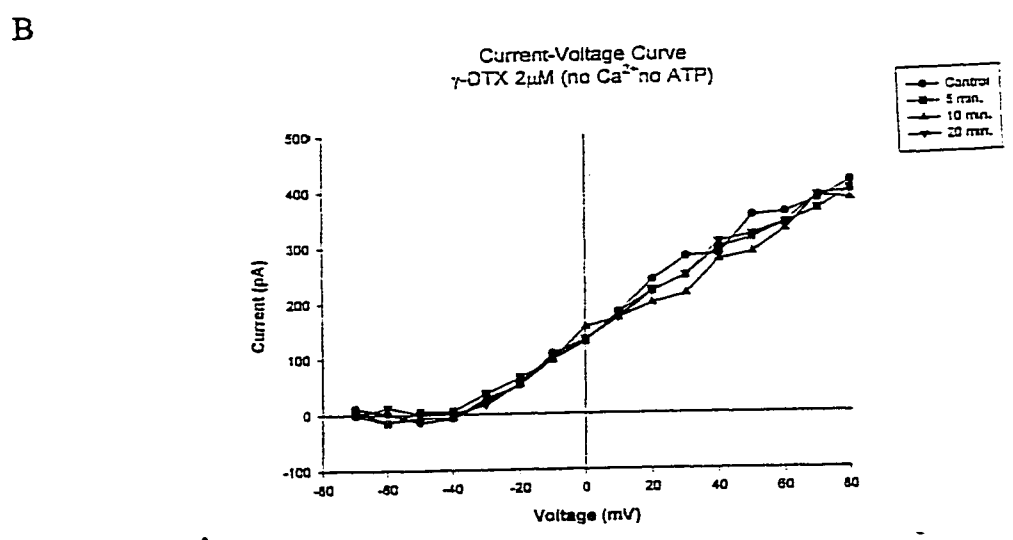
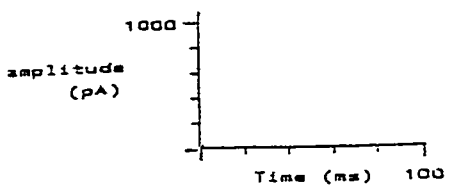
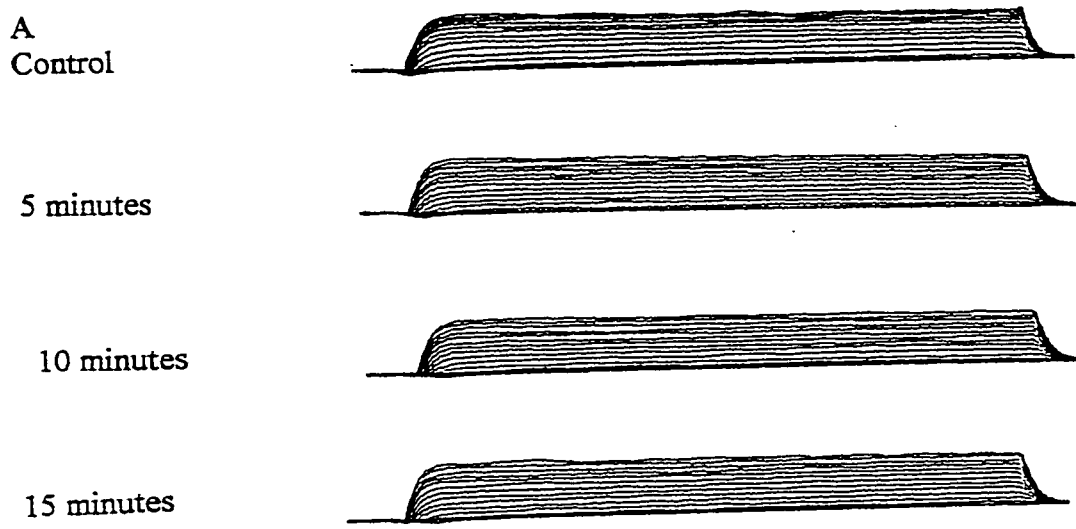


Figure III-17. Effect of  $2\mu\text{M}$   $\gamma$ -DTX application on whole-cell  $\text{K}^+$  currents recorded in the presence of pipette EGTA, and absence of ATP and  $\text{Ca}^{2+}$ . A series of representative original current traces (A) from a single cell, showing the response to a series of voltage pulses before, 5, 10, and 15 minutes after the application of  $\gamma$ -DTX, and the corresponding I-V plot (B). Note the lack of a significant change in outward current even after 15 minutes, and the absence of current run-down.



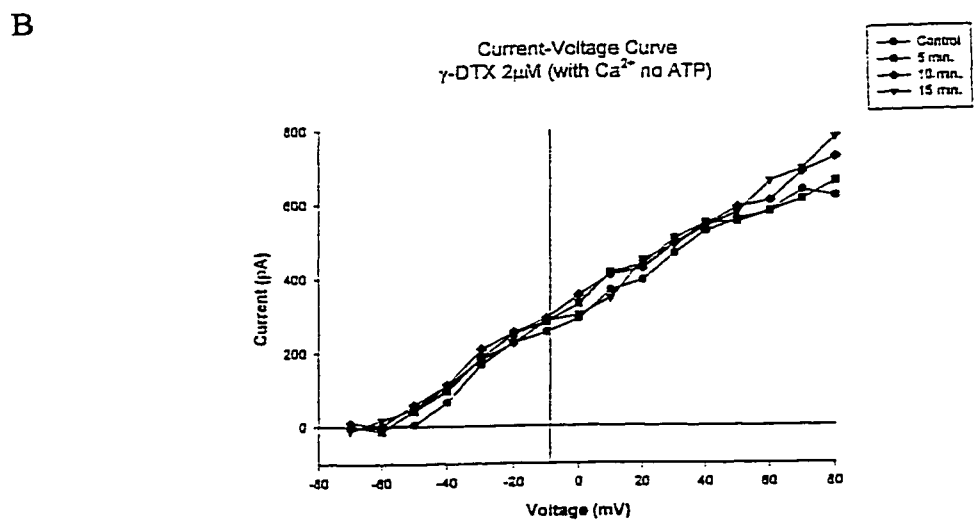
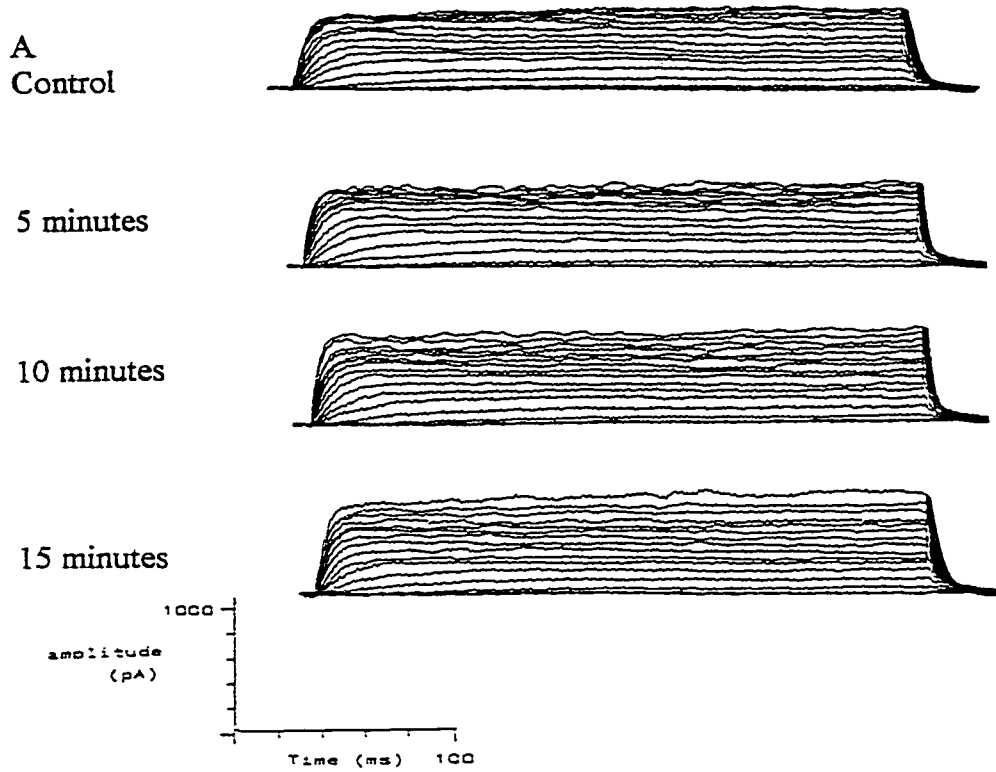


Figure III-18. Effect of  $2\ \mu\text{M}$   $\gamma$ -DTX application on whole-cell  $\text{K}^+$  currents recorded in the presence of pipette  $\text{Ca}^{2+}$  and EGTA, and absence of ATP. A series of representative original traces from a single cell (A) showing the response to a series of voltage pulses before and 5, 10, and 15 minutes after the application of  $2\ \mu\text{M}$   $\gamma$ -DTX, and the corresponding I-V plot (B). Note the lack of a significant change in the outward current even after 15 minutes, and the absence of current run-down.

## Chapter IV

### Single Channel Results

#### 4.1 Introduction

While  $\text{Ca}^{2+}$ -activated  $\text{K}^+$  channels have been studied in DMSO-differentiated cells, they have not been characterized in undifferentiated N1E 115 cells. In DMSO-differentiated cells large and small conductance  $\text{Ca}^{2+}$ -activated  $\text{K}^+$  channels have been identified, and have been shown to have a similar kinetics, pharmacology, and  $\text{Ca}^{2+}$  activation profiles to those found in other cells (Leinders and Vijverberg, 1992; Diserbo, Antonny and Verdeti, 1994; see Section I-1.4 for discussion). Distributions of  $\text{Ca}^{2+}$ -activated  $\text{K}^+$  channels in differentiated and undifferentiated cells are variable and dependent on several factors, including cell cycle, hormonal stimulation and second messenger modulation (Haylett and Jenkinson, 1990; Hinrichsen, 1993).

#### 4.2 Experimental Design

##### 4.2.1 Characterization of Single Channels

Outside-out patches of undifferentiated N1E 115 cells were obtained by removing the pipette from the cell, following the establishment of a high  $\text{G}\Omega$  seal, and a whole-cell recording mode. Only undifferentiated cells were used in single channel experiments since DMSO-treatment rendered cell membranes too unstable for outside-out patches.

The pipette and bath solutions were designed to study  $\text{Ca}^{2+}$ -activated  $\text{K}^+$  channels— pipette free  $[\text{Ca}^{2+}]$  was adjusted to be within the 1  $\mu\text{M}$  range suggested by Diserbo (in this study pipette free calcium ranged from 500 nM to 5  $\mu\text{M}$ ), Antony and Verdeti (1994) to be optimal for BK(Ca) activity in differentiated N1E 115 cells, and the  $[\text{Ca}^{2+}]$  in the bath solution was higher than that used in whole-cell recordings (from 2 to 4 mM; see text for discussion). Two types of recording mode were used: patches were either pulsed from a holding potential of  $-80$  mV to potentials of  $-20$ , 0,  $+20$ , or  $+40$  mV, or were held at  $-20$ , 0,  $+20$ , or  $+40$  mV throughout the recording period. Using both types of recording enabled the characterization of  $\text{Ca}^{2+}$ -activated  $\text{K}^+$  channels with and without voltage-gated  $\text{Ca}^{2+}$  channel contribution, respectively.

#### **4.2.2 Pharmacology of the Single Channels**

Various  $\text{Ca}^{2+}$ -activated  $\text{K}^+$  channel blockers were used to determine the nature of the channels studied. The  $\text{Ca}^{2+}$  channel blocker nifedipine (10  $\mu\text{M}$ ) was used on the pulsed patches, and the ionophore ionomycin (at 1 nM, or 10 nM) was used on both pulsed patches, and patches held at various voltages to determine the  $\text{Ca}^{2+}$  dependence of the channels studied. The scorpion toxin iberiotoxin (IbTX; a specific BK(Ca) blocker; 1  $\mu\text{M}$ ) the bee venom toxin apamin (a specific SK(Ca) blocker; 100 nM), the non-specific  $\text{K}^+$  channel blocker TEA (1 mM), and the  $\text{Cl}^-$  channel blocker SITS (1 mM) were used to characterise the  $\text{Ca}^{2+}$ -activated  $\text{K}^+$  channels in the patch. Traces recorded at a holding potential of  $+20$  mV were used to compare open probability before (control) and after drug application. Recordings prior to the application of drugs were used as control; each patch acted as its own control.

### 4.2.3 Effect of $\gamma$ -DTX on Single Channels

Based on the whole-cell results, several concentrations of  $\gamma$ -DTX (200 nM, 20 nM, and 2 nM) were used to determine the effect of this toxin on  $\text{Ca}^{2+}$ -activated  $\text{K}^+$  channels in the patch. While the whole-cell results for  $\beta$ -DTX were far more variable,  $\beta$ -DTX (200 nM) was also used for comparison. Finally,  $\alpha$ -DTX (200 nM), which had no effect in whole-cell recordings, was used as a control. Traces recorded at a holding potential of +20 mV were used to compare open probabilities before (control) and after drug application. Recordings prior to the application of drugs were used as control; each patch acted as its own control.

## 4.3 Results

### 4.3.1 Characterization of Single Channels

Two  $\text{Ca}^{2+}$ -activated  $\text{K}^+$  channels were found in N1E 115 cell outside-out patches (see Figure IV-1), with widely different conductance, kinetic and pharmacological profiles. Channel conductances, measured under asymmetrical  $\text{K}^+$  gradient (high pipette  $\text{K}^+$ , and low bath  $\text{K}^+$ , see Section 2.3.2), were 187 pS, and 63 pS, and are in the range for BK(Ca) and IK(Ca) channels (Hinrichsen, 1993), respectively, in both types of patch protocol (see Figure IV-2). Generally, the 63 pS channels were found in more of the patches (70%) than the BK(Ca) channels, and were far more common than the 187 pS channels in patches held at positive potentials. In the patches studied, the 63 pS channels exhibited bursting open patterns, characterized by periods of frequent opening, followed by long periods of silence (see Figure IV-3). The 63 pS channel was weakly voltage sensitive within a narrow range (0 mV to 20 mV), increased voltage consistently resulted

in a decreased open probability (see Figure IV-4). IK(Ca) subtypes in several cell systems, including erythrocytes, lymphocytes and macrophages, have been reported to be weakly voltage-dependent, or even voltage-insensitive (Haylett and Jenkinson, 1990; Hinrichsen, 1993). The 187 pS channel generally exhibited an increase in the probability of opening as the voltage increased, but was characterized by shifts in open probability, so that recordings on the same day, under the same conditions, varied widely (see Figure IV-5). Within a single recording the 187 pS channel cycled through phases of high opening probability, followed by virtually no openings (see Figure IV-6). This pattern of BK(Ca) channel activity has been characterized by other researchers (Bowlby and Levitan, 1996; Silberberg et al., 1996) and termed “wanderlust kinetics” (Silberberg et al., 1996). In some patches held at positive potentials 187 pS channel activity was lost within the course of control recordings; these patches were not used in this study, but inactivating BK(Ca) subtypes have been reported by others (Reinhart, Chung and Levitan, 1989; Solaro et al., 1995; Bowlby and Levitan, 1996).

#### **4.3.2 Pharmacology of the Single Channels**

In patches pulsed from a holding potential of  $-80$  mV to various potentials ( $-20$ ,  $0$ ,  $20$ , and  $40$  mV) both channels were sensitive to the  $\text{Ca}^{2+}$  channel blocker nifedipine ( $10$   $\mu\text{M}$ ). The 187 pS channel was comparatively more sensitive to  $\text{Ca}^{2+}$  channel blockade by nifedipine since channel open probability dropped dramatically by  $89.2 \pm 5.6\%$  after 5 minutes, and  $93.1 \pm 3.2\%$  after 10 minutes ( $n=3$ ; significantly different from control,  $p < 0.01$ ; see Figure IV-7). In comparison, the 63 pS channel open probability decreased by  $75 \pm 3.2\%$  after 5 minutes and  $81 \pm 2.6\%$  after 10 minutes ( $n=3$ ;

significantly different from control,  $p < 0.01$ ; see Figure IV-8) in response to nifedipine application. IK(Ca) channels are reported to be more sensitive to intracellular  $[Ca^{2+}]$  than BK(Ca) channels (Hinrichsen, 1993), thus, differences in the response of these two channels to nifedipine could be explained by the 63 pS channel being more sensitive to lower concentrations of  $Ca^{2+}$ . Although channel activity was significantly greater in the pulsed patches (channel openings were rarely seen in patches held at positive potentials, even with a doubling of the extracellular  $[Ca^{2+}]$  to 4 mM), application of ionomycin (1 nM, or 10 nM) was effective in returning the activity of both channels to the level seen in pulsed patches (see Figure IV-9 and IV-10). The response to nifedipine and to ionomycin indicated that patches held at positive potentials during recording required a higher free  $Ca^{2+}$  concentration in the recording pipette to generate IK(Ca) and BK(Ca) channel activity, reflecting a loss of voltage-gated  $Ca^{2+}$  channel activity as the patches are held at positive potentials (especially since increasing extracellular  $[Ca^{2+}]$  did not result in a subsequent increase in channel activity), rather than pulsed from a holding potential of  $-80$  mV. Patches held at positive potentials were preferentially used to compare the effect of applied drugs since large baseline fluctuations in pulsed patches made data analysis more difficult.

The  $Cl^-$  channel blocker SITS (1 mM,  $n = 4$  for each channel) had no effect on the activity of either channel in outside-out patches held at positive potentials (i.e. no change in open probability compared to control, see Figure IV-11), revealing that these are not large conductance  $Ca^{2+}$ -sensitive  $Cl^-$  channels. The 63 pS channel open probability did not change in response to application of the SK(Ca) channel blocker apamin (100 nM,  $n = 3$ ) in pulsed patches (see Figure IV-12), confirming that this channel is an IK(Ca)

channel, which is not known to be sensitive to apamin (Haylett and Jenkinson, 1990; Hinrichsen, 1993). The non-specific  $K^+$  channel blocker TEA (1 mM) had no effect on opening probability of the 63 pS channel ( $n = 3$ ; see Figure IV-13), which is consistent with known profiles of some IK(Ca) subtypes (Haylett and Jenkinson, 1990; Hinrichsen, 1993). An IK(Ca) channel subtype in *Aplysia* neurons was reported to have an apparent  $K_D$  for TEA of at least 100 mM (Hermann and Erxleben, 1987). However, application 1 mM TEA resulted in a decrease in 187 pS channel open probability of  $73.1 \pm 4.5\%$  after 5 minutes and  $89.1 \pm 3.4\%$  after 10 minutes ( $n=4$ ; significantly different from control,  $p < 0.01$ ; see Figure IV-14). BK(Ca) channels have been reported to be sensitive to external application of TEA in the  $\mu\text{M}$  range (MacKinnon and Miller, 1988; Reinhart, Chung and Levitan, 1989; Hinrichsen, 1993). Similarly the specific BK(Ca) channel blocker IBTX (1  $\mu\text{M}$ ) had no effect on the 63 pS channel ( $n = 4$ ; see Figure IV-15), but did block the 187 pS channel in patches held at positive potentials—187 pS channel opening probability decreased by  $86.2 \pm 6.4\%$  at 5 minutes and  $92.6 \pm 4.5\%$  after 10 minutes ( $n = 4$ ; significantly different from control,  $p < 0.01$ ; see Figure IV-16). IbTX has not been reported to block IK(Ca) channels, but is known to be a specific and potent blocker of BK(Ca) channels (Hinrichsen, 1993).

#### 4.3.3 Effect of $\gamma$ -DTX on Single Channels

Based on the whole-cell data, it was predicted that not all of the DTXs would have an effect on the  $\text{Ca}^{2+}$ -activated  $K^+$  channels in these cells. Neither the 63 pS channel, nor the 187 pS channel was sensitive to the application of 200 nM  $\alpha$ -DTX ( $n = 4$ ), as would be predicted on the basis of the whole-cell data (see Figure IV-17, and IV-

18, respectively). Neither 200 nM  $\beta$ -DTX (n = 5), nor 200 nM  $\gamma$ -DTX (n = 6) had any effect on the 63 pS channel in either patch protocol (see Figures IV-19, and IV-20, respectively). In contrast, the 187 pS channel responded to both  $\beta$ - and  $\gamma$ -DTX, though to varying degrees.

Response of the 187 pS channel to the application of 200 nM  $\beta$ -DTX was as variable in the outside-out patch recordings as it was in the whole-cell recordings: in some patches  $\beta$ -DTX application decreased open probability of the 187 pS channel, while in others it had no effect (n = 5; see Figure IV-21). It is interesting to note that in most (4 out of 6) patches application of  $\beta$ -DTX resulted in increased 187 pS channel opening after 5 minutes, which reversed within 10 minutes (see Figure IV-21). Overall, the effect of  $\beta$ -DTX was not statistically significant given the degree of variability.

Unlike  $\beta$ -DTX, application of  $\gamma$ -DTX consistently altered the open probability of the 187 pS channel at concentrations of 200 nM, 20 nM, and 2 nM. There was, however, a sharp decrease in the onset of block over the 10- to 100-fold decrease in toxin concentration. At 200 nM,  $\gamma$ -DTX completely blocked 187 pS channel activity within 2 to 3 minutes (n = 8; see Figure IV-22, and IV-25). In contrast, application of 20 nM  $\gamma$ -DTX resulted in a slower onset of block, so that the 187 pS channel opening was decreased by  $72.2 \pm 6.7\%$  after 5 minutes, and was completely blocked within 10 minutes (n = 5; see Figure IV-23, and IV-25). Application of 2 nM  $\gamma$ -DTX did not significantly alter 187 pS channel opening after 5 minutes, but did decrease channel opening by  $43.3 \pm 5.2\%$  after 10 minutes (n = 3; see Figure IV-24, and IV-26). In all cases, application of  $\gamma$ -DTX did not alter conductance of the 187 pS channel.



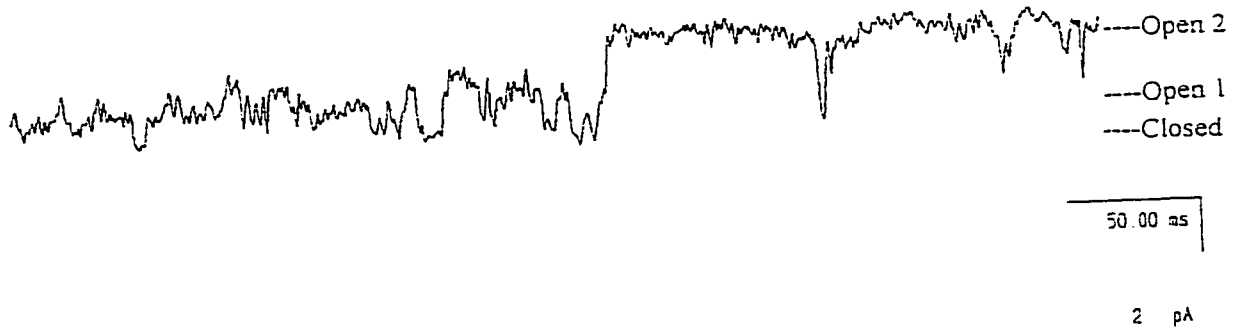
Interestingly,  $\gamma$ -DTX block, at all concentrations tested, was found to be voltage-dependent since patches held at 0 mV, 20 mV, and 40 mV exhibited significantly decreased channel opening, but in patches held at -20 mV, channel opening was not decreased from control recordings even 10 minutes after toxin application (see Figure IV-23, IV-25, and IV-26). Also, of interest was the observation that, like  $\beta$ -DTX,  $\gamma$ -DTX was found, at the lower concentrations of 20 nM and 2 nM in most patches, to transiently increase open probability before the onset of block. As toxin concentration decreased this transient increase in open probability was delayed, so that an increase in open probability was seen within 3 to 4 minutes following application of 20 nM  $\gamma$ -DTX, and was delayed to 6 to 8 minutes following the application of 2 nM  $\gamma$ -DTX.

These results are novel since there have been no other reports that external application of any member of the DTX family would block  $\text{Ca}^{2+}$ -activated  $\text{K}^+$  channels (Hinrichsen, 1993). In fact, in several cell systems application of DTX has been found to have no effect on the  $\text{Ca}^{2+}$ -activated  $\text{K}^+$  channels, and BK(Ca) channels in particular (Tauc, Gasteineau, and Poujeol, 1993). It is of interest to note, however, that intracellular application of DTX-I has been found to increase subconductance events in BK(Ca) channels (Lucchesi, and Moczydlowski, 1991; Moss and Moczydlowski, 1996).

A

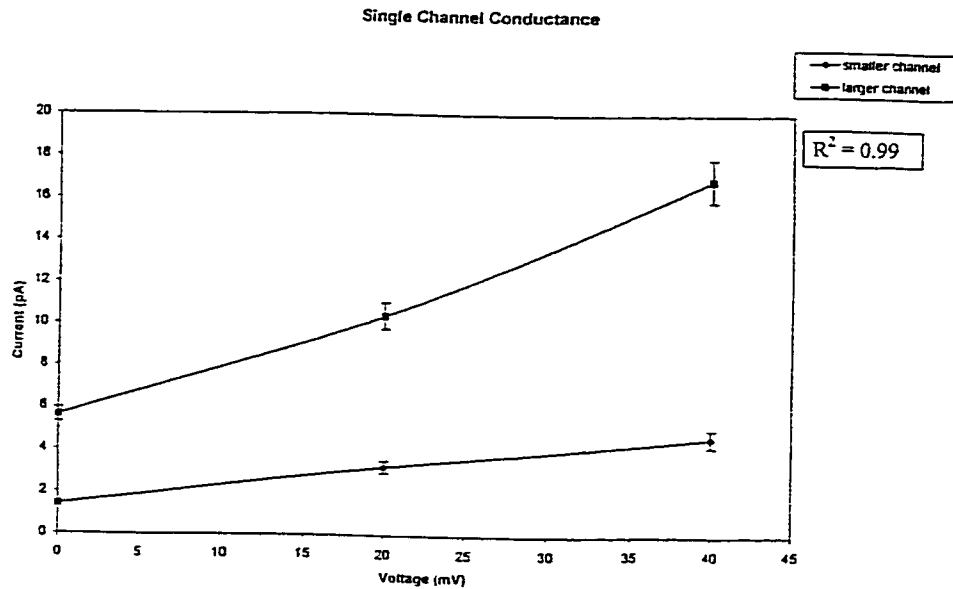


B

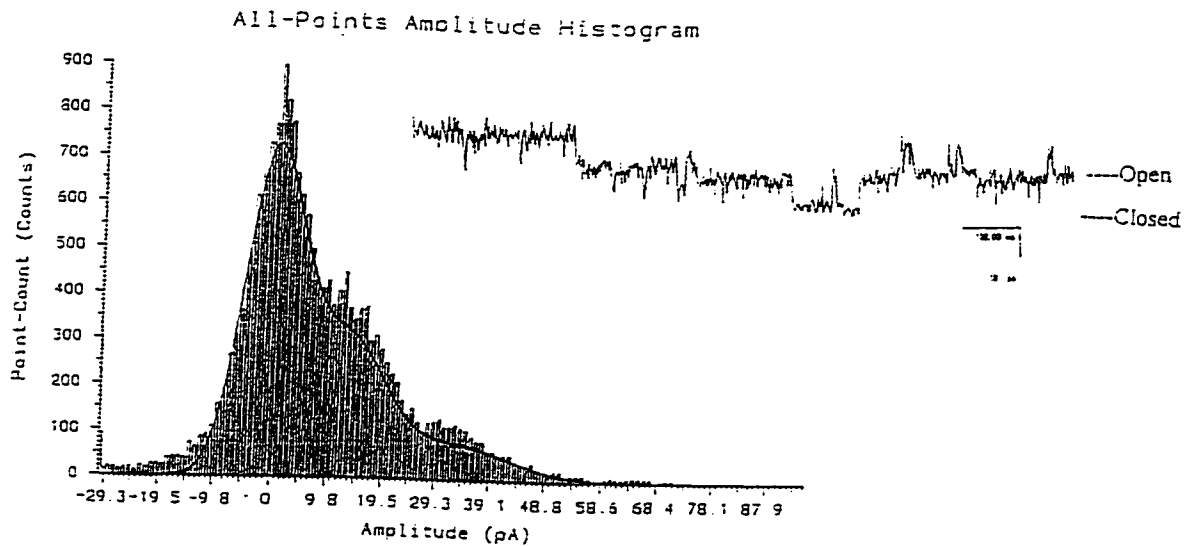


IV-1. Outside-out patches from undifferentiated N1E 115 cells exhibited 2 channel types active in the patch under the conditions used. See section 2.3 for details. Traces are from 2 different representative patches. In patches pulsed from  $-80$  mV to  $0$  mV (shown in (A)) and in patches held at  $0$  mV (shown in (B)) a larger and much smaller channel are seen to open. Patches were far more likely to exhibit  $63$  pS channel activity. Open 1 marks the open level of the  $63$  pS channel and open 2 marks the open level of the  $187$  pS channel, while both channels are closed at the baseline. Open and closed states are noted on all subsequent traces.

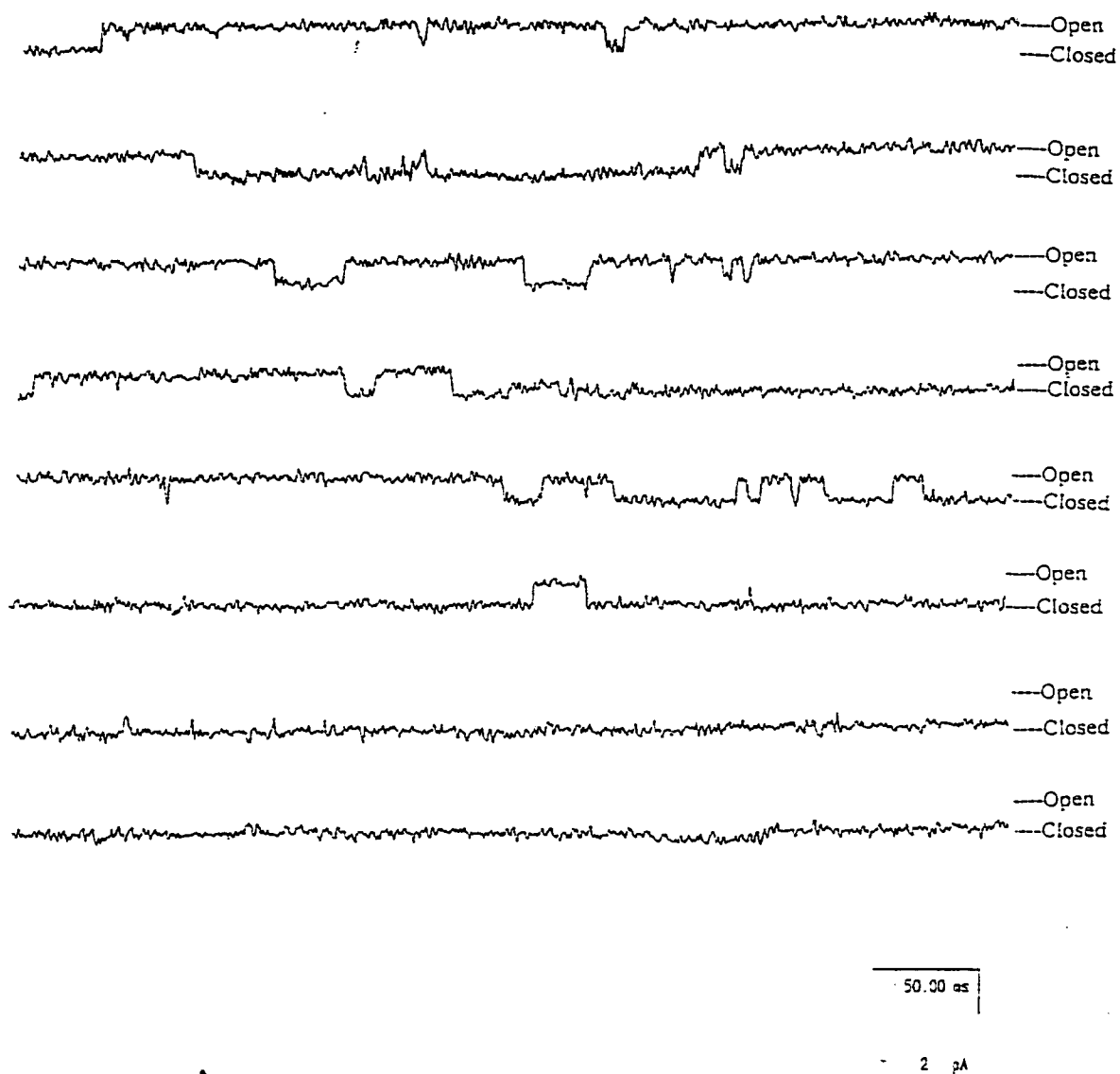
A



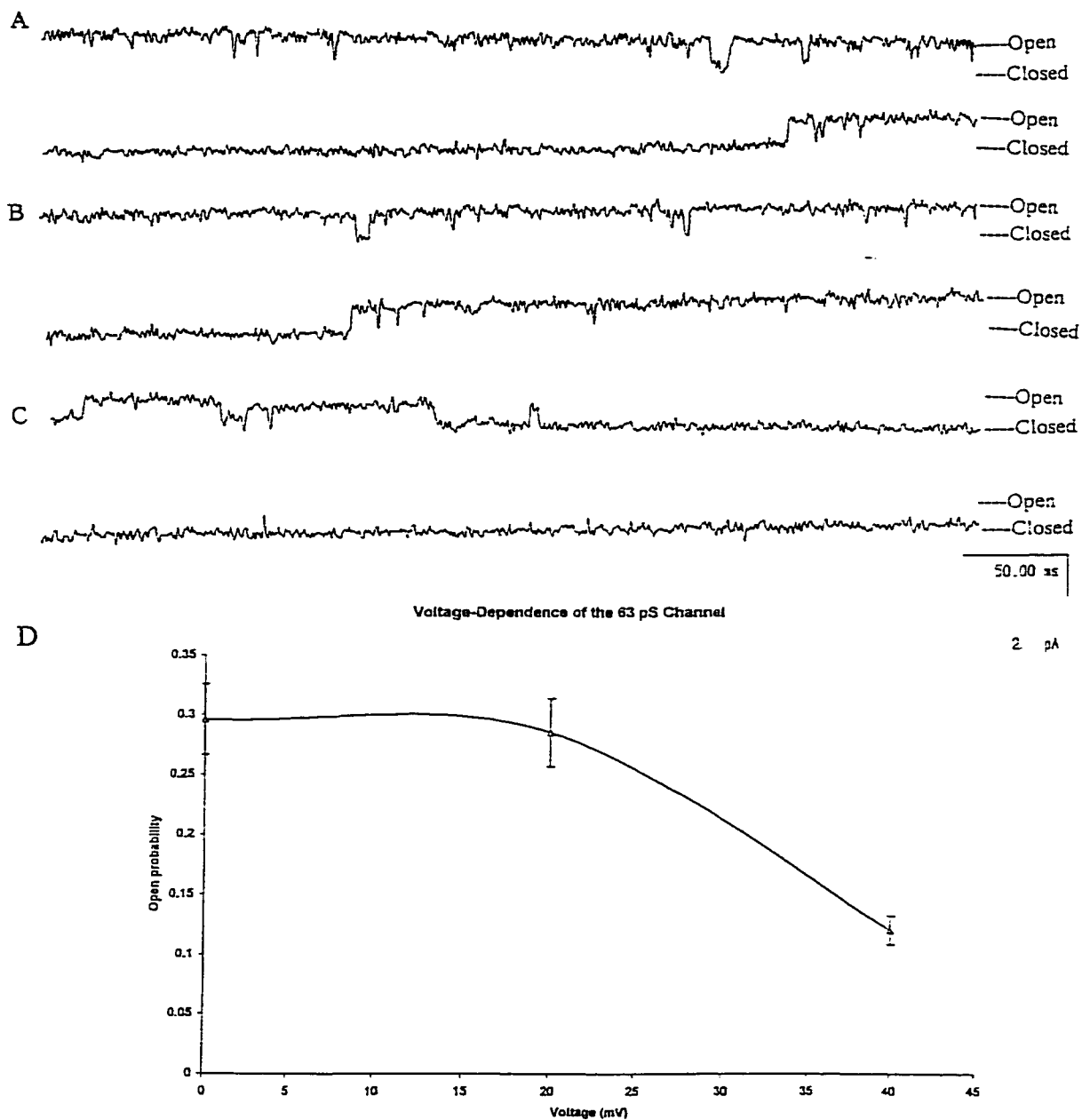
B



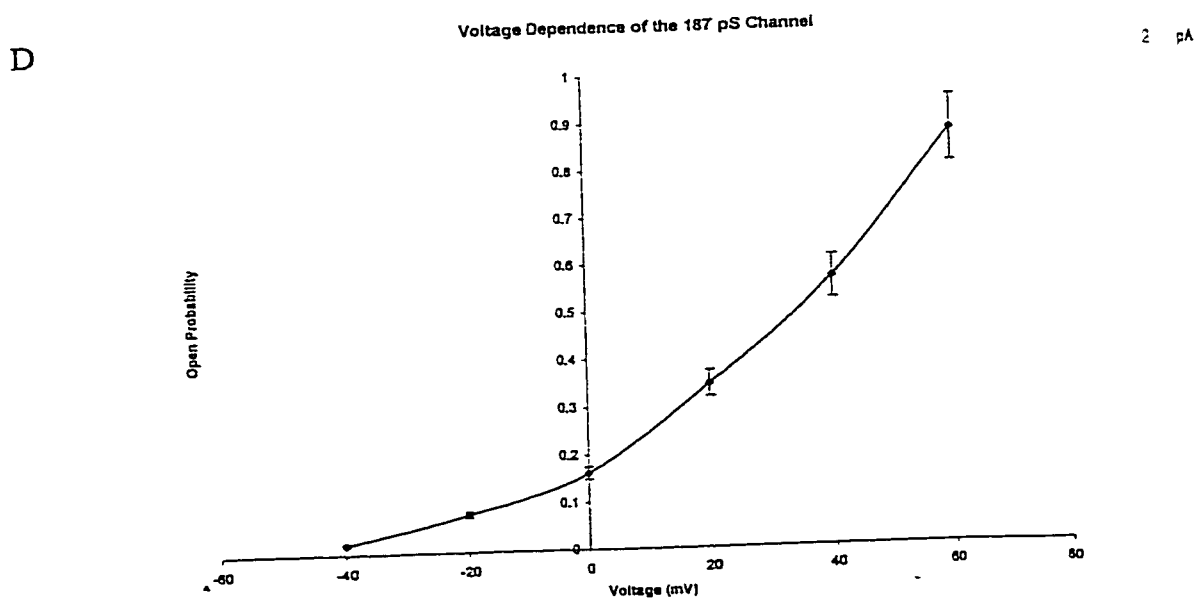
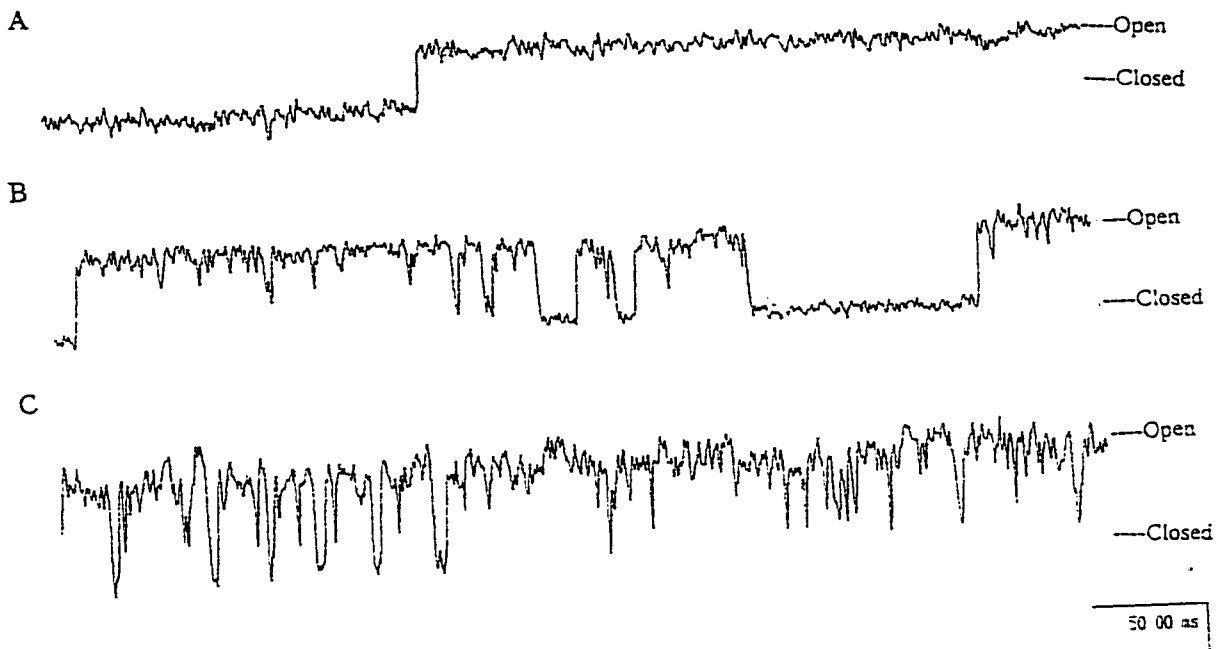
IV-2. Determination of single channel conductance based on linear regression of a current-voltage plot, and an all-points histogram from a recording of the larger channel are shown. In (A) a graph of the amplitude of channel current versus voltage is fitted by linear regression to give the conductance of each channel. The regression line is described by  $y = mx + b$ , with  $y$  = current measured,  $x$  = voltage pulse,  $m$  = conductance,  $b$  = intercept, for the larger channel,  $m = 0.187$ , and  $b = 2.67$ , for a conductance of 187 pS, and the smaller channel,  $m = 0.063$ , and  $b = 1.56$ , for a conductance of 63 pS. Channel current was measured in outside-out patches under asymmetrical  $[K^+]$ , and an average of samples taken from both pulsed and holding patch protocols was used ( $n = 10$ ). In (B) a representative all-points histogram from an original channel recording of the 187 pS channel in which an outside-out patch was pulsed from  $-80$  mV to 20 mV (see inset; channel open and closed states are marked) is shown. The histogram shows that channel openings are significantly different from the baseline.



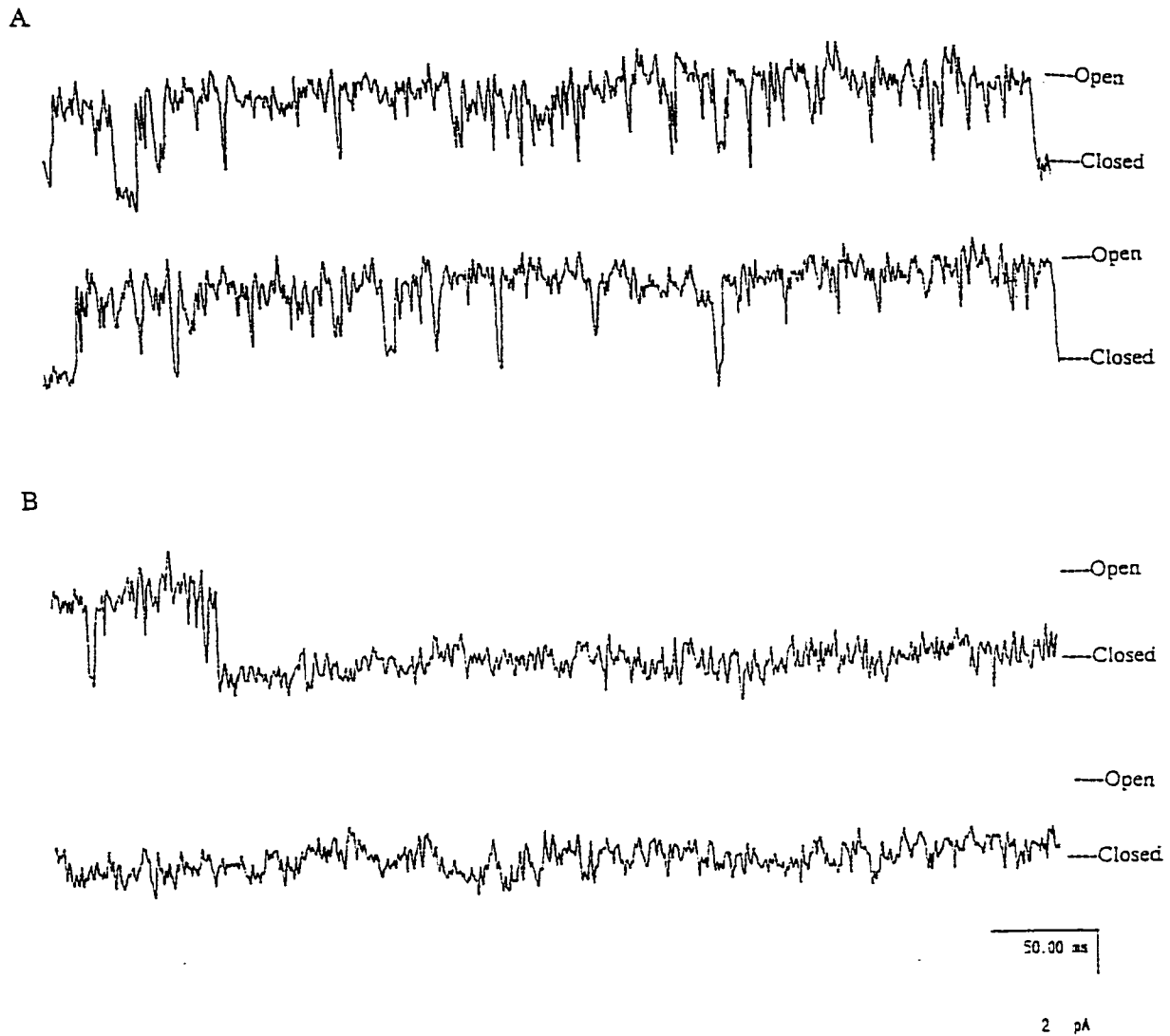
IV-3. The 63 pS channel exhibited a characteristic pattern of cycling through periods of burst openings followed by several seconds of silence. Each trace is from the same patch in which only the 63 pS channel was active and the traces represent a sequence of control recordings at a holding potential of 0 mV within a 6 second recording period. Channel closed and open states are marked on the traces.



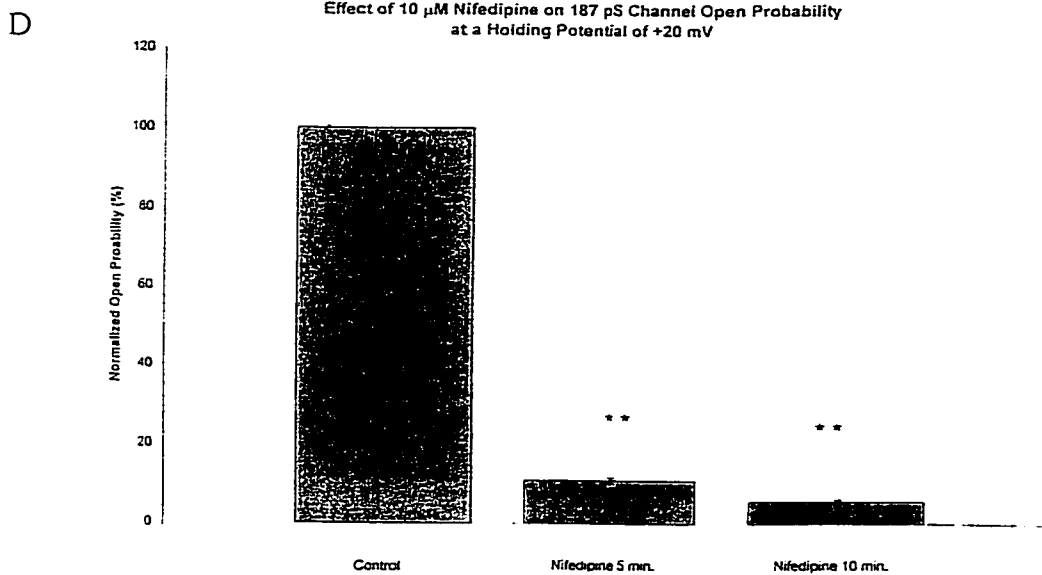
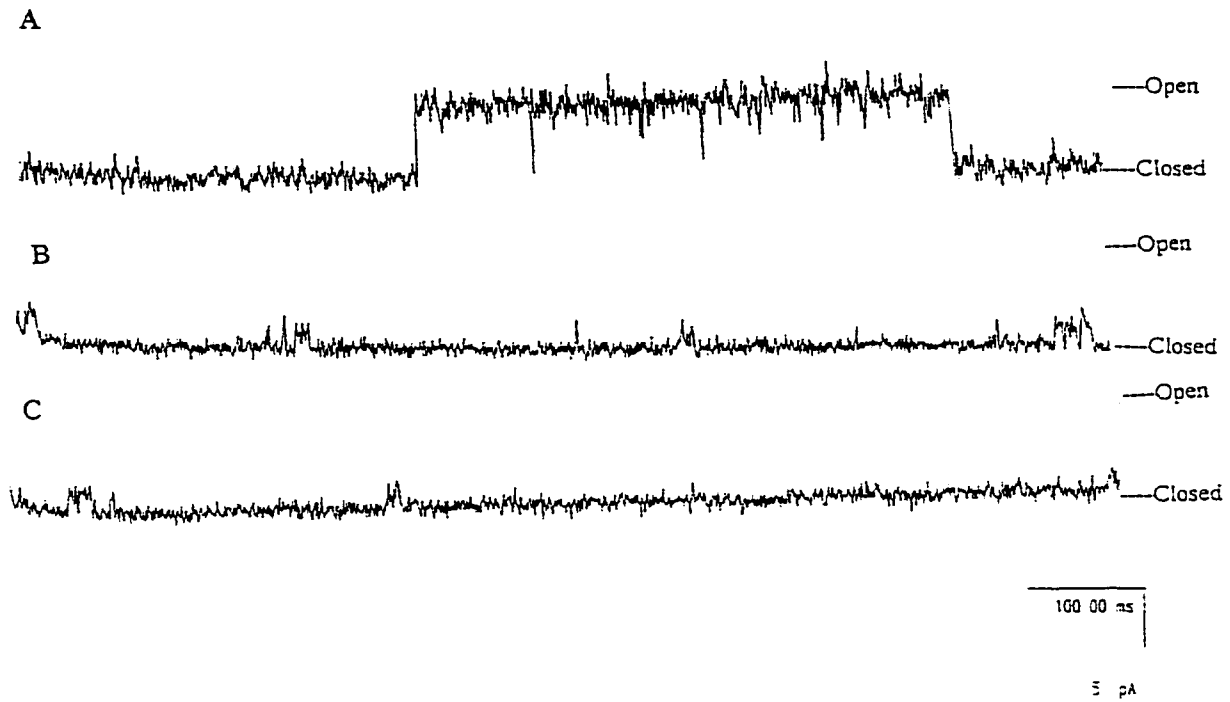
IV-4. The 63 pS channel was found to be weakly voltage-dependent. Increasing the holding potential from 0 mV to 20 mV did not significantly affect channel open probability, but at holding potential of 40 mV (C) 63 pS channel open probability is consistently much lower. These traces are from the same patch, and show a consistent pattern of opening at holding potentials of 0 mV (A), and 20 mV (B), but not at a holding potential of 40 mV. In (D) a plot of open probability versus voltage clearly illustrates this weak voltage-dependence ( $n = 8$ ).



IV-5. Unlike the 63 pS channel, the 187 pS channel exhibited a characteristic pattern of voltage-dependence. The traces shown are from a single patch and show the usual increase in open probability as the holding potential increases from 0 mV (A) to 20 mV (B) to 40 mV (C). In (D) an open probability versus voltage plot illustrates this increase in open probability in response to increases in voltage ( $n = 9$ ).

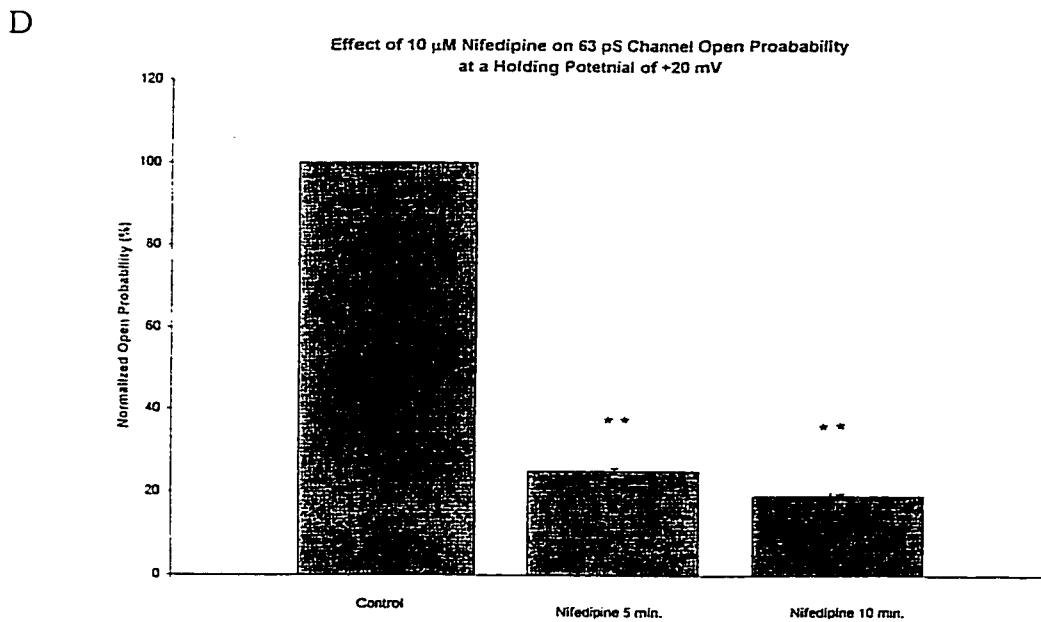
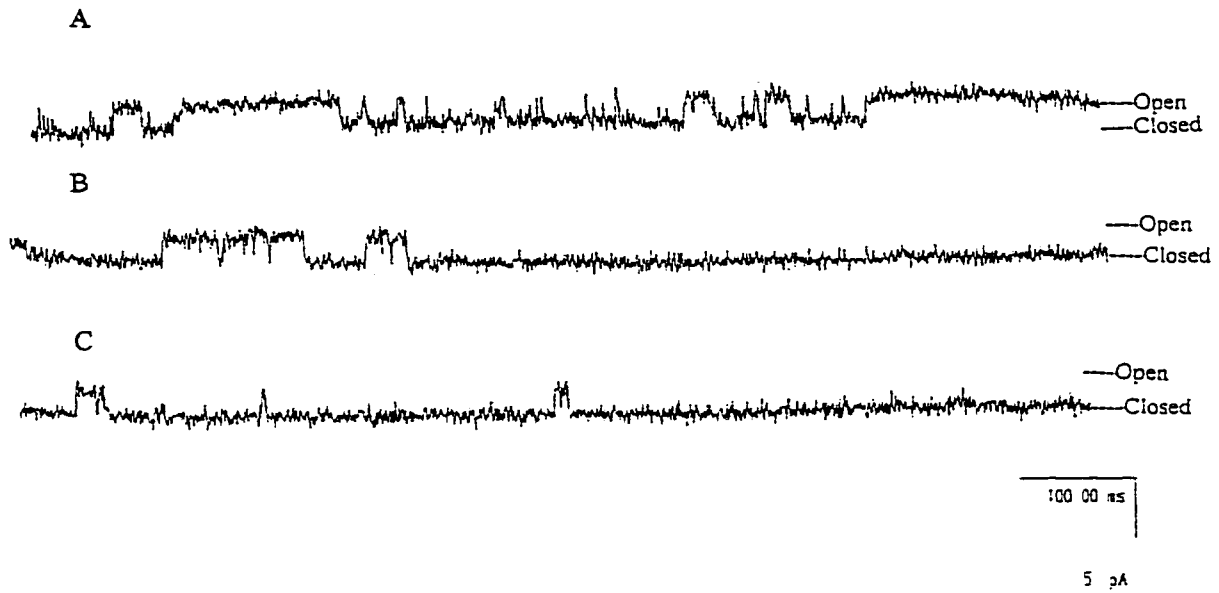


IV-6. The 187 pS channel showed great variations in open probability. In the same patch and at the same holding potentials (40 mV in these traces) the channel open probability went from very high (A) to very low (B) within the course of control recordings; both sets of traces were recorded within the same 6 second recording period. Patches in which the 187 pS channel exhibited such great shifts in open probability were not used in this study.

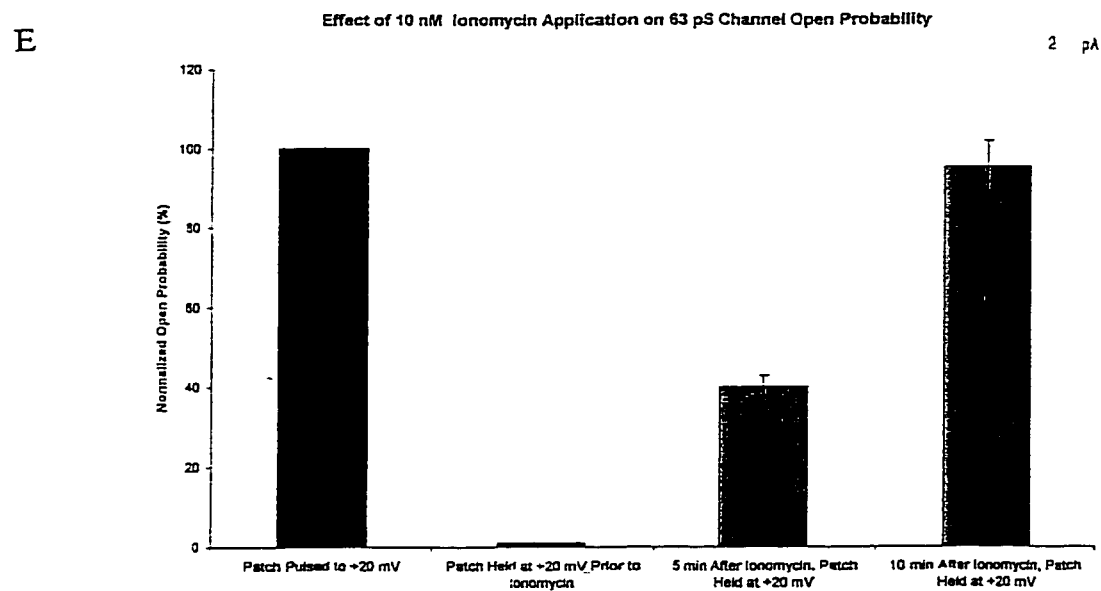
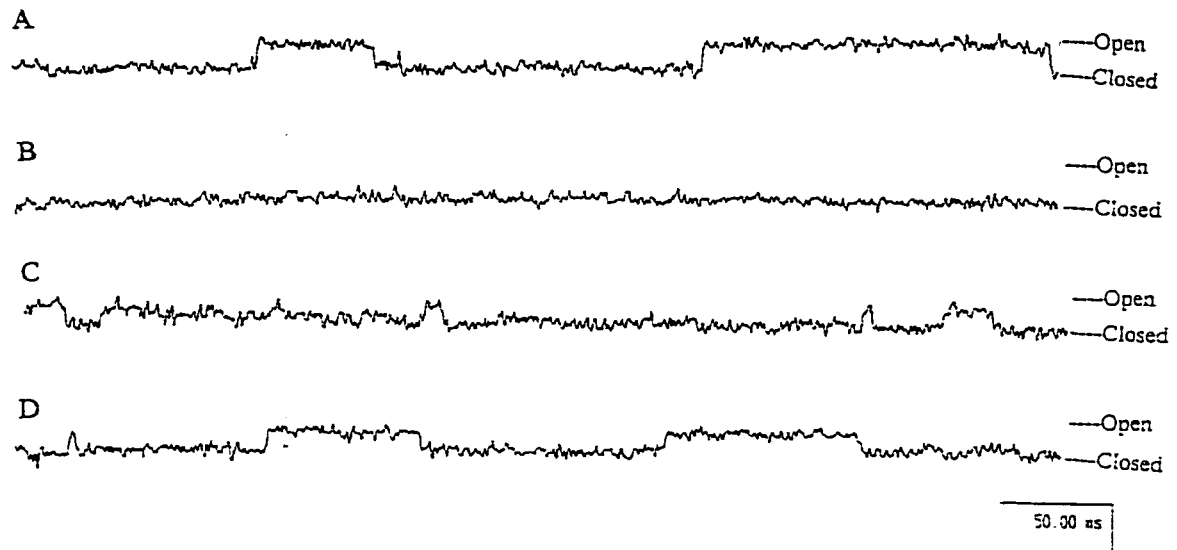


IV-7. The 187 pS channel is very sensitive to  $\text{Ca}^{2+}$  channel blockade by 10  $\mu\text{M}$  nifedipine. These traces from a representative patch pulsed from  $-80$  mV to 0 mV. Traces shown are recorded prior to (A), and 5 (B) and 10 (C) minutes after nifedipine application: in this patch, the 187 pS channel is completely blocked within 5 minutes. Note that 63 pS channel opening is still seen at both 5 and 10 minutes after nifedipine application. In (D) decreases in open probability are compared to control values (defined as 100% to standardize data;  $n = 3$ ; values after nifedipine treatment are statistically significant,  $p < 0.01$ ).

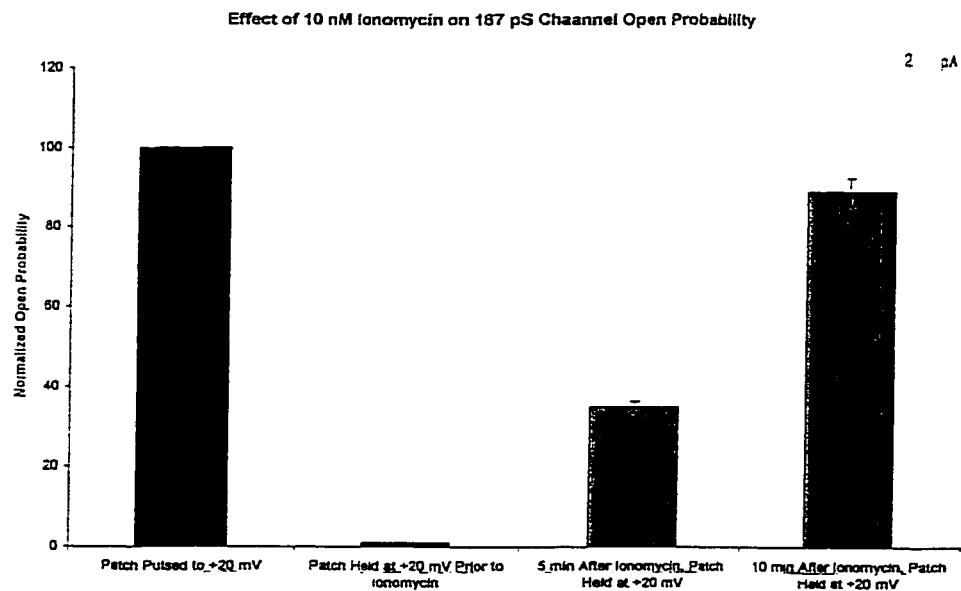
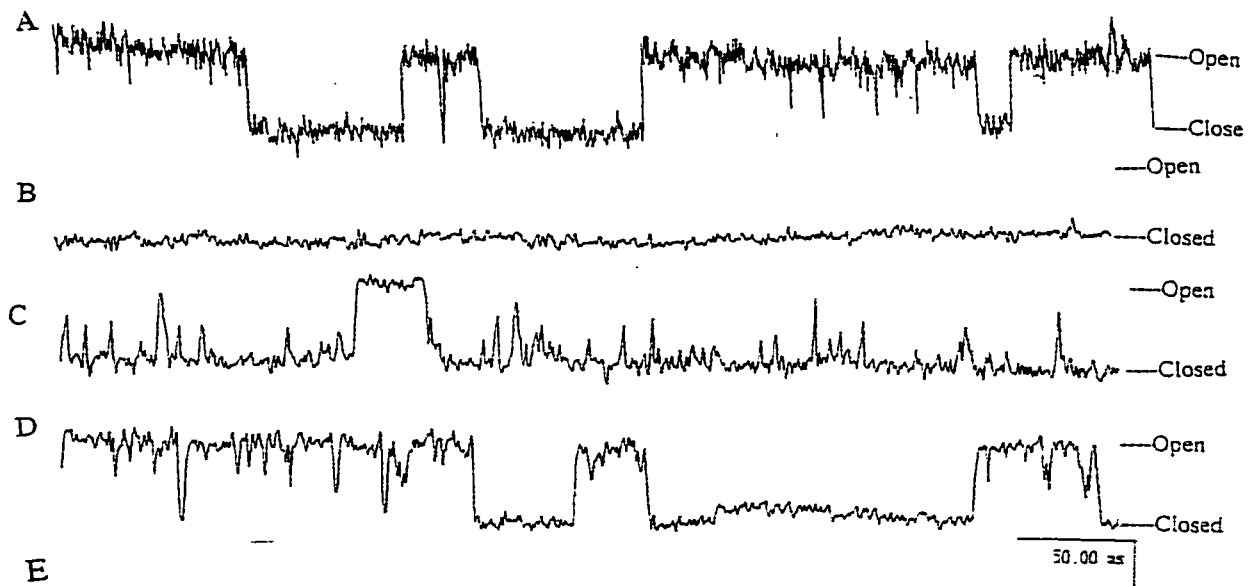




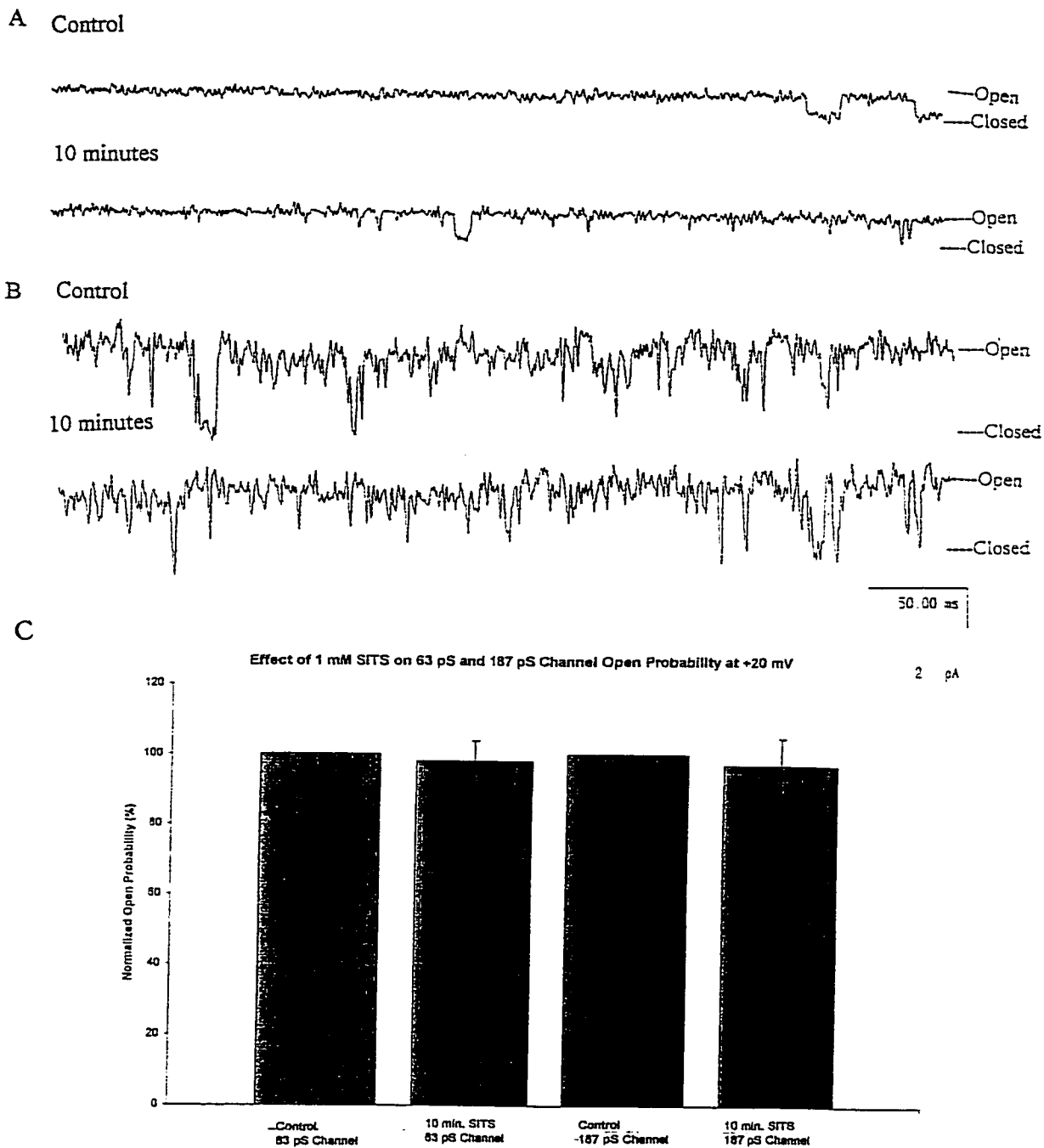
IV-8. The 63 pS channel is also sensitive to  $\text{Ca}^{2+}$ -channel blockade by 10  $\mu\text{M}$  nifedipine. These traces from a patch pulsed from  $-80$  mV to 0 mV. While numerous channel openings can be seen in control conditions (A), open probability is reduced by 5 minutes (B), and channel opening, while greatly reduced, is still seen at 10 minutes (C). In (D) the decrease in open probability is graphed compared to control (defined as 100% to standardize data;  $n = 3$ ; values following nifedipine treatment are statistically different from control,  $p < 0.01$ )



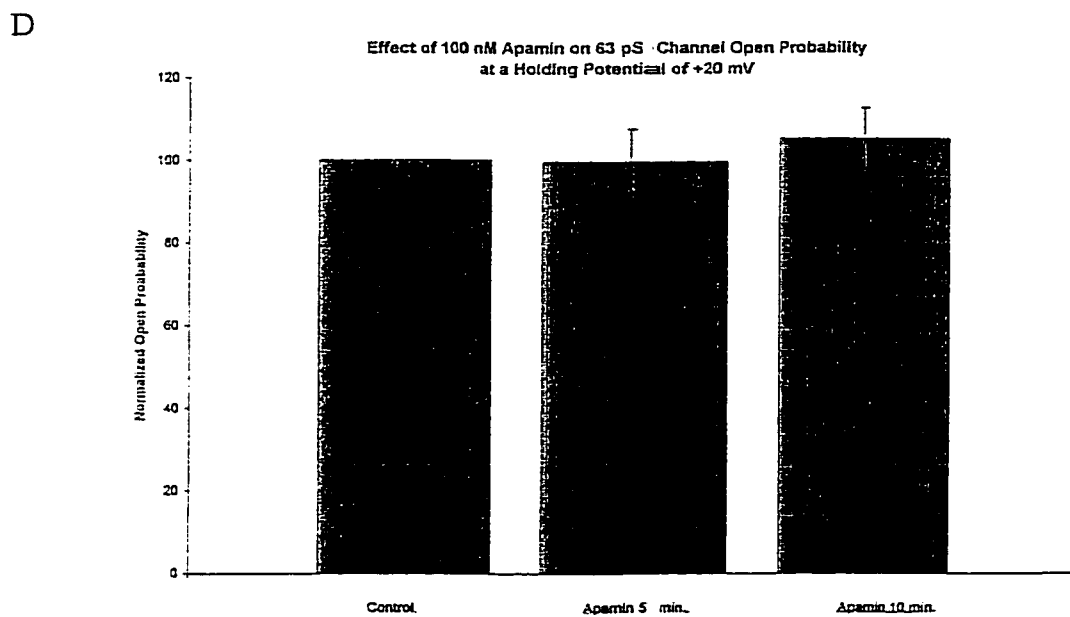
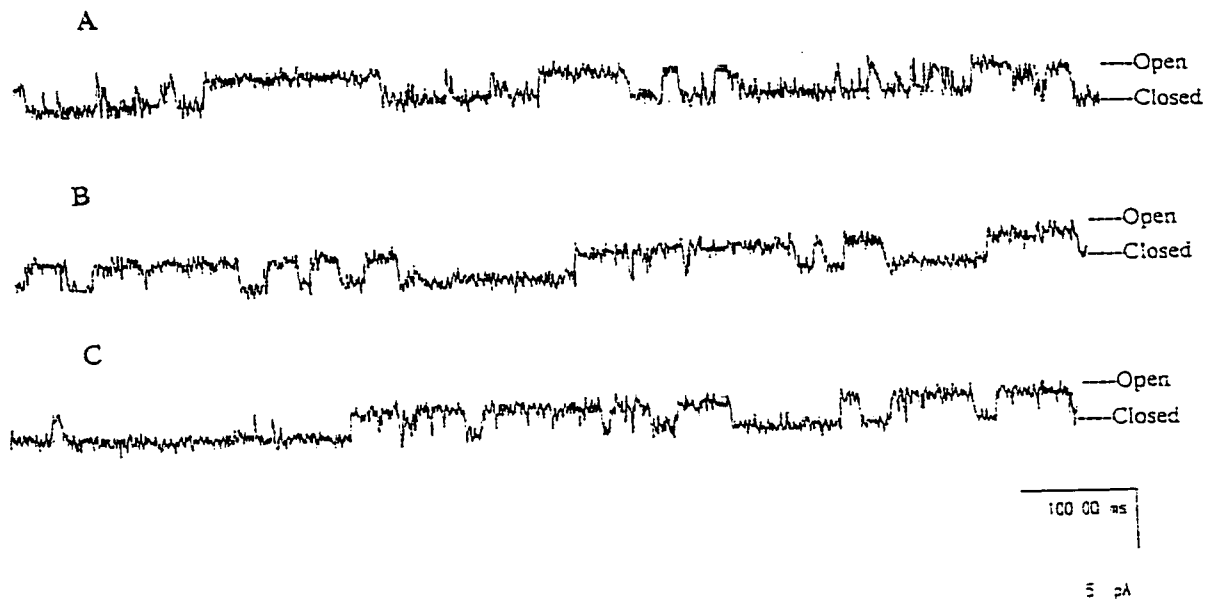
IV-9. Effect of 10 nM ionomycin application on 63 pS channel open probability in patches held at positive potentials. These traces are from a single, representative outside-out patch with 63 pS channel activity. In (A) the patch was pulsed from a holding potential of  $-80$  mV to  $20$  mV, and in (B) the patch was held at  $20$  mV prior to the application of ionomycin; in (C) and (D) the patch was held at  $20$  mV  $5$  and  $10$  minutes, respectively, after the application of ionomycin. Note the increased channel opening following longer exposure to ionomycin, which is comparable to the channel open probability seen in pulsed patches. In the absence of ionomycin no channel openings were seen in control patches held at positive potentials. Alternately, increasing pipette free  $[Ca^{2+}]$  had the same effect as application of ionomycin. In (E) changes in open probability are graphed compared to controls from pulsed patches (defined as 100% to standardize data;  $n = 4$ ).



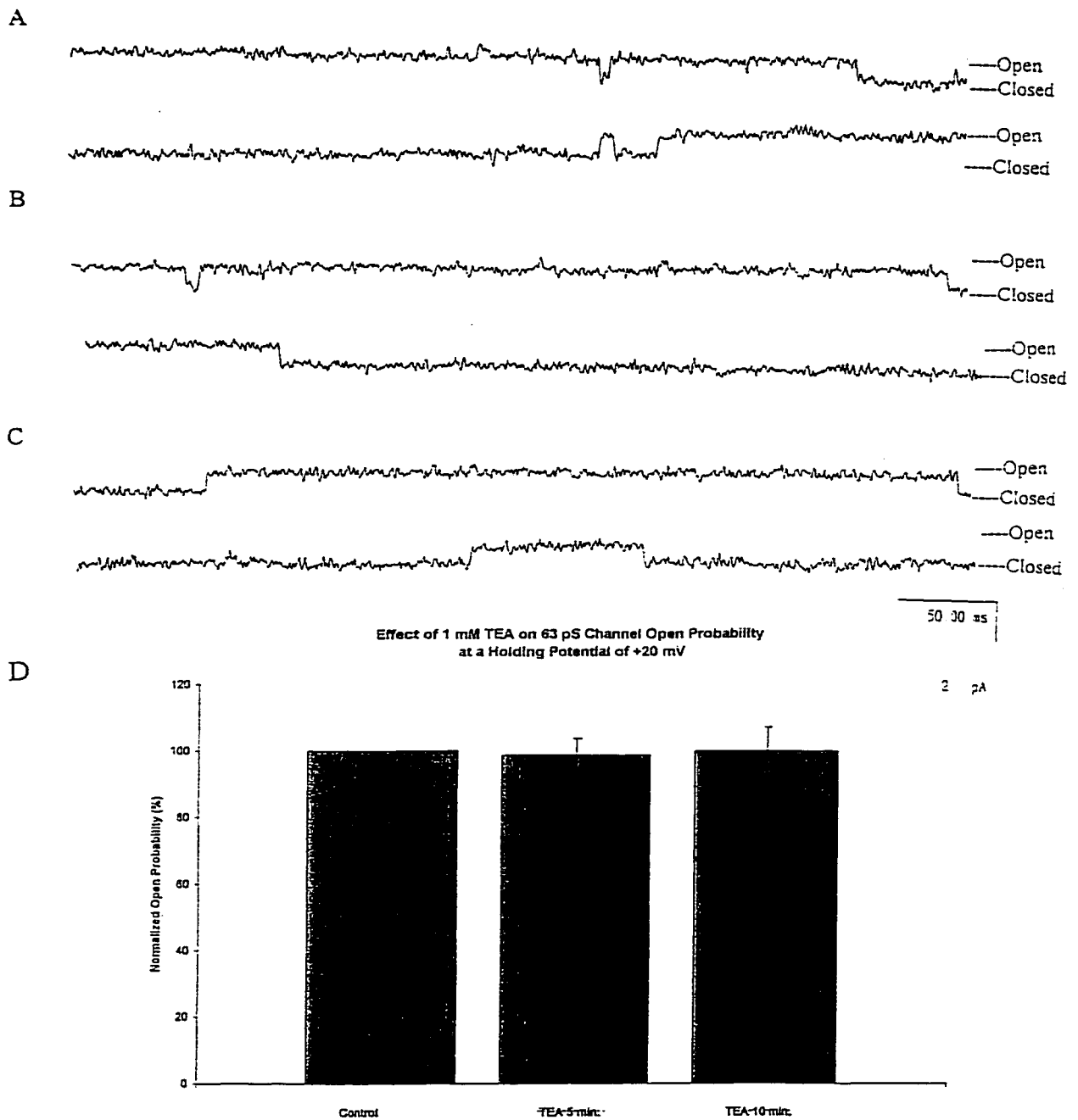
IV-10. Effect of 10 nM ionomycin application on 187 pS channel open probability in patches held at positive potentials. These traces are from a single, representative outside-out patch with 187 pS channel activity. In (A) the patch was pulsed from a holding potential of  $-80$  mV to  $20$  mV, and in (B) the patch was held at  $20$  mV prior to the application of ionomycin; in (C) and (D) the patch was held at  $20$  mV 5 and 10 minutes, respectively, after the application of ionomycin. Note the increased channel opening following prolonged exposure to ionomycin, which is comparable to the channel open probability seen in pulsed patches. In the absence of ionomycin no channel openings were seen in patches held at positive potentials. Alternately, increasing pipette free  $[Ca^{2+}]$  had the same effect as application of ionomycin. In (E) changes in open probability are graphed compared to controls from pulsed patches (defined as 100% to standardize data;  $n = 4$ ).



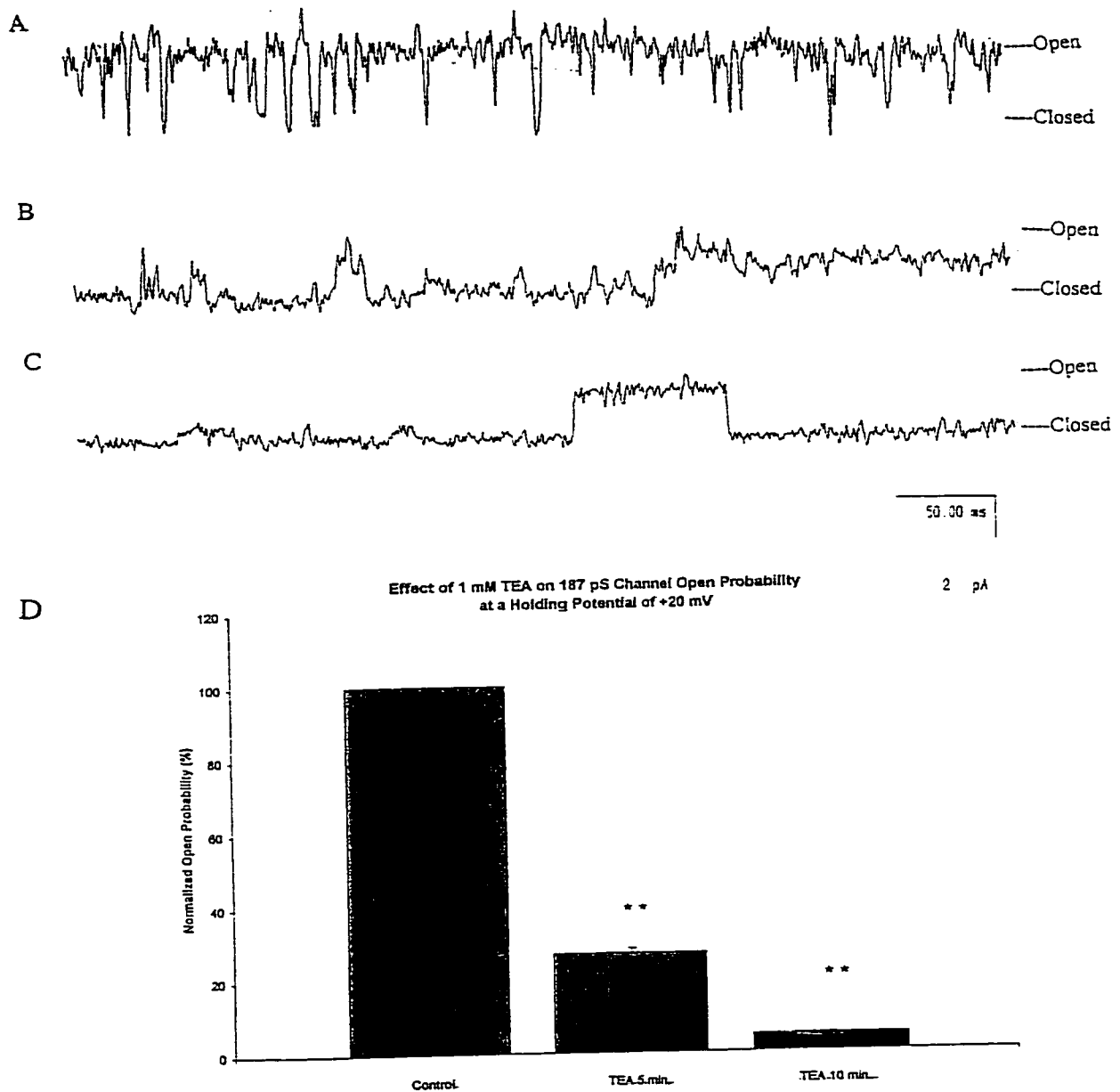
IV-11. Neither the 63 pS channel (A), nor the 187 pS channel (B) were sensitive to application of the Cl<sup>-</sup> channel blocker SITS (1 mM). The traces shown here were from 2 separate, representative patches in which only one channel or the other was present; the patches were held at a potential of 20 mV and recordings were made prior to, and 10 minutes after application of SITS. Note that the open probability of both channels did not change. In (C) the open probability of each channel 10 minutes after SITS application is graphed compared to control (defined as 100% to standardize data; n = 4).



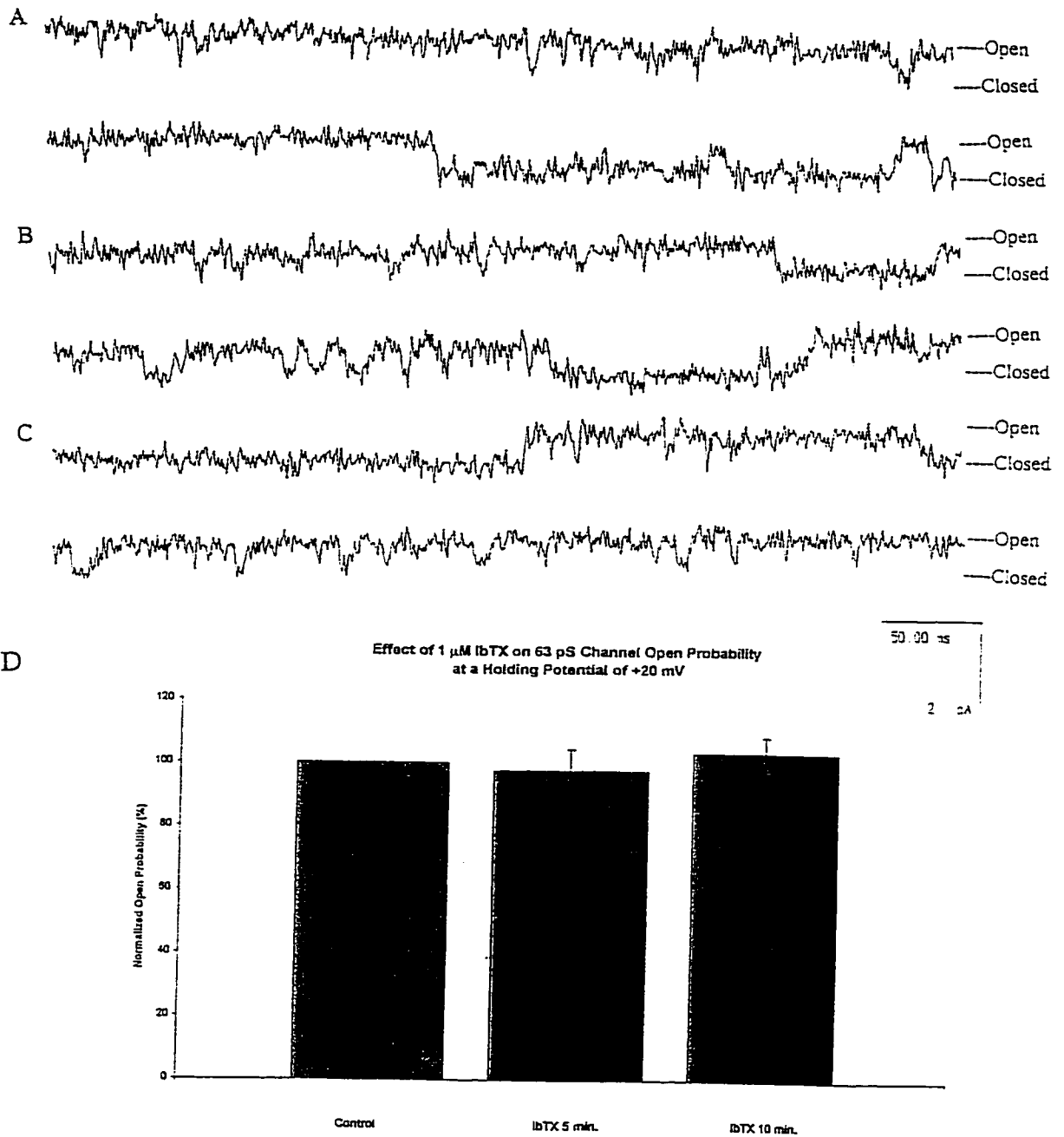
IV-12. The 63 pS channel is insensitive to application of the SK(Ca) channel blocker apamin (100 nM). These traces are from a single, representative patch in which only the 63 pS channel was present; the traces were recorded at a holding potential of 0 mV prior to (A) and 5 (B) and 10 (C) minutes after the application of apamin. Note that channel open probability did not change after toxin application. In (D) channel open probability 5 and 10 minutes after apamin application are compared to control (defined as 100% to standardize data; n = 3).



IV-13. Effect of 1 mM TEA application on 63 pS channel open probability in patches held at positive potentials. These traces are from a single, representative patch held at 0 mV, in which only the 63 pS channel was present: the traces were recorded before (A) and 5 (B) and 10 (C) minutes after the application of TEA. Note that there is no significant change in 63 pS channel open probability despite application of TEA. In (D) open probability 5 and 10 minutes after TEA application are compared to control (defined as 100% to standardize data; n = 3).

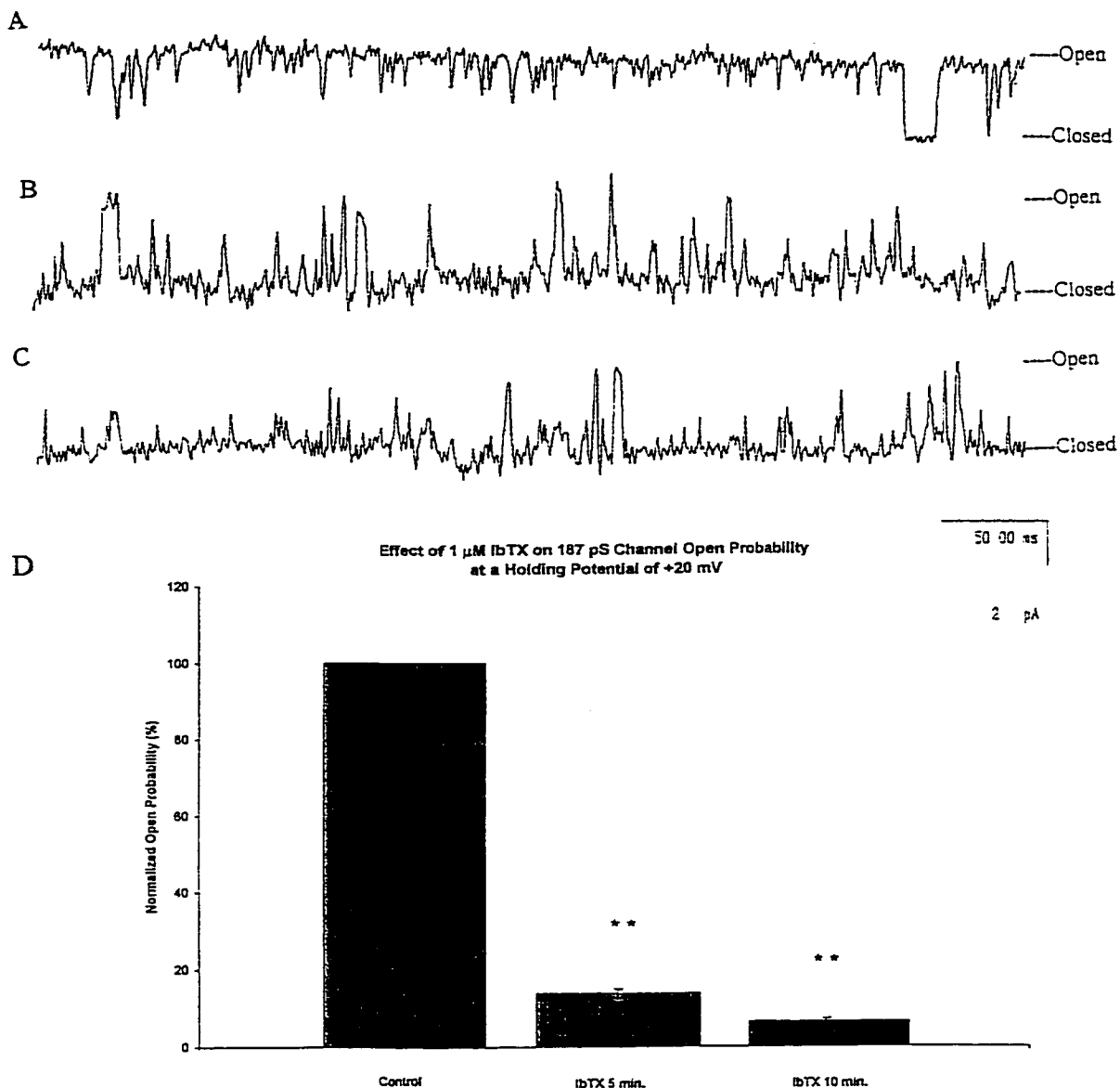


IV-14. Effect of 1 mM TEA application on 187 pS channel open probability in patches held at positive potentials. These traces are from a single, representative patch held at 20 mV and they show the sensitivity of the 187 pS channel to application of TEA. When compared to control (A) recordings, a significant decrease in channel open probability can be seen 5 (B) and 10 (C) minutes after TEA application. Note that TEA at this concentration does not completely block channel activity. In (D) changes in open probability are graphed compared to control (defined as 100% to standardize data; n = 4; values following TEA treatment are statistically different from control,  $p < 0.01$ ).

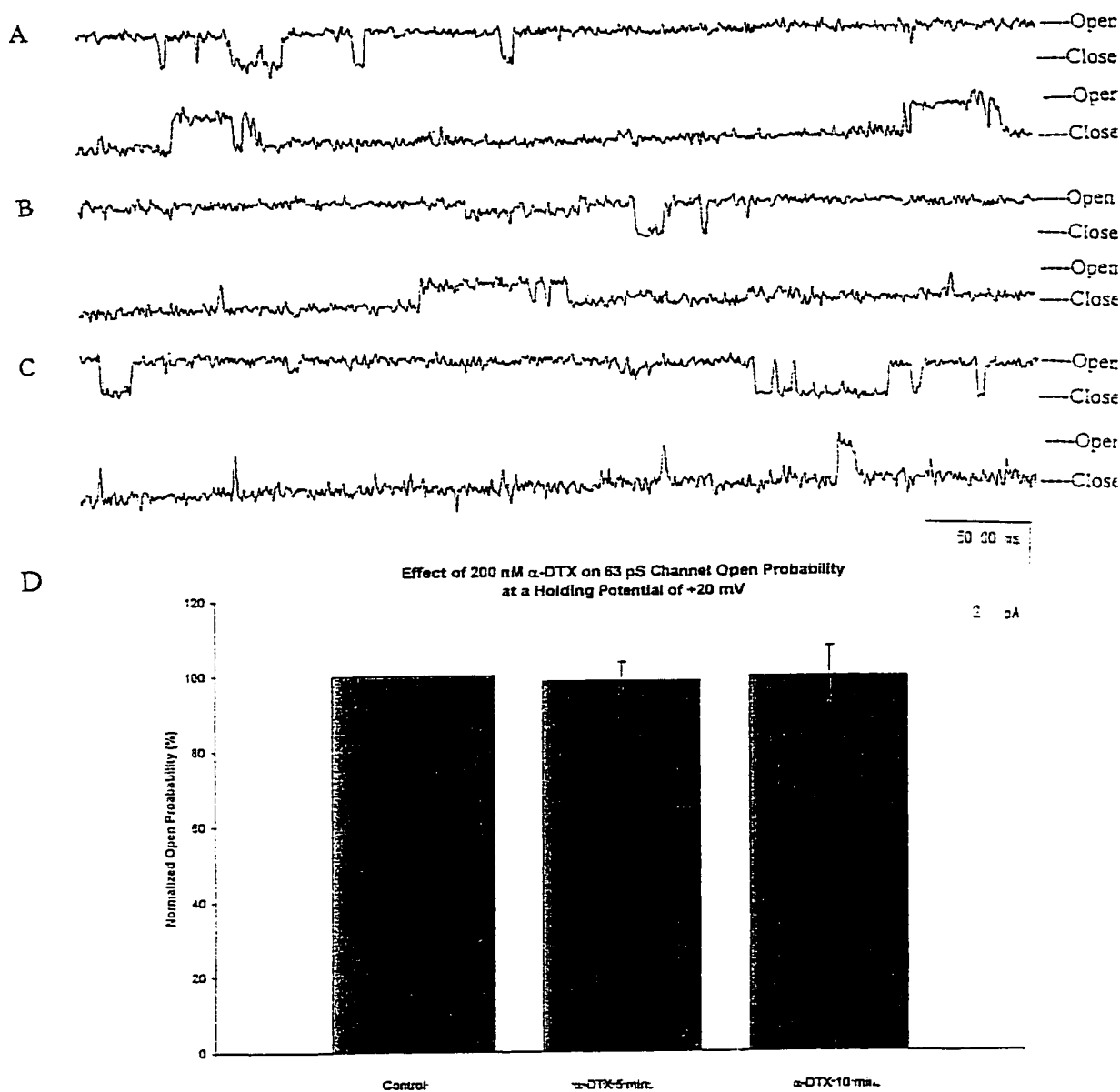


IV-15. Effect of application of 1  $\mu\text{M}$  IbTX on 63 pS channel open probability in patches held at positive potentials. These traces are recorded from a single, representative patch held at 20 mV, in which only the 63 pS channel was present, and they show the insensitivity of this channel to application of the large conductance  $\text{Ca}^{2+}$ -activated  $\text{K}^+$  channel blocker IbTX. Note that when compared to control (A) recordings, no change in open probability can be seen 5 (B) and 10 (C) minutes after application of IbTX. In (D) open probability 5 and 10 minutes after IbTX application are compared to control (defined as 100% to standardize data;  $n = 4$ ).

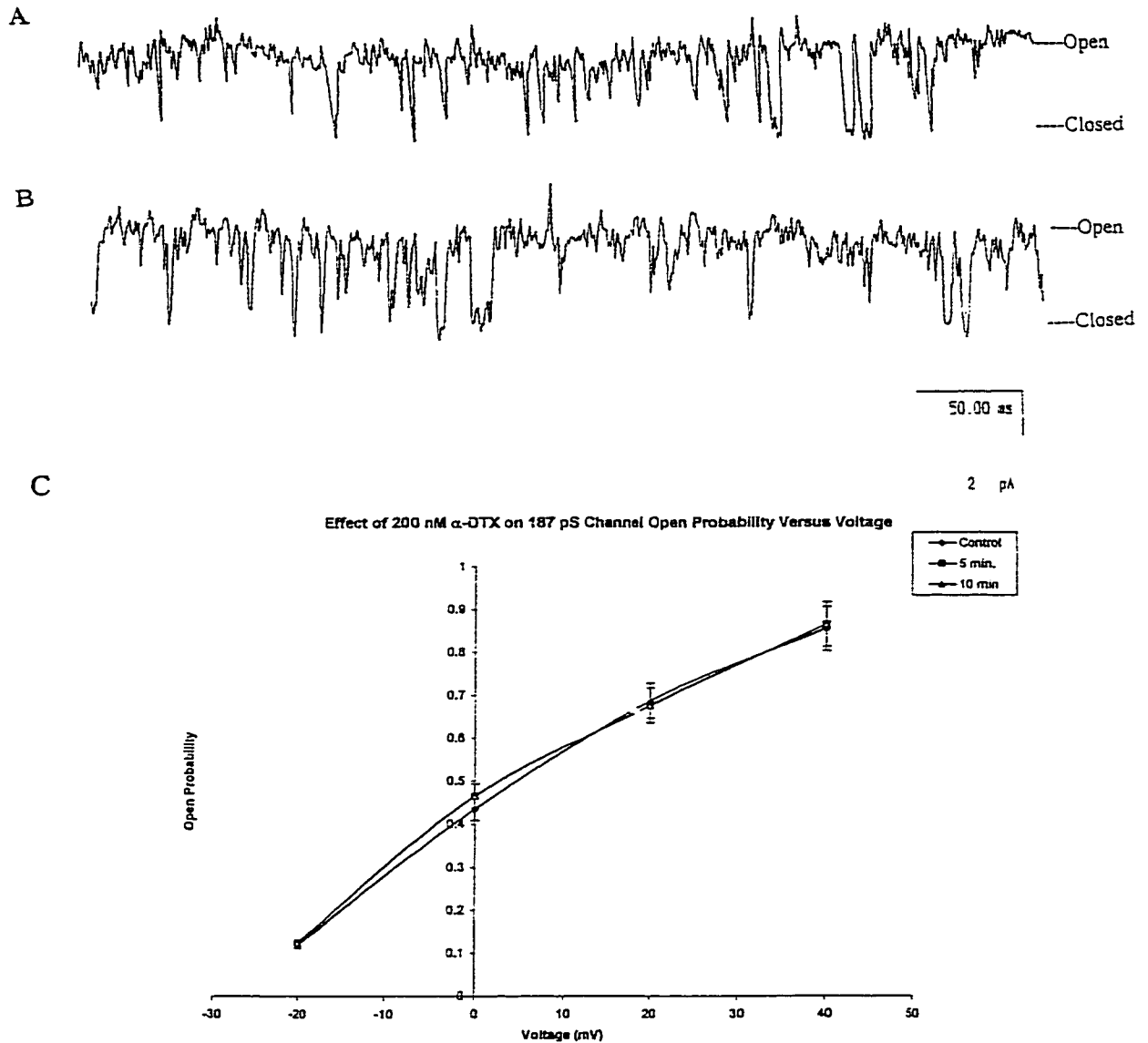




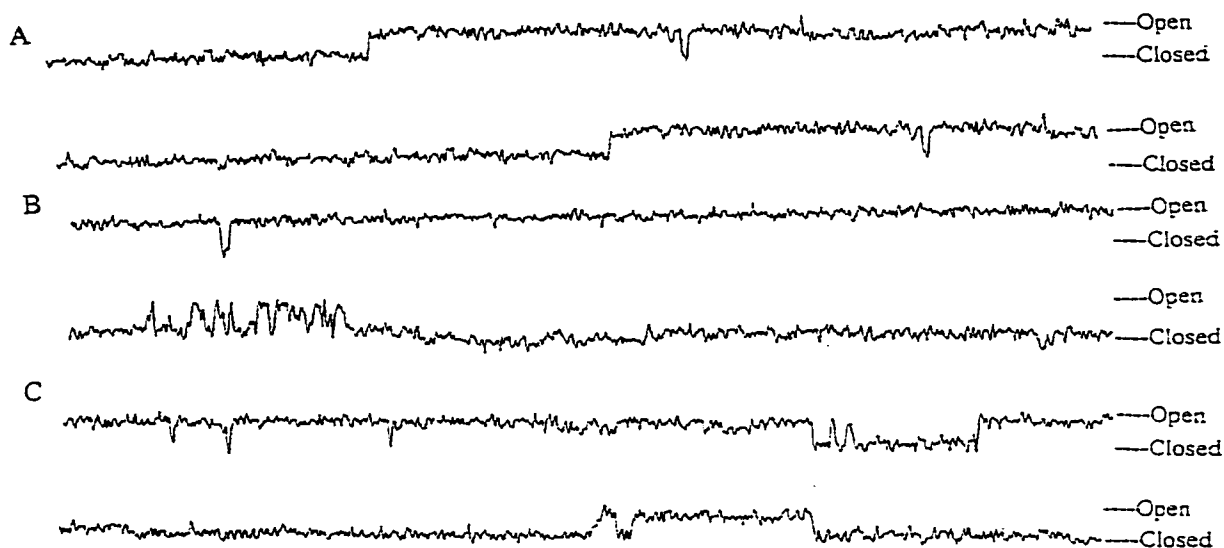
IV-16. Effect of 1  $\mu\text{M}$  IbTX application on 187 pS channel open probability in patches held at positive potentials. These traces are recorded from a single, representative patch held at 20 mV, in which only the 187 pS channel was present, and they show the sensitivity of this channel to application of the large conductance  $\text{Ca}^{2+}$ -activated  $\text{K}^+$  channel blocker IbTX. Note that when compared to before (A) application of IbTX, there is a significant decrease in channel open probability 5 (B) and 10 (C) minutes after toxin application, although the toxin does not completely block channel activity. In (D) changes in open probability are graphed compared to control (defined as 100% to standardize data;  $n = 4$ ; values following IbTX treatment are statistically different from control,  $p < 0.01$ ).



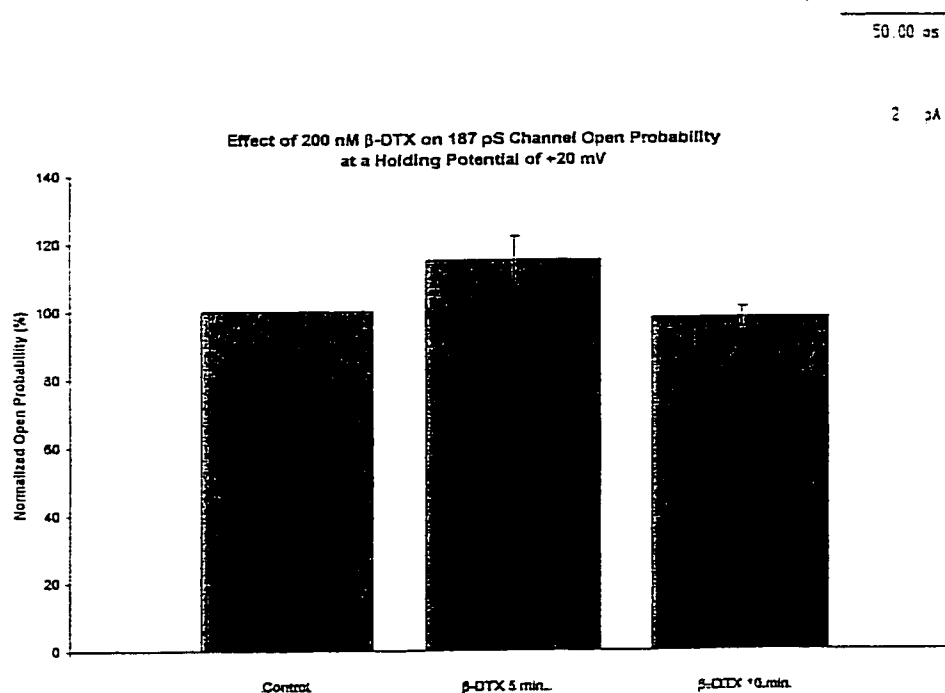
IV-17. Effect of 200 nM  $\alpha$ -DTX application on 63 pS channel open probability in patches held at positive potentials. These traces are recorded from a single, representative patch held at 20 mV, in which only the 63 pS channel was present, and they show the insensitivity of this channel to application of  $\alpha$ -DTX. Note that when compared to control (A) recordings, there is not significant change in open probability 5 (B) and 10 (C) minutes after application of  $\alpha$ -DTX; this insensitivity to  $\alpha$ -DTX was also seen at holding potentials of 0 mV and 40 mV. In (D) open probability 5 and 10 minutes after  $\alpha$ -DTX application are compared to control (defined as 100% to standardize data; n = 4).



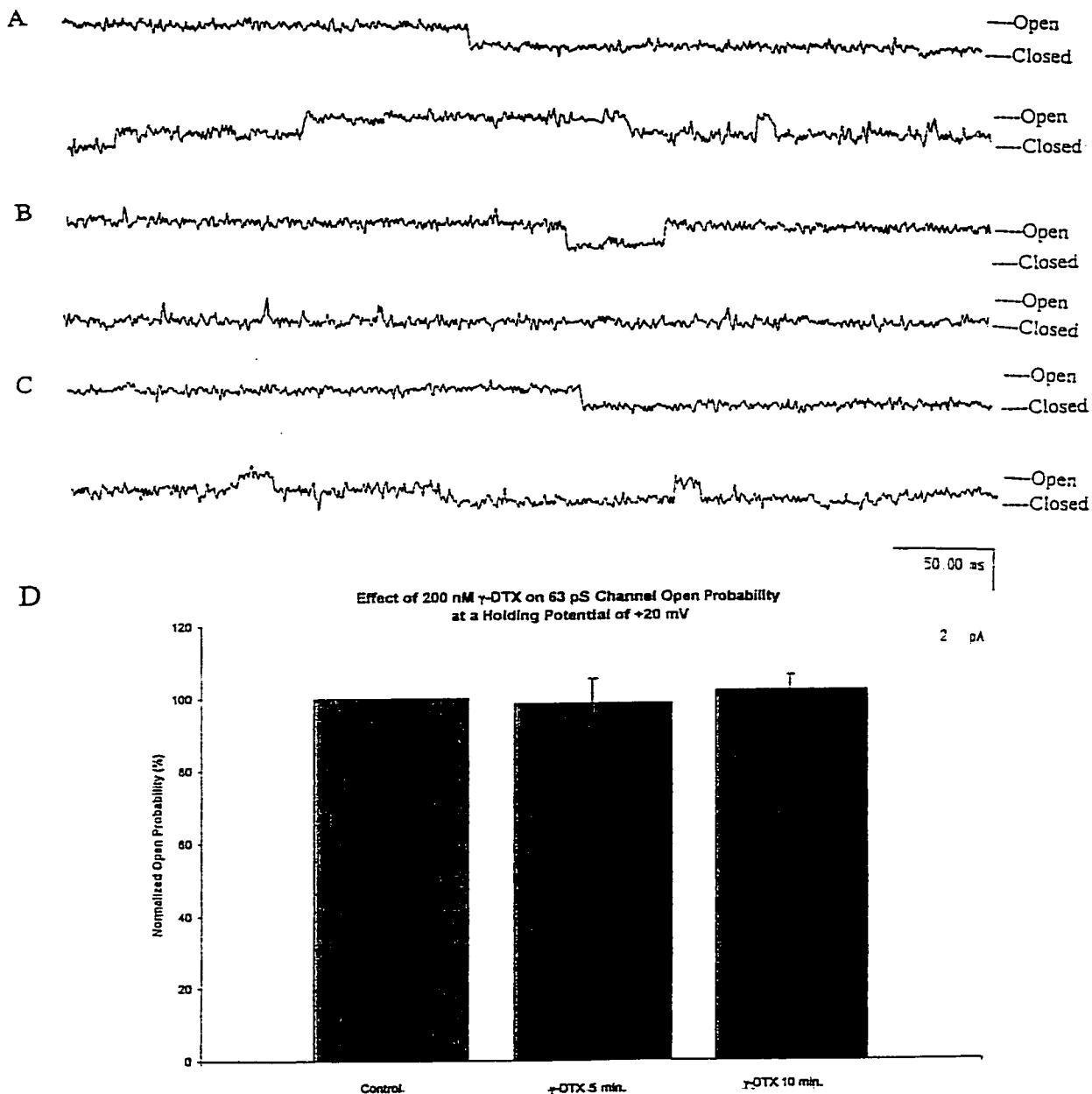
IV-18. Effect of 200 nM  $\alpha$ -DTX application on 187 pS open probability in patches held at various potentials. These traces are recorded from a single, representative patch recorded at a holding potential of 40 mV, and they show the insensitivity of the 187 pS channel to  $\alpha$ -DTX. No change was seen in 187 pS channel open probability when compared to control (A), even 10 minutes (B) after application of  $\alpha$ -DTX; recordings 5 and 10 minutes after toxin application did not differ from control at holding potentials of 0 mV or 20 mV, as can be seen in (C). In (C) open probability is graphed as a function of voltage; values 5 and 10 minutes after  $\alpha$ -DTX application are compared to control (n = 4).



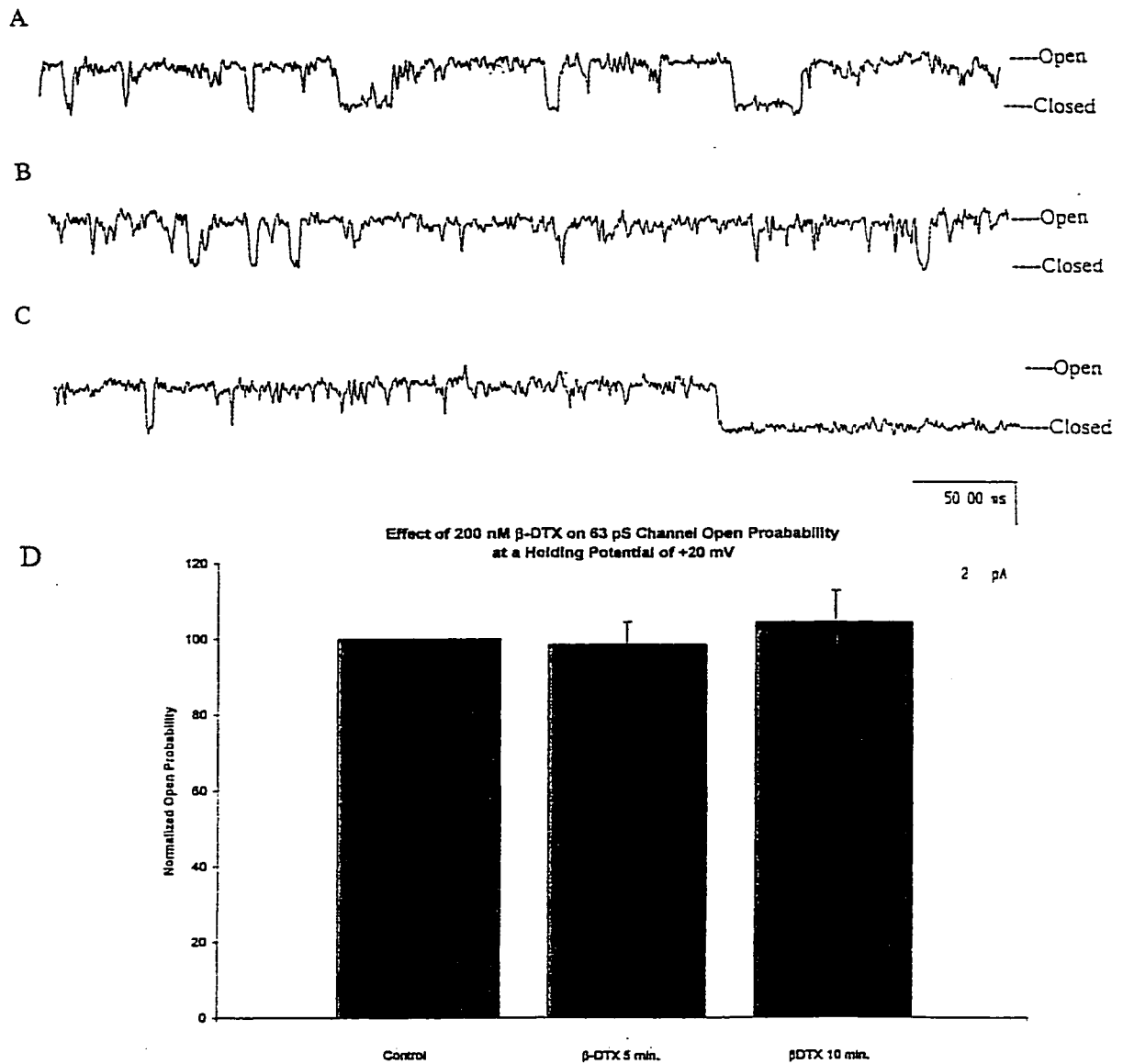
D



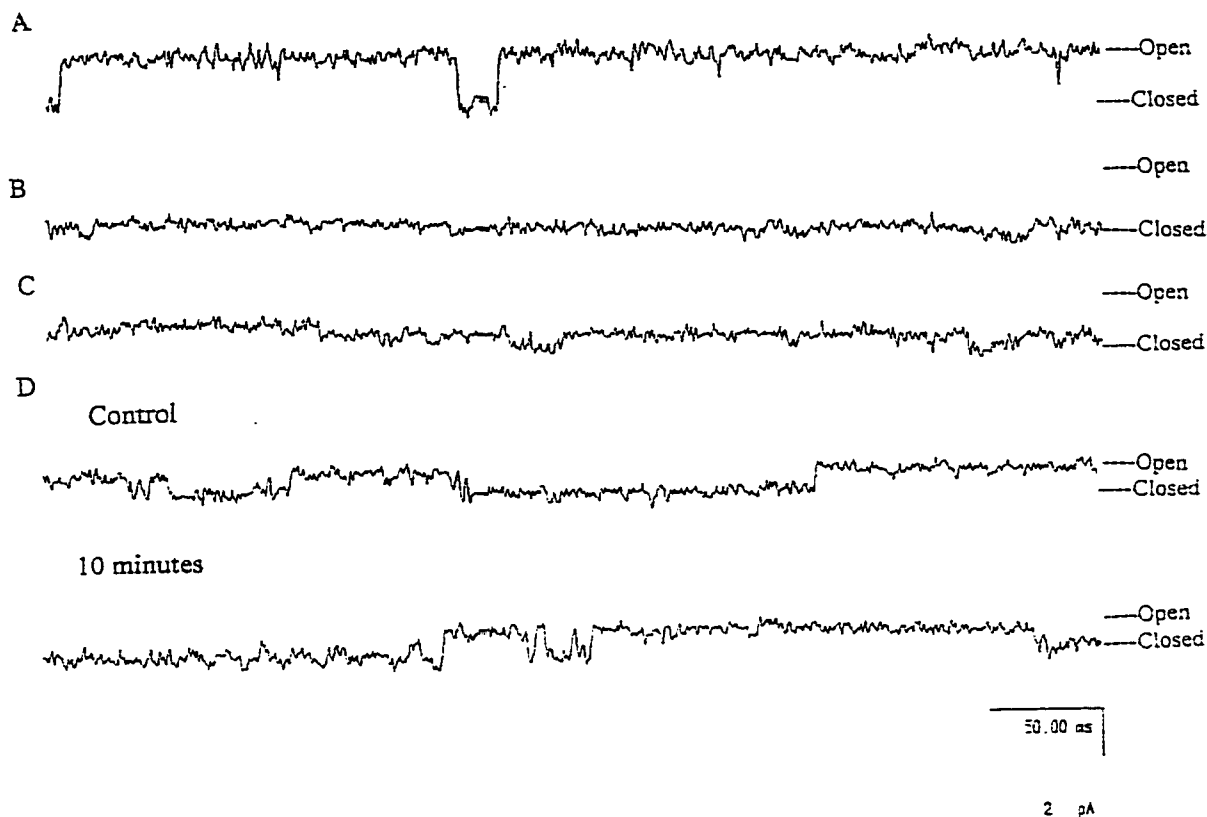
IV-19. Effect of 200 nM  $\beta$ -DTX application on 63 pS channel open probability in patches held at positive potentials. These traces are recorded from a single, representative patch at a holding potential of 20mV in which the 63 pS channel was present and are representative of the insensitivity of this channel to  $\beta$ -DTX. No change was seen in 63 pS channel open probability when compared to control (A) at both 5 minutes (B) and 10 minutes (C) after application of  $\beta$ -DTX. Recordings 5 and 10 minutes after toxin application did not differ from control at holding potentials of 0 mV or 40 mV. In (D) open probability 5 and 10 minutes after  $\alpha$ -DTX application are compared to control (defined as 100% to standardize data; n = 4).



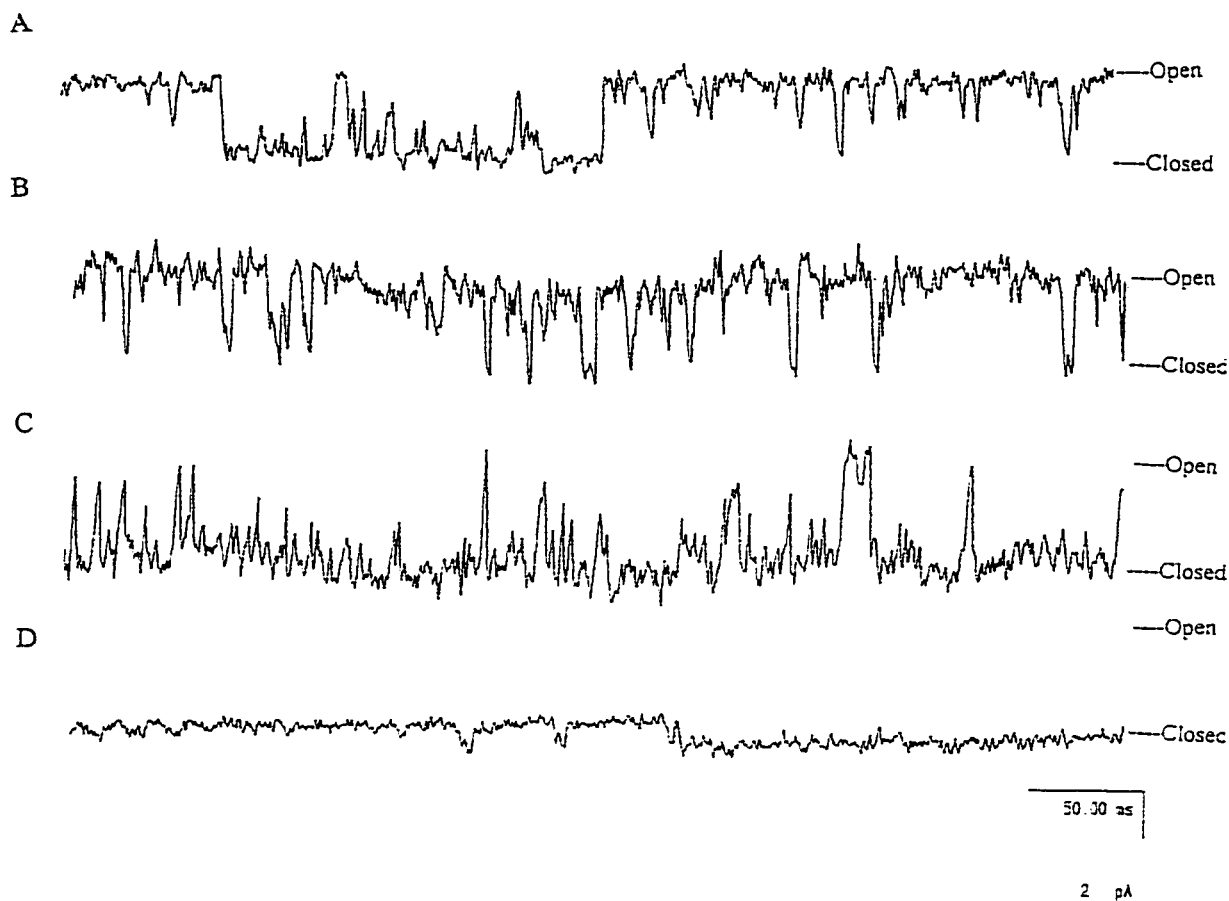
IV-20. Effect of 200 nM  $\gamma$ -DTX on 63 pS channel open probability in patches held at positive potentials. These traces are recorded from a single, representative patch at a holding potential of 0 mV, in which the 63 pS channel was present, and are representative of the insensitivity of this channel to  $\gamma$ -DTX. No change was seen in 63 pS channel open probability when compared to control (A) at both 5 (B) and 10 (C) minutes after application of  $\gamma$ -DTX. Recordings 5 and 10 minutes after toxin application were not significantly different from control at holding potentials of 20 mV or 40 mV. In (D) open probability 5 and 10 minutes after  $\gamma$ -DTX application are compared to control (defined as 100% to standardize data; n = 4).



IV-21. Effect of 200 nM  $\beta$ -DTX application on 187 pS channel open probability in patches held at positive potentials. The traces shown here are from a single, representative patch recorded at a holding potential of 0 mV. Response of the 187 pS channel to  $\beta$ -DTX was variable: when compared to control (A), most patches exhibited an increase in open probability 5 minutes (B) after application of  $\beta$ -DTX, followed by a decrease in open probability 10 minutes (C) after toxin application. These changes in open probability were not significantly different from control due to large variability. A similar pattern of response to  $\beta$ -DTX (i.e. transient increase in opening, followed by a decrease in opening) was seen at holding potentials of 20 mV and 40 mV. In (D) changes in open probability are graphed compared to control (defined as 100% to standardize data; n = 5).

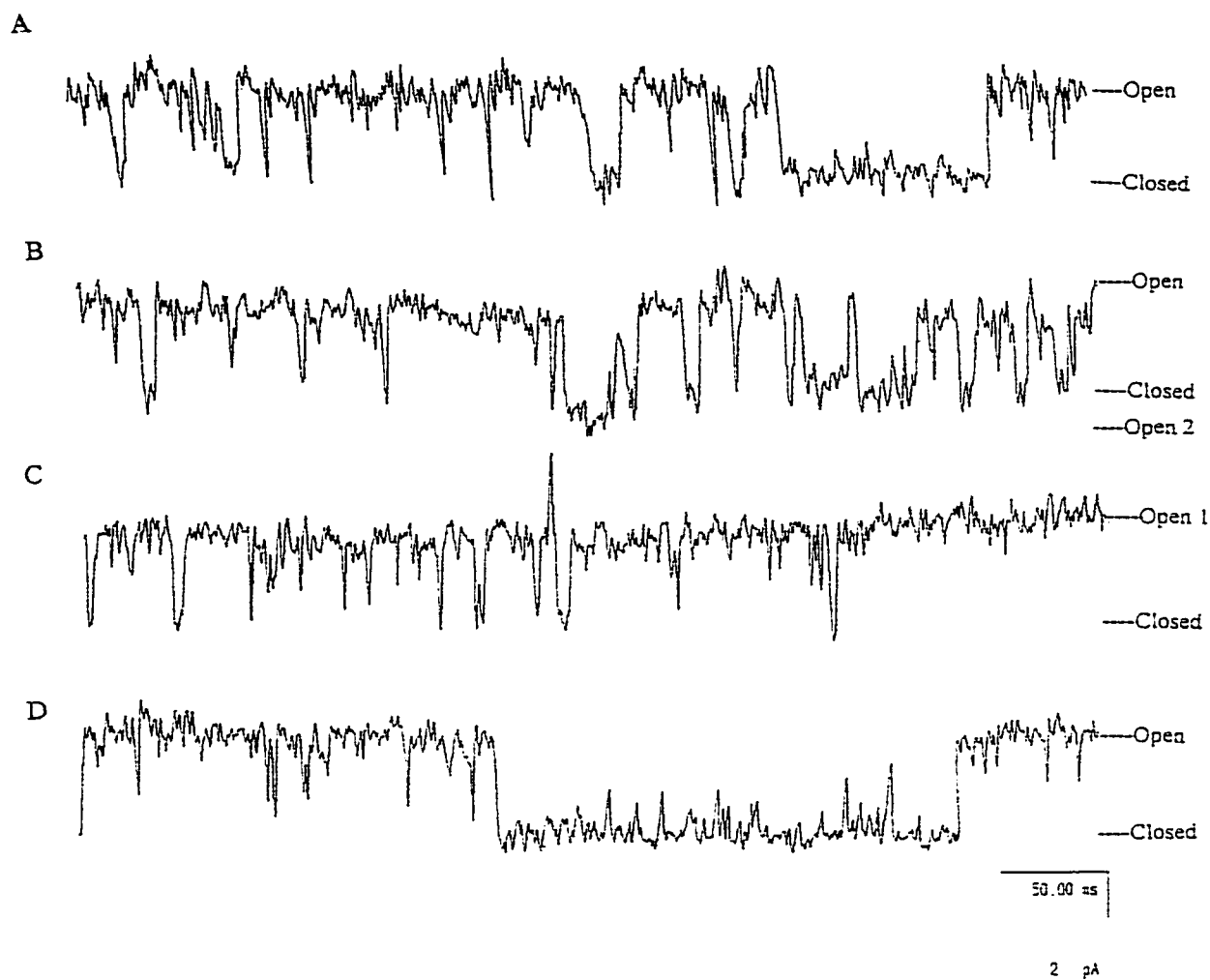


IV-22. The effect of 200 nM  $\gamma$ -DTX on the 187 pS channel is shown in these representative traces are from a single patch, recorded at holding potentials of 0 mV (traces (A), (B), and (C)), and -20 mV (trace (D)). When compared to control (A), no 187 pS channel openings are seen 5 (B), or 10 (C) minutes after application of  $\gamma$ -DTX. In most patches, complete block of the 187 pS channel occurred 2 to 3 minutes after application of 200 nM  $\gamma$ -DTX at holding potentials of 0 mV, 20 mV, and 40 mV. A transient increase in open probability was not seen prior to the onset of complete channel block (seen with 200 nM  $\beta$ -DTX, and with lower concentrations of  $\gamma$ -DTX). Toxin block was found to be voltage-dependent: at a holding potential of -20 mV, the 187 pS channel opened consistently, at control levels, even 10 minutes (D) after application of  $\gamma$ -DTX (see Figure IV-25).



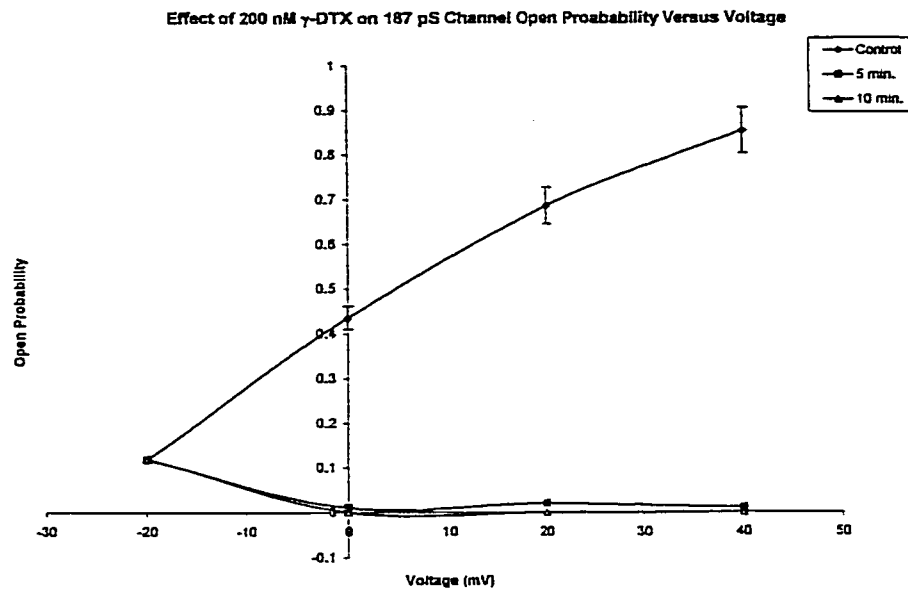
IV-23. Effect of 20 nM  $\gamma$ -DTX application on 187 pS channel open probability in patches held at various potentials. The traces shown here are from a single, representative patch in which both channels are present, and are recorded at a holding potential of 20 mV. When compared to control (A), 187 pS channel opening is reduced at 5 (C) minutes, and completely blocked at 10 (D) minutes after the application of  $\gamma$ -DTX (this pattern of block was also seen at holding potentials of 0 mV, and 40 mV, but not at -20 mV, see Figure IV-25). Note that the 63 pS channel was still opening at both 5 (B) and 10 (C) minutes after toxin application. A transient increase in 187 pS channel open probability was seen in most patches within 3 to 4 minutes after  $\gamma$ -DTX was added to the bath solution (B).



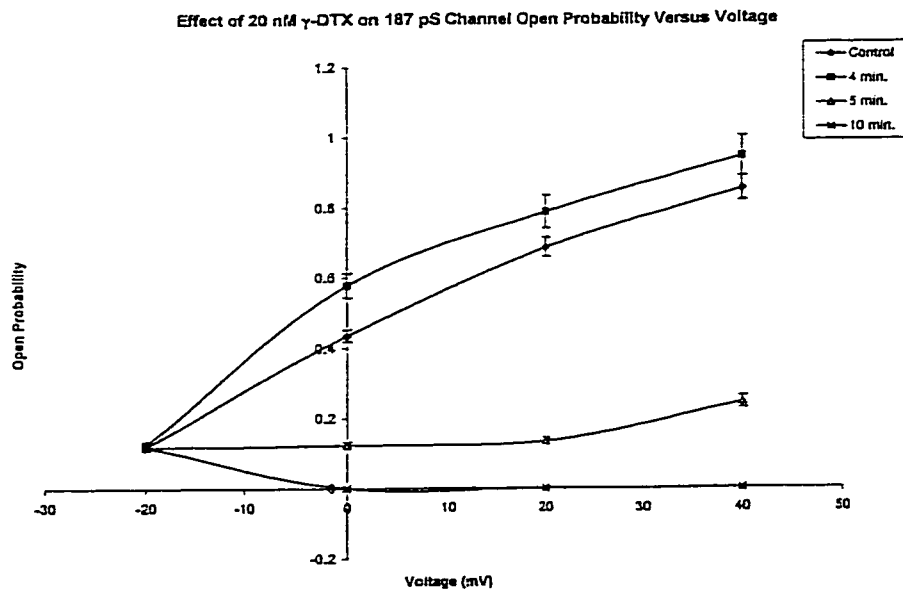


IV-24. Effect of 2 nM  $\gamma$ -DTX application on 187 pS channel open probability in patches held at various potentials. The traces shown are from a single, representative patch in which both channels are present, and are recorded at a holding potential of 40 mV. When compared to control (A), channel opening was not significantly different at 5 (B) minutes, and did not change significantly until 10 (D) minutes after toxin application (this pattern of partial block was also seen at holding potentials of 0 mV and 20 mV, but not -20 mV, see Figure IV-26). Note that 63 pS channel opening, while masked in trace (A), is noticeable in traces (B) and (D). A transient increase in 187 pS channel open probability was seen in most patches 6 to 8 minutes after  $\gamma$ -DTX was added to the bath solution (C).

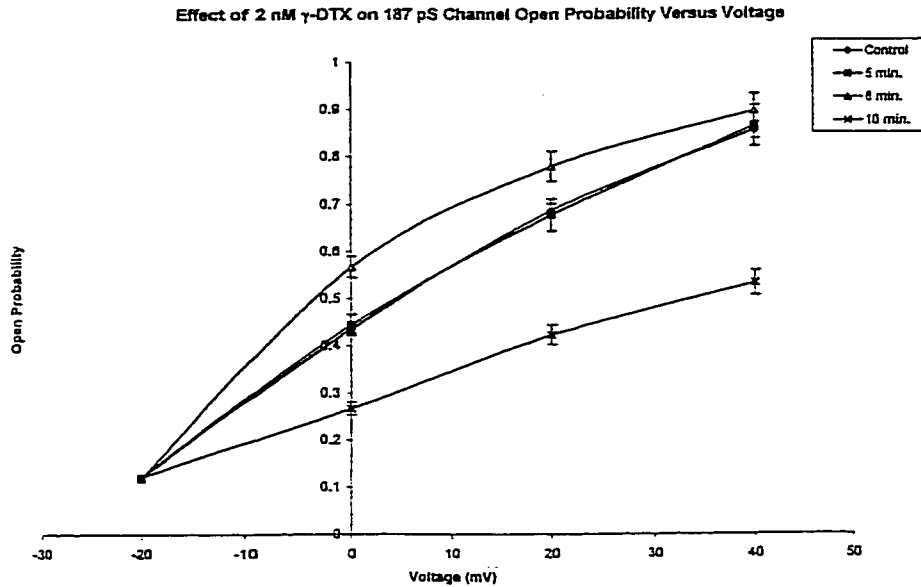
A



B



IV-25. Graph of the effect of (A) 200 nM or (B) 20 nM  $\gamma$ -DTX application on 187 pS channel open probability as a function of the holding potential. In (A) the voltage-dependence of  $\gamma$ -DTX-induced channel block can be seen as the open probability at  $-20$  mV does not differ from control, yet at 0, 20 and 40 mV the channel is completely blocked ( $n = 8$ ; values at 0, 20, and 40 mV are significantly different from control,  $p < 0.01$ ). In (B) a transient increase in open probability is seen prior to the onset of channel block, which is delayed compared to the time course of 200 nM  $\gamma$ -DTX-induced block ( $n = 5$ ; values 5 and 10 minutes after toxin application are significantly different from control at 0, 20, and 40 mV,  $p < 0.01$ ).



IV-26. Graph of the effect of 2 nM  $\gamma$ -DTX application on 187 pS channel open probability as a function of the holding potential. Onset of  $\gamma$ -DTX-induced channel block is further delayed at 2 nM, compared to both 200 and 20 nM, as is the onset of the transient increase in open probability, compared to 20 nM. Also, at 2 nM  $\gamma$ -DTX does not completely block channel opening, even after 10 minutes ( $n = 3$ , values are significantly different from control 10 minutes after toxin application at 0, 20, and 40 mV,  $p < 0.01$ ). Similar to both 200 nM, and 20 nM  $\gamma$ -DTX, however, even at 2 nM, the open probability at -20 mV does not change after toxin application.

## Chapter V

### Discussion

#### 5.1 Whole-cell Results

Based on pharmacological and kinetic characterization,  $K^+$  channels contributed to the currents recorded from undifferentiated N1E 115 cells under the conditions used. The calculated reversal potential within the range for the equilibrium potential for  $K^+$ , and the sensitivity to TEA and 4-AP all supported the description of the recorded current as a  $K^+$  current. The cell population in these cultured undifferentiated N1E 115 cells was found to exhibit great variability in  $K^+$  current amplitude and kinetics. Large cell-to-cell variation in whole cell current amplitude, variations in the presence of saturating currents, and fluctuations in the deactivation time constant, regardless of pipette solution composition, all support the conclusion that in these cells the channel population fluctuates. Given that this cell line is known to spontaneously differentiate (Quandt, 1994), and that cells are subcultured prior to patch clamp recordings, it is not unreasonable to assume that the cell population is heterogeneous. Fluctuations in  $K^+$  channel number and type altering  $K^+$  current amplitude and kinetics have been shown to occur during the cell cycle in the mouse lymphocytes (Deutsch 1990), and during neuronal differentiation (Ribera and Spitzer, 1992). Also, a similar variability in  $K^+$  current amplitude has been shown to occur following the maturation of voltage-gated and

Ca<sup>2+</sup>-activated K<sup>+</sup> currents as neurons mature in culture (O'Dowd, Ribera, and Spitzer, 1988).

Several lines of evidence indicated that Ca<sup>2+</sup>-activated K<sup>+</sup> currents were responsible for the development of saturating currents in the recordings from these whole-cell preparations. The composition of the pipette solution dictated whether or not saturating currents were seen in whole-cell recordings, so that in the presence of high pipette EGTA (a Ca<sup>2+</sup> chelator), or in the absence of Ca<sup>2+</sup> and ATP (to prevent the run-down of Ca<sup>2+</sup> channels) currents recorded did not saturate. Thus, Ca<sup>2+</sup> was found to play a crucial role in the saturation of these K<sup>+</sup> currents. Also, activation of Ca<sup>2+</sup>-activated K<sup>+</sup> currents has been shown to cause the saturation of recorded K<sup>+</sup> currents in other preparations (O'Dowd, Ribera and Spitzer, 1988).

DTX-sensitivity of the whole-cell K<sup>+</sup> currents recorded in this preparation of N1E 115 cells varied widely. The whole-cell currents were insensitive to application of either  $\alpha$ -, or the structurally similar  $\delta$ -DTX at 200 nM, regardless of the composition of the pipette solution. Application of  $\beta$ -, or  $\gamma$ -DTX, however, was found to be sensitive to the composition of the pipette solution, and, specifically to the presence of saturating currents: neither  $\beta$ -, nor  $\gamma$ -DTX had any effect on whole-cell currents in the absence of saturating currents. The response to 200 nM  $\beta$ -DTX, in cells with saturating currents, was variable, ranging from increases to decreases to no change in overall K<sup>+</sup> current, so that no significant effect was seen. In contrast, 200 nM  $\gamma$ -DTX was found to consistently affect whole-cell K<sup>+</sup> currents, either increasing, or decreasing overall current depending on the presence or absence of saturation following toxin application. Data from the

whole-cell recordings indicated that block of outward currents by 200 nM  $\gamma$ -DTX was  $\text{Ca}^{2+}$ -sensitive:  $\gamma$ -DTX had no effect on  $\text{K}^+$  currents in the presence of high EGTA, or absence of  $\text{Ca}^{2+}$  and ATP in the recording pipette. Also, given that  $\gamma$ -DTX, in cells in which  $\gamma$ -DTX blocked outward currents, was unable to completely block outward currents, it was postulated that  $\text{Ca}^{2+}$ -activated  $\text{K}^+$  channels, of the 3 classes of  $\text{K}^+$  channels reported to be present in these cells, were responding to the toxin. Thus, increases in outward currents could occur in cells in which block of  $\text{Ca}^{2+}$ -activated  $\text{K}^+$  channels would remove their saturating effects, and as the voltage-gated channels are activated the current would increase. On the other hand, decreases in current could be a result of  $\text{Ca}^{2+}$ -activated  $\text{K}^+$  channels being the major active channel and therefore block would reduce the current. One possible explanation for directional changes in  $\text{K}^+$  current response to  $\gamma$ -DTX application would be a reflection of a changing channel population as the cell's electrical excitability matures and shifts away from  $\text{Ca}^{2+}$ -activated  $\text{K}^+$  channel based to more voltage-gated representation, as documented for maturing neurons in culture (O'Dowd, Ribera, and Spitzer, 1988).

## 5.2 Single Channel Results

Two channel types were found in outside-out patches of N1E 115 cells, and these channels had very different conductances, patterns of opening, and voltage-dependence, but shared sensitivity to  $\text{Ca}^{2+}$  availability. These channels were found to have single channel conductances, measured under asymmetrical  $[\text{K}^+]$ , of 63 pS and 187 pS. Both of these channels, while within the conductance range of  $\text{Cl}^-$  channels, were insensitive to

the Cl<sup>-</sup> channel blocker SITS. Also, both channels were sensitive to the Ca<sup>2+</sup> channel blocker nifedipine, and to loss of voltage-gated Ca<sup>2+</sup> channel activity when patches were held at positive potentials--channel activity was restored by application of ionomycin, or by increasing the free [Ca<sup>2+</sup>] in the pipette solution. This is consistent with reports that BK(Ca) and IK(Ca) channels are closely associated with voltage-gated Ca<sup>2+</sup> channels (Haylett and Jenkinson, 1990; McManus, 1991), and that opening of BK(Ca) channels in particular is linked to opening of the voltage-gated Ca<sup>2+</sup> channels (McManus, 1991; Hinrichsen, 1993). The 63 pS channel exhibited a characteristic pattern of burst openings followed by silence, was not voltage-dependent, was insensitive to the SK(Ca) blocker apamin, the BK(Ca) blocker IbTX, and to TEA. Such characteristics place the 63 pS channel in the IK(Ca) category of channel types: relative voltage-insensitivity, burst openings, an insensitivity to apamin, TEA, and the specific BK(Ca) blocker ChBTX have been reported for channels of this class (Deitmer and Eckbert, 1985; Haylett and Jenkinson, 1990; Hinrichsen, 1993). The 187 pS channel exhibited variations in both open probability and voltage-dependence, even in patches recorded under the same conditions on the same day, and was sensitive to both TEA and IbTX. Thus, the 187 pS channel has the reported characteristics of BK(Ca) channels (Haylett and Jenkinson, 1990; Hinrichsen, 1993), including a tendency toward what Silberberg et al. (1996) term "wanderlust kinetics" (variations in open probability and voltage-sensitivity within a patch and among patches under the same conditions).

DTX sensitivity of the Ca<sup>2+</sup>-activated K<sup>+</sup> channels found in these outside-out patches varied. As would be predicted on the basis of whole-cell data, neither channel was sensitive to 200 nM  $\alpha$ -DTX. The 63 pS channel was found to be insensitive to

application of either 200 nM  $\beta$ -, or 200 nM  $\gamma$ -DTX. Interestingly, the 187 pS channel was far more sensitive to  $\gamma$ -DTX over a range of concentrations (200 nM, 20 nM and 2 nM), but only mildly sensitive to 200 nM  $\beta$ -DTX application. Again, as would be predicted on the basis of the whole-cell data, the effect of  $\beta$ -DTX on the 187 pS channel was variable—decreases in channel open probability were too variable to be significantly different from control. In contrast, at a concentration of 200 nM,  $\gamma$ -DTX completely blocked the 187 pS channel within 5 minutes. At lower concentrations (20 nM, and 2 nM),  $\gamma$ -DTX-induced channel block was delayed, and was preceded by a transient increase in open probability. Although application of 2 nM  $\gamma$ -DTX, unlike the higher concentrations, did not induce complete channel block, open probability of the 187 pS channel was significantly decreased. Interestingly, application of 200 nM  $\beta$ -DTX also resulted in a transient increase in open probability, similar to that seen with either 20 nM, or 2 nM  $\gamma$ -DTX block. These results indicate that  $\beta$ - and  $\gamma$ -DTX probably act at the same site, but, while  $\beta$ -DTX is far less potent a blocker of the 187 pS channel,  $\gamma$ -DTX is a specific blocker of 187 pS channel activity. It is possible that such an increase in open probability prior to block could be a consequence of the electrostatic interaction between negatively charged residues lining the channel pore and the positively charged DTX residues prior to toxin occlusion of the pore. Perhaps prior to toxin binding the positively charged toxin molecule acts on ion gating sites within the channel mouth to stimulate ion flow. Such a possibility is reinforced by studies of block by cations, which suggest that a site on the extracellular surface of the  $K^+$  channel destabilizes channel closing (Neyton and Pelleschi, 1991; Demo and Yellen, 1992); this theory is reinforced by the discovery



that the site on the DTX molecule which is thought to interact with the  $K^+$  channel has a high concentration of positively charged amino acids (Swaminathan et al., 1996).

Finally, the transient increase in open probability seen prior to the onset of  $\gamma$ -DTX-induced channel block would be consistent with the conclusion that this toxin is an open channel blocker.

### 5.3 Implications and Significance

Several results are reported here for the first time: the discovery of an IK(Ca) channel in this cell line, and the discovery of an extracellular site of action for  $\gamma$ -DTX on a  $Ca^{2+}$ -activated  $K^+$  channel. DTXs have been reported to block large conductance  $Ca^{2+}$ -activated  $K^+$  channels when applied to the intracellular side of the channel (Lucchesi and Moczydlowski, 1991), but not when exposed to the external face (Tauc, Gastineau, and Poujeol, 1993). Application of DTX-I, or the structurally similar BPTI to the intracellular face of BK(Ca) channels has been found to increase subconductance events (Lucchesi and Moczydlowski, 1991). This study represents the first indication that a member of the DTX family may block  $Ca^{2+}$ -activated  $K^+$  channels from an extracellular site. It is not surprising, however, that BK(Ca) channels in one tissue would be insensitive to DTXs (Tauc, Gastineau, and Poujeol, 1993), while another would not: DTX sensitivity is not universal for voltage-gated  $K^+$  channels, and has been found to be tissue-specific (Dolly et al., 1987; Tygat et al., 1995; Harvey, 1997). The implications of this finding are dependent on further study into the nature of the binding site itself, and the function of these channels in this cell line. It is possible, however, that BK(Ca) channel sensitivity to  $\gamma$ -DTX is a reflection of greater structural similarities between

functionally distinct channel types (such as voltage-gated and  $\text{Ca}^{2+}$ -activated  $\text{K}^+$  channels) than originally thought, and that the DTX-sensitive channel subunit expression is related to the channel's physiological role. Further studies to determine whether other BK(Ca) channels in other cell types express a sensitivity to DTXs in general, and  $\gamma$ -DTX in particular, and the place this channel subtype would hold in the  $\text{K}^+$  channel family would also be necessary. This discovery raises many questions as to the nature of  $\text{K}^+$  channel makeup, the relationship between  $\text{Ca}^{2+}$ -activated  $\text{K}^+$  channel and voltage-gated  $\text{K}^+$  channel structure and gene expression.

The discovery of an IK(Ca) channel in this cell line raises interesting questions as to its functional significance. While IK(Ca) channels have been found in mammalian neuronal tissue (Haylett and Jenkinson, 1990), they have not been reported to be present in DMSO-differentiated N1E 115 cells. Since it has not been reported to be one of the channel classes in differentiated N1E 115 cells, the possibility exists that its presence in undifferentiated cells is linked either to differentiation, or cell growth and maturation. Given that  $\text{K}^+$  channels have been shown to play a role in mitogenesis (Deutsch, 1990), and in neuronal differentiation (Ribera and Spitzer, 1992), such a possibility exists. One possibility, suggested by Deutsch (1990) is that  $\text{K}^+$  channels, and IK(Ca) in particular, play a similar role in regulating the ionic environment during mitogenesis, as the cell membrane grows, that they do in the volume regulation pathway. It is noteworthy that IK(Ca) channels in other cell types, most notably in red cells, which are involved in volume regulation are also (like the 63 pS channel found in the N1E 115 cells) voltage-insensitive; while IK(Ca) channels which play a role in cellular excitability are voltage-sensitive (Haylett and Jenkinson, 1990). Further study into the kinetics, pharmacology,

and structure of this channel, and its correlation to both BK(Ca) and voltage-gated  $K^+$  channels would also be of interest—IK(Ca) channel structure, and its genetic relationship to the other classes of  $K^+$  channel has not been reported.

## References

- Adams DJ, and Nonner W (1990) Voltage-dependent ion channels: gating, permeation and block. In: *Potassium Channels: Structure, Classification, Function and Therapeutic Potential*, pp. 40-69, N Cook (ed.). Ellis Horwood Limited, West Sussex.
- Adams PR, Constanti A, Brown DA, and Clark RB (1982) Intracellular  $\text{Ca}^{2+}$  activates a fast voltage-sensitive  $\text{K}^+$  current in vertebrate sympathetic neurones. *Nature* **262**: 746-749.
- Adelman JP, Shen KZ, Kavanaugh MP, Warren RA, Wu YN, Lagrutta A, Bond CT, and North RA (1992) Calcium-activated potassium channels expressed from cloned complimentary DNAs. *Neuron* **9**: 209-216.
- Amano T, Richelson E, and Nirenberg M (1972) Neurotransmitter synthesis by neuroblastoma clones. *Proc. Natl. Acad. Sci. USA* **69**: 258-263.
- Anderson CS, MacKinnon R, Smith C, and Miller C (1988) Charybdotoxin block of single  $\text{Ca}^{2+}$ -activated  $\text{K}^+$  channels. Effects of channel gating, voltage and ionic strength. *J. Gen. Physiol.* **91**: 317-333.
- Awan KA, and Dolly JO (1991) Potassium channel subtypes in rat brain: characteristic locations revealed using  $\beta$ -bungaratoxin,  $\alpha$ - and  $\delta$ -dendrotoxins. *Neurosci.* **40**: 29-39.
- Atkinson NS, Robertson GA, and Ganetzky B (1991) A component of calcium-activated potassium channels encoded by the *Drosophila slo* locus. *Science* **253**: 551-554.
- Bagetta G, Nistico G, and Dolly JO (1992) Production of seizures and brain damage in rats by  $\alpha$ -dendrotoxin, a selective  $\text{K}^+$  channel blocker. *Neurosci. Lett.* **139**: 34-40.
- Bagetta G, Nair S, Nistico G, and Dolly JO (1994) Hippocampal damage produced in rats by  $\alpha$ -dendrotoxin—a selective  $\text{K}^+$  channel blocker—involves non-NMDA receptor activation. *Neurochem. Int.* **24**: 81-90.
- Bednarek MA, Bugianni RM, Leonard RJ, Felix JP (1994) Chemical synthesis and structure-function studies of margatoxin, a potent inhibitor of voltage-dependent potassium channel in human T-lymphocytes. *Biophys. Res. Comm.* **198**: 619-625.

- Benishin CG, Sorenson RG, Brown WE, Krueger BK, and Blaustein MP (1988) Four polypeptide components of green mamba venom selectively block certain potassium channels in rat brain synaptosomes. *Molecular Pharmacology* **34**: 152-159.
- Bentoit E, and Dubois J-M (1986) Toxin I from the snake *Dendroaspis polylepis polylepis*: a highly specific blocker of one type of potassium channel in myelinated nerve fibre. *Brain Res.* **377**: 374-377.
- Bowlby MR, and Levitan IB (1996) Kinetic variability and modulation of *dslo*, a cloned calcium-dependent potassium channel. *Neuropharmacol.* **35**: 867-875.
- Brayden JE (1996) Potassium channels in vascular smooth muscle. *Clin. Exp. Pharmacol. Physiol.* **23**: 1069-1076.
- Brugnara C, Armsby CC, De Franceschi L, Crest M, Martin Euclaire M-F, and Alper SL (1995) Ca<sup>2+</sup>-activated K<sup>+</sup> channels of human and rabbit erythrocytes display distinctive patterns of inhibition by venom peptide toxins. *J. Membrane Biol.* **147**: 71-82.
- Butler A, Tsunoda S, McCobb DP, Wei A, and Salkoff L (1993) *mSlo*, a complex mouse gene encoding "maxi" calcium-activated potassium channels. *Science* **261**: 221-224.
- Chandy KG (1991) Simplified gene nomenclature. *Nature Lond.* **352**: 26.
- Christopherson P (1991) Ca-activated K channel from human erythrocyte membranes: single channel rectification and selectivity. *J. Membrane Biol.* **119**: 75-83.
- Choi KL, Aldrich RW, and Yellen G (1991) Tetraethylammonium distinguishes two inactivation mechanisms in voltage-activated K<sup>+</sup> channels. *Proc. Natl. Acad. Sci. USA* **88**: 5092-5095.
- Choi KL, Mossman C, Aube J, and Yellen G (1993) The internal quaternary ammonium receptor site of Shaker potassium channels. *Neuron* **10**: 533-541.
- Christie MJ (1995) Molecular and functional diversity of K<sup>+</sup> channels. *Clin. Exp. Pharmacol. Physiol.* **22**: 944-951.
- Christie MJ, North RA, Douglas J, and Adelman JP (1990) Heteropolymeric potassium channels expressed in *Xenopus oocytes* from cloned subunits. *Neuron* **2**: 405-411.
- Cook NS (1988) The pharmacology of potassium channels and their therapeutic potential. *TiPS* **9**: 21-28.
- Crest M, Jacquet G, Gola M, Zerrouk H, Benslimane A, Rochat H, Mansuelle P, Martin-Euclaire MF (1992) Kaliotoxin, a novel peptidyl inhibitor of neuronal BK-type Ca<sup>2+</sup>-

activated K<sup>+</sup> channels characterized from *Androctonus mauretanicus mauretanicus* venom. *J. Biol. Chem.* **267**: 1640-1647.

Dawson DC (1991) Ion channels and colonic salt transport. *Ann. Rev. Physiol.* **53**: 321-339.

Deitmer JW, and Eckbert R (1985) Two components of Ca-dependent potassium current in identified neurones of *Aplysia californica*. *Pflugers Arch.* **403**: 353-359.

Demo SD, and Yellen G (1992) Ion effects on gating of the Ca<sup>2+</sup>-activated K<sup>+</sup> channel correlate with occupancy of the pore. *Biophys. J.* **61**: 639-648.

Demo SD, and Yellen G (1991) The inactivation gate of the Shaker K<sup>+</sup> channel behaves like an open channel blocker. *Neuron* **7**: 743-753.

Deutsch C (1990) K<sup>+</sup> channels and mitogenesis. In *Potassium Channels: Basic Function and Therapeutic Aspects*, Proceedings of the 29<sup>th</sup> Annual A. N. Richards Symposium, pp. 251-271, Colatsky TJ (ed.). Wiley-Liss, New York.

Diserbo M, Antonny B, and Verdetti J (1994) Biophysical and pharmacological properties of large conductance Ca<sup>2+</sup>-activated K<sup>+</sup> channels in N1E-115 cells. *Biochem. Biophys. Res. Commun.* **205**: 596-602.

Dolly JO, Rettig J, Scott VES, Parcej DN, Wittkat R, Sewing S, and Pongs O (1994) Oligomeric and subunit structures of neuronal voltage-sensitive K<sup>+</sup> channels. *Biochem. Soc. Trans.* **22**:473-478.

Dolly JO, Stansfeld CE, Breeze AL, Pelchen-Matthews A, Marsh SJ, and Brown DA (1987) Neuronal acceptor sub-types for dendrotoxin and their relation to K<sup>+</sup> channels. In: *Neurotoxins and their Pharmacological Implications*, pp.81-96, Jenner PG (ed.). Raven Press, New York.

Drakopoulou E, Zinn-Justin S, Guenneugues M, Gilquin B, Ménez A, and Vita C (1996) Changing the structural context of a functional  $\beta$ -hairpin: synthesis and characterization of a chimera containing the curaremimetic loop of a snake toxin in the scorpion  $\alpha/\beta$  scaffold. *J. Biol. Chem.* **271**: 11979-11987.

Dworetzky SI, Trojnacki JT, and Gribkoff VK (1994) Cloning and expression of a human large-conductance calcium-activated potassium channel. *Mol. Brain Res.* **27**: 189-193.

Ennis C, and Minchin MCW (1993) The effect of toxin I, a K<sup>+</sup> channel inhibitor, on [<sup>3</sup>H]noradrenaline release from rat cerebral cortex. *Eur. J. Pharmacol.* **248**: 85-88.

Foray M-F, Lancelin J-M, Hollecker M, and Marion D (1993) Sequence-specific  $^1\text{H}$ -NMR assignment and secondary structure of black mamba dendrotoxin I, a highly selective blocker of voltage-gated potassium channels. *Eur. J. Biochem.* **211**: 813-820.

Franciolini F (1994) The S4 segment and gating of voltage-dependent cationic channels. *Biochim. Biophys. Acta* **1197**:227-236.

Garcia ML, Knaus H-G, Munujos P, Slaughter RS and Kaczorowski GJ (1995) Charybdotoxin and its effects on potassium channels. *Am. J. Physiol.* **269**: C1-C10.

Garcia-Calvo M, Knaus H-G, McManus OB, Giangiacomo KM, Kaczorowski GJ, and Garcia ML (1994) Purification and reconstitution of the high-conductance calcium-activated potassium channel from tracheal smooth muscle. *J. Biol. Chem.* **269**: 676-682.

Garcia-Calvo M, Leonard RJ, Novick J, Stevens SP, Schmalhofer W, Kaczorowski J and Garcia ML (1993) Purification, characterization and biosynthesis of margatoxin, a component of *Centurroides margaritatus* venom that selectively inhibits voltage-dependent K channels. *J. Biol. Chem.* **268**: 18866-18874.

Garcia-Calvo M, Vazquez J, Smith M, Kaczorowski GJ, and Garcia ML (1991) Characterization of solubilized charybdotoxin receptor from bovine aortic smooth muscle. *Biochem.* **30**: 111517-11164.

Gardos G (1959) The permeability of human erythrocytes to potassium. *Acta Physiol. Acad. Sci. Hungary* **10**: 185-189.

Goh JW, Kelly MEM, Pennefather PS, Chicchi GG, Cascier MA, Garcia ML, and Kaczorowski GJ (1992) Effect of charybdotoxin and leiurotoxin I on potassium currents in bullfrog sympathetic ganglion and hippocampal neurons. *Brain Res.* **591**: 165-170

Goldstein SAN and Miller C (1993) Mechanism of charybdotoxin block of a *Shaker*  $\text{K}^+$  channel. *Biophys. J.* **65**: 1613-1619.

Gribkoff VK, Lum-Ragan JT, Boissard CG, Post-Munson DJ, Meanwell NA, Starrett JE Jr., Kozlowski ES, Romine JL, Trojnacki JT, McKay C, Zhong J, and Dworetzky SI (1996) Effects of channel modulators on cloned large-conductance calcium-activated potassium channels. *Mol. Pharmacol.* **50**: 206-217.

Grissmer S, Nygyen AN, Aiyar J, Hanson DC, Mather RJ, Gutmari GA, Karmilowicz MJ, Auperin DD, and Chandy KG (1994) Pharmacological characterization of five cloned voltage-gated  $\text{K}^+$  channels, types  $\text{Kv}1.1$ ,  $1.2$ ,  $1.3$ ,  $1.5$ , and  $3.1$  stably expressed in mammalian cell lines. *Mol. Pharmacol.* **45**: 1227-1234.

Grynkiewicz G, Poenie M, and Tsien RY (1985) A new generation of  $\text{Ca}^{2+}$  indicators with greatly improved fluorescence properties. *J. Biol. Chem.* **260**: 2440-2450.

Guy HR, and Durrell SR (1994) Using sequence homology to analyse the structure and function of voltage-gated channels. In: *Molecular Evolution of Physiological Processes*, Society of General Physiologists Symposium 47, pp. 197-212, Fambrough DM (ed.). Rockefeller University Press.

Guy HR, and Conti F (1990) Pursuing the structure and function of voltage-gated channels. *Trends Neurosci.* **13**: 201-206.

Hamill OP, Marty A, Neher E, Sakmann B, and Sigworth FJ (1981) Improved patch-clamp techniques for high-resolution current recording from cells and cell-free membrane patches. *Pflugers Arch.* **391**: 85-100.

Hall A, Stow J, Sorenson R, Dolly JO, and Owen D (1994) Blockade by DTX homologues of voltage-dependent  $K^+$  currents in cultured sensory neurons from neonatal rats. *Br. J. Pharmacol.* **113**: 959-967.

Halperin JA, Brugnara C, and Nicholson-Weller A (1989)  $Ca^{++}$  activated  $K^+$  efflux limits complement mediated lysis of human erythrocytes. *J. Clin. Invest.* **83**: 1466-1471.

Hartmann HA, Kirsch GE, Drewe JA, Tagliatela M, Joho RH, and Brown AM (1991) Exchange of conduction pathways between the pores of two related  $K^+$  channels. *Science Wash. DC* **251**: 942-944.

Harvey AL (1997) Recent studies on dendrotoxins and potassium ion channels. *Gen. Pharmacol.* **28**: 7-12.

Harvey AL, Rowan EG, Vatanpour H, Fatehi M, Castaneda O, and Karlsson E (1994) Potassium channel toxins and transmitter release. *Ann. N. Y. Acad. Sci.* **710**: 1-10.

Harvey AL, Marshall DL, and Possani LD (1992) Dendrotoxin-like effects of noxiustoxin. *Toxicon.* **30**: 1497-1500.

Harvey AL, and Karlsson E (1982) Protease inhibitor homologues from mamba venoms: facilitation of acetylcholine release and interactions with prejunctional blocking toxins. *Br. J. Pharmacol.* **77**: 153-161.

Haylett DG, and Jenkinson DH (1990) Calcium-activated potassium channels. In: *Potassium Channels: Structure, Classification, Function and Therapeutic Potential*, pp. 71-95, N Cook (ed.). Ellis Horwood Limited, West Sussex.

Heginbotham L, Lu Z, Abramson T, and MacKinnon R (1994) Mutations in the  $K^+$  channel signature sequence. *Biophys. J.* **66**: 1061-1067.



Heinemann SH, Rettig J, Grack HR, and Pongs O (1996) Functional characterization of Kv channel  $\beta$ -subunits from rat brain. *J. Physiol.* **493**: 625-633.

Hinrichsen HD (1993) *Calcium-dependent potassium channels*. Molecular Biology Research Unit. RG Landes Company, Austin, Texas.

Herbert SC, Friedman PA, and Andreoli TE (1984) Effects of antidiuretic hormone on cellular conductive pathways in mouse medullary thick ascending limbs of Henle: I ADH increases transcellular conductance pathways. *J. Membr. Biol.* **80**: 201-219.

Hermann A, and Erxleben C (1987) Charybdotoxin selectively blocks small Ca-activated K channels in *Aplysia* neurons. *J. Gen. Physiol.* **90**: 27-47.

Hirsh JK, and Quandt FN (1993) Aminopyridine block of potassium channels in mouse neuroblastoma cells. *J. Pharmacol. Exp. Ther.* **267**: 604-611.

Hodgkin AL, and Huxley AF (1952) A quantitative description of membrane current and its application to conduction and excitation in nerve. *J. Physiol. (Lond)* **116**: 500-544.

Hollecker M, Marshall DL, and Harvey AL (1993) Structural features important for the biological activity of the potassium channel blocking dendrotoxins. *Br. J. Pharmacol.* **110**: 790-794.

Hopkins WF, Demas V, and Tempel BL (1994) Both N- and C-terminal regions contribute to the assembly and functional expression of homo- and heteromultimeric voltage-gated K<sup>+</sup> channels. *J. Neurosci.* **14**: 1385-1393.

Hoshi T, Zagotta WN, Aldrich RW (1990) Biophysical and molecular mechanisms of Shaker potassium channel inactivation. *Science Wash. DC* **250**: 533-538.

Hugues M, Romey G, Duval D, Vincent JP, and Lazdunski M (1982) Apamin as a selective blocker of the calcium-dependent potassium channel in neuroblastoma cells: voltage-clamp and biochemical characterization of the toxin receptor. *Proc. Natl. Acad. Sci. USA* **79**: 1308-1312.

Isacoff EY, Jan YN, and Jan LY (1991) Putative receptor for the cytoplasmic inactivation gate in the Shaker K<sup>+</sup> channel. *Nature Lond.* **353**: 86-90.

Jan LY, and Jan YN (1989) Voltage sensitive ion channels. *Cell* **56**: 13-25.

Kem WR, Parten B, Pennington MW, Price DA, and Dunn BM (1989) Isolation, characterization and amino acid sequence of a polypeptide neurotoxin occurring in the sea anemone *Stichodactyla helianthus*. *Biochem.* **28**: 3483-3489.

- Keynes RD (1994) The kinetics of voltage-gated ion channels. *Quarterly Rev. Biophysics* **27**: 339-434.
- Kimhi Y, Palfrey C, Spector I, Barak Y, and Littauer UZ (1976) *Proc. Natl. Acad. Sci. USA* **73**: 462-466.
- Kirsch GE and Drewe JA (1993) Gating-dependent mechanism of 4-aminopyridine block in two related potassium channels. *J. Gen. Physiol.* **102**: 797-816.
- Kirsch GE, Shieh CC, Drewe JA, Vener DF, and Brown AM (1993) Segmental exchanges define 4-aminopyridine binding at the inner mouth of K<sup>+</sup> pores. *Neuron* **11**: 503-512.
- Knaus H, Folander F, Garcia-Calvo M, Garcia ML, Kaczorowski GJ, Smith M, and Swanson R (1994) Primary sequence and immunological characterization of  $\beta$ -subunit of high conductance Ca<sup>2+</sup>-activated K<sup>+</sup> channel from smooth muscle. *J. Biol. Chem.* **269**: 17274-17278.
- Kramer RH, Goulding E, and Siegelbaum SA (1994) Potassium channel inactivation peptide blocks cyclic nucleotide-gated channels by binding to the conserved pore domain. *Neuron* **12**: 655-662.
- Kukuljan M, Labarca P, and Latorre R (1995) Molecular determinants of ion conduction and inactivation in K<sup>+</sup> channels. *Am. J. Physiol.* **268**: C535-C556.
- Lagutta A, Shen KZ, North RA, and Adelman JP (1994) Functional differences among alternatively spliced variants of Slowpoke, a Drosophila calcium-activated potassium channel. *J. Biol. Chem.* **269**: 20347-20351.
- Larsson HP, Baker OS, Dhillon DS, and Isacoff EY (1996) Transmembrane movement of the Shaker K<sup>+</sup> channel S4. *Neuron* **16**: 387-397.
- Latorre R, Oberhauser A, Labarca P, and Alvarez O (1989) Varieties of calcium-activated potassium channels. *Ann. Rev. Physiol.* **51**: 385-399.
- Leicher T, Roeper J, Weber K, Wang X, and Pongs O (1996) Structural and functional characterization of human potassium channel subunit family  $\beta$ 1(KCN1B). *Neuropharmacology* **35**: 787-795.
- Leinders T, and Vijverberg HPM (1992) Ca<sup>2+</sup> dependence of small Ca<sup>2+</sup>-activated K<sup>+</sup> channels in cultured N1E-115 mouse neuroblastoma cells. *Pflugers Arch.* **422**: 223-232.
- Leonard RJ, Garcia ML, Slaughter RS, and Reuben JP (1992) Selective blockers of voltage-gated K<sup>+</sup> channels depolarize human T lymphocytes: mechanism of antiproliferative effect of charybdotoxin. *Proc. Natl. Acad. Sci. USA* **89**: 10094-10098.

Lewis RS, and Calahan MD (1990) Ion channels and signal transduction in lymphocytes. *Ann. Rev. Physiol.* **52**: 415-430.

Lewis RS and Calahan MD (1995) Potassium and calcium channels in lymphocytes. *Ann. Rev. Immunol.* **13**: 623-653.

Li M, Jan YN, and Jan LY (1992) Specification of subunit assembly by the hydrophilic amino-terminal domain of the *Shaker* potassium channel. *Science* **257**: 1225-1230.

Liman ER, Hess P, Weaver F, and Koren G (1991) Voltage-sensing residues in the S4 region of the mammalian K<sup>+</sup> channel. *Nature Lond.* **353**: 752-756.

Logothetis DE, Movahedi S, Salter C, Lindpainter K, and Nadal-Ginard B (1992) Incremental reductions of positive charge within the S4 region of a voltage-gated K<sup>+</sup> channel result in corresponding decreases in gating charges. *Neuron* **8**: 531-540.

Lopez GA, Jan YN, and Jan LY (1994) Evidence that the S6 segment of *Shaker* voltage-gated K<sup>+</sup> channel comprises part of the pore. *Nature Lond.* **367**: 179-182.

López-Barneo J, Hoshi T, Heinemann SH, and Aldrich RW (1993) Effects of external cations and mutations in the pore region on C-type inactivation of *Shaker* potassium channels. *Recept. Channels* **1**: 61-71.

Lucchesi KJ, and Moczydlowski E (1991) On the interaction of bovine pancreatic trypsin inhibitor with maxi Ca<sup>2+</sup>-activated K<sup>+</sup> channels: a model for analysis of peptide-induced subconductance states. *J. Gen. Physiol.* **97**: 1295-1319.

MacKinnon R, Aldrich R, and Lee AW (1993) Functional stoichiometry of *Shaker* potassium channel inactivation. *Science Wash. DC* **262**: 757-759.

MacKinnon R, Heginbotham L, and Abramson T (1990) Mapping the receptor site for charybdotoxin, a pore-blocking potassium channel inhibitor. *Neuron* **5**: 767-771.

MacKinnon R, and Miller C (1989) Mutant potassium channels with altered binding of charybdotoxin, a pore-blocking peptide inhibitor. *Science Wash. DC* **245**: 1382-1385.

MacKinnon R, and Miller C (1988) Mechanisms of charybdotoxin block of *Shaker* K<sup>+</sup> channels suggests that different types of K<sup>+</sup> channels share common structural features. *Neuron* **1**: 997-1001.

MacKinnon R, Reinhart PH, and White MM (1988) Charybdotoxin block of *Shaker* K<sup>+</sup> channels suggests that different types of K<sup>+</sup> channels share common structural features. *Neuron* **1**: 997-1001.

Mannuzzu LM, Moronne MM, and Isacoff EY (1996) Direct physical measure of conformational rearrangement underlying potassium channel gating. *Science Wash. DC* **271**: 213-216.

McCobb DP, Fowler NL, Featherstone T, Lingle C, Mitsuyoshi S, Knause JE, and Salkoff L (1995) A human calcium-activated potassium channel gene expressed in vascular smooth muscle. *Am. J. Physiol.* **269**: H767-H777.

McCormack K, Lin JW, Iverson LE, and Rudy B (1990) Shaker K<sup>+</sup> channel subunits form heteromultimeric channels with novel functional properties. *Biochem. Biophys. Res. Commun.* **3**: 1361-1371.

McCormack T, and McCormack K (1994) Shaker K<sup>+</sup> channel  $\beta$  subunits belong to an NAD(P)H-dependent oxido-reductase superfamily. *Cell* **79**: 1133-1135.

McManus OB, Helms LMH, Pallancki L, Ganetzky B, Swanson R, and Leonard RJ (1995) Functional role of the  $\beta$  subunit of high conductance calcium-activated potassium channels. *Neuron* **14**: 1-20.

McManus OB (1991) Calcium-activated potassium channels: regulation by calcium. *J. Bioenerg. Biomem.* **23**: 537-560.

Mienville M-C, and Baker JL (1996) Immature properties of large-conductance calcium-activated potassium channels in rat neuroepithelium. *Pflügers Arch. Eur. J. Physiol.* **431**: 763-770.

Mienville M-C (1994) Gating mode conversion by proteolysis in a large conductance K<sup>+</sup> channel from embryonic rat telencephalon. *J. Physiol. (Lond)* **481**: 293-298.

Miller C (1995) The charybdotoxin family of K<sup>+</sup> channel-blocking peptides. *Neuron* **15**: 5-10.

Miller C (1988) Competition for block of a Ca<sup>2+</sup>-activated K<sup>+</sup> channel by charybdotoxin and tetraethylammonium. *Neuron* **1**: 1003-1006.

Moolenaar WH and Spector I (1978) Ionic currents in cultured mouse neuroblastoma cells under voltage clamp. *J. Physiol.* **278**: 265-286.

Moss GWJ, Marshall J, Morabito M, Howe JR, and Moczydlowski E (1996) An evolutionarily conserved binding site for serine protease inhibitors in large conductance calcium-activated potassium channels. *Biochem.* **35**: 16024-16035.

Moss GWJ, and Moczydlowski E (1996) Rectifying conductance substates in a large conductance Ca<sup>2+</sup>-activated K<sup>+</sup> channel: evidence for a fluctuating barrier mechanism. *J. Gen. Physiol.* **107**: 47-68.

Muniz ZM, Parcej DN, and Dolly JO (1992) Characterization of monoclonal antibodies against voltage-dependent K<sup>+</sup> channels raised using  $\alpha$ -dendrotoxin acceptors purified from bovine brain. *Biochem.* **31**: 12297-12303.

Murrell-Lagnado RU, and Aldrich RW (1993) Interactions of the amino terminal domains of Shaker channels with a pore blocking site studied with synthetic peptides. *J. Gen. Physiol.* **102**: 949-975.

Munujos P, Knaus HG, Kaczorowski GJ, and Garcia ML (1995) Cross-linking of charybdotoxin to high-conductance calcium-activated potassium channels: identification of the covalently modified toxin residue. *Biochem.* **34**: 10771-10776.

Naini AA, Shimony E, Kozlowski E, Shaikh T, Dang W and Miller C (1996) Interaction of Ca<sup>2+</sup>-activated K<sup>+</sup> channels with refolded charybdotoxins mutated at a central interaction residue. *Neuropharmacol.* **35**: 915-921.

Narahashi T, Tsunoo A, and Yoshii M (1987) Characterization of two types of calcium channels in mouse neuroblastoma cells. *J. Physiol.* **383**: 231-249.

Neyton J, and Pelleschi M (1991) Multi-ion occupancy alters gating in high conductance, Ca<sup>2+</sup>-activated K<sup>+</sup> channels. *J. Gen. Physiol.* **97**: 641-665.

Neyton J, and Miller C (1988a) Discrete Ba<sup>2+</sup> block as a probe of ion occupancy and pore structure in the high conductance Ca<sup>2+</sup>-activated K<sup>+</sup> channel. *J. Gen. Physiol.* **92**: 427-429.

Neyton J, and Miller C (1988b) Potassium block barium permeation through a calcium-activated potassium channel. *J. Gen. Physiol.* **92**: 549-567

Oakes SG, Schlager JJ, Santone KS, Abraham RT, and Powis G (1990) Doxorubicin blocks the increase in intracellular Ca<sup>++</sup>, part of a second messenger system in N1E-115 murine neuroblastoma cells. *J. Pharmacol. Exp. Ther.* **252**: 979-83.

Owen DG, Hall A, Stephens G, Stow J, and Robertson B (1997) The relative potencies of dendrotoxins as blockers of the cloned voltage-gated K<sup>+</sup> channel, mKv1.1 (MK-1), when stably expressed in Chinese hamster ovary cells. *Br. J. Pharmacol.* **120**: 1029-1034.

O'Dowd DK, Ribera AB, and Spitzer NC (1988) Development of voltage-dependent calcium, sodium and potassium currents in *Xenopus* spinal neurons. *J. Neurosci.* **8**: 792-805.

Papazian DM, Timpe LC, Jan YN, and Jan LY (1991) Alteration of voltage-dependence of *Shaker* potassium channel by mutations in the S4 sequence. *Nature Lond.* **349**: 305-310.

- Parcej DN, Scott VES, and Dolly JO (1992) Oligomeric properties of an  $\alpha$ -dendrotoxin-sensitive potassium ion channels purified from bovine brain. *Biochem. 31*: 11084-11088.
- Park C-S and Miller C (1992) Mapping function to structure in a channel-blocking peptide: electrostatic mutants of charybdotoxin. *Biochem. 31*: 7749-7755.
- Pelchen-Matthews A, and Dolly JO (1989) Distribution in the rat central nervous system of acceptor sub-types for dendrotoxin, a  $K^+$  channel probe. *Neurosci. 29*: 347-361.
- Penner R, Petersen M, Pierau F-K, and Dreyer F (1986) Dendrotoxin: a selective blocker of non-inactivating potassium current in guinea-pig dorsal root ganglion neurones. *Pflügers Arch. Gen. Physiol. 407*: 365-369.
- Quandt FN (1994) Recording sodium and potassium currents from neuroblastoma cells. *Methods in Neuroscience 19*: 3-20.
- Quandt FN (1988) Three kinetically distinct potassium channels in mouse neuroblastoma cells. *J. Physiol. 395*: 401-418.
- Quandt FN, and Narahashi T (1984) Isolation and kinetic analysis of inward currents in neuroblastoma cells. *Neurosci. 13*: 249-262.
- Reinhart PH, Chung S, and Levitan IB (1989) A family of calcium-dependent potassium channels from rat brain. *Neuron 2*: 1031-1041.
- Ren J, Karpinski E, and Benishin C (1994) Inhibition of a  $K^+$  current by  $\beta$ -dendrotoxin in primary and subcultured vascular smooth muscle cells. *J. Pharmacol. Exp. Ther. 269*: 209-214.
- Rettig JS, Heinemann SH, Wunder F, Lorra C, Parcej DN, Dolly JO, and Pongs O (1994) Inactivation properties of voltage-gated  $K^+$  channels altered by presence of  $\beta$  subunit. *Nature Lond. 369*: 289-294.
- Ribera AB, and Spitzer NC (1992) Developmental regulation of potassium channels and the impact on neuronal differentiation. In *Ion Channels*, Vol. 3, pp. 1-38, Narahashi T (ed.). Plenum Press, New York.
- Robertson B, Owen D, Stow J, Butler C, and Newland C (1996) Novel effects of dendrotoxin homologues on subtypes of mammalian Kv1 potassium channels expressed in *Xenopus oocytes*. *FEBS Lett. 383*: 26-30.
- Ruppertsburg JP, Schröter KH, Sakmann B, Stocker M, Sewing S, and Pongs O (1990) Heteromultimeric channels formed in rat brain potassium-channel proteins. *Nature (Lond) 345*: 535-537.

- Reinhart PH, Chung S, and Levitan IB (1989) A family of calcium-dependent potassium channels from rat brain. *Neuron* **2**: 1031-1041.
- Romi R, Crest M, Grola M, Sampieri F, Jacquett G, Zerrouk H, Mansuelle P, Sorokine O, Van Dorrselauer A, Rochat H, Martin-Euclaire MF, and Van Rietschoten J (1993) Synthesis and characterization of kaliotoxin. Is the 26-32 sequence essential for potassium channel recognition? *J. Biol. Chem.* **268**: 26302-26309.
- Sah P (1996)  $\text{Ca}^{2+}$ -activated  $\text{K}^+$  currents in neurones: types, physiological roles and modulation. *Trends Neurosci.* **19**: 150-154.
- Salkoff L, and Jegla T (1995) Surfing the DNA databases for  $\text{K}^+$  channels nets yet more diversity. *Neuron* **15**: 489-492.
- Schultz SG (1984) A cellular model for active sodium absorption by mammalian colon. *Ann. Rev. Physiol.* **46**: 435-451.
- Schweitz H, Bidard J-N, Maes P and Lazdunski M (1989) Charybdotoxin is a new member of the  $\text{K}^+$  channel toxin family that includes dendrotoxin I and mast cell degranulating peptide. *Biochem.* **28**: 9708-9714.
- Scott et al. (1994a) Primary structure of a  $\beta$  subunit of  $\alpha$ -DTX sensitive  $\text{K}^+$  channels from bovine brain. *PNAS* **91**: 1637-41.
- Scott VES, Muniz ZA, Sewing S, Lichtinghagen R, Parcej DN, Pongs O, and Dolly JO (1994b) Antibodies specific for distinct Kv subunits unveil a heterooligomeric basis for subtypes of an  $\alpha$ -dendrotoxin-sensitive  $\text{K}^+$  channels in bovine brain. *Biochem.* **33**: 11084-11088.
- Sheng M, Liao YJ, Jan YN, and Jan LY (1993) Presynaptic A-current based on heteromultimeric  $\text{K}^+$  channels detected in vivo. *Nature (Lond)* **365**: 72-75.
- Silberberg SD, Lagutta A, Adelman JP, and Magleby KL (1996) Wanderlust kinetics and variable  $\text{Ca}^{2+}$ -sensitivity of *dslo*, a large conductance  $\text{Ca}^{2+}$ -activated  $\text{K}^+$  channel expressed in oocytes. *Biophys. J.* **70**: 2640-2651.
- Skarzynski T (1992) Crystal structure of  $\alpha$ -dendrotoxin from the green mamba venom and its comparison with the structure of bovine pancreatic trypsin inhibitor. *J. Mol. Biol.* **224**: 671-683.
- Slesinger P, Jan YN, and Jan LY (1993) The S4-S5 loop contributes to the ion-selective pore of potassium channels. *Neuron* **11**: 739-749.

Smith LA, Lafaye PJ, LaPontiere HF, Spain T, and Dolly JO (1993) Cloning and functional expression of dendrotoxin K from black mamba, a K<sup>+</sup> channel blocker. *Biochem. J.* **32**: 5692-5697.

Solaro CR, Prakriya M, Ding JP, and Lingle CJ (1995) Inactivating and noninactivating Ca<sup>2+</sup>- and voltage-dependent K<sup>+</sup> current in rat adrenal chromaffin cells. *J. Neurosci.* **15**: 6110-6123.

Sprunger LK, Stewig NJ, and O'Grady SM (1996) Effects of charybdotoxin on K<sup>+</sup> channel (Kv1.2) deactivation and inactivation kinetics. *Eur. J. Pharmacol.* **314**: 357-364.

Swaminathan P, Hariharan M, Murali R, and Singh CU (1996) Molecular structure, conformational analysis, and structure-activity studies of Dendrotoxin and its homologues using molecular mechanics and molecular dynamics techniques. *J. Mol. Chem.* **39**: 2141-2155.

Taglialatela M, and Brown AM (1995) Structural motifs underlying voltage-dependent K<sup>+</sup> channel function. *Kidney Int.* **48**: 918-922.

Tauc M, Gastineau M, and Poujeol P (1993) Toxin sensitivity of the calcium-dependent rubidium efflux in Mabin-Darby canine kidney cells. *Biochem. Biophys. Res. Commun.* **190**: 596-601.

Torro L, Stefani E, and Latorre R (1992) Internal blockade of a Ca<sup>2+</sup>-activated K<sup>+</sup> channel by shakerB inactivating "ball" peptide. *Neuron* **9**: 237-245.

Tseng-Crank J, Yao JA, Berman MF, and Tseng GN (1994a) Functional role of the NH<sub>2</sub>-terminal cytoplasmic domain of a mammalian A-type K<sup>+</sup> channel. *J. Gen. Physiol.* **102**: 1057-1083.

Tseng-Crank J, Foster CD, Krauz JD, Mertz R, Godinot N, Dilhara TJ, and Reinhart PH (1994b) Cloning, expression and distribution of functionally distinct Ca<sup>2+</sup>-activated K<sup>+</sup> channel isoforms from human brain. *Neuron* **13**: 1315-1330.

Tytgat J, Debont T, Carmeliet E, and Daenens P (1995) The  $\alpha$ -dendrotoxin footprint on a mammalian potassium channel. *J. Biol. Chem.* **270**: 24776-24781.

Wang H, Kunze DD, Martin TM, Shwartzkron PA, and Tempel BL (1993) Heteromultimeric K<sup>+</sup> channels in terminal and juxtaparanodal regions of neurons. *Nature (Lond)* **365**: 75-79.

Wang R (1991) *Characterization of voltage-dependent calcium channels and their modulation by parathyroid hormone in three types of cells.* PhD Thesis.



- Wei, A, Jegla, T, and Salkoff L (1996) Eight potassium channel families revealed by the *C. elegans* genome project. *Neuropharmacology* **35**: 805-829.
- Wei A, Solaro C, Lingle C, and Salkoff L (1994) Calcium sensitivity of BK-type  $K_{Ca}$  channels determined by a separable domain. *Neuron* **13**: 671-681.
- Werkman TR, Kawamura T, Yokoyama S, Higashida H, and Rogawski MA (1992) Charybdotoxin, dendrotoxin and mast cell degranulating peptide block the voltage-activated  $K^+$  current of fibroblast cells stably transfected with NGK1 (Kv1.2)  $K^+$  channel complementary DNA. *Neurosci.* **50**: 935-946.
- Winters CJ, Reeves WB, Andreoli TE (1991) A survey of transport properties of the thick ascending limb. *Semin. Nephrol.* **11**: 236-247.
- Wu JV, Shuttleworth TJ, and Stampe P (1996) Clustered distribution of calcium sensitivities: an indication of hetero-tetrameric gating components in  $Ca^{2+}$ -activated  $K^+$  channels reconstituted from avian nasal gland. *J. Membrane Biol.* **154**: 275-282.
- Yellen G, Sodickson D, Chen T-Y, and Jurman ME (1994) An engineered cysteine in the external mouth of a  $K^+$  channel allows inactivation to be modulated by metal binding. *Biophys. J.* **66**: 1068-1075.
- Yellen G, Jurman ME, Abramson T, and Mackinnon R (1991) Mutations affecting internal TEA blockade identify the probable pore forming region of a  $K^+$  channel. *Science Wash. DC* **251**: 939-942.
- Yool AJ, and Schwarz TL (1991) Alteration of ionic selectivity of a  $K^+$  channel by mutation of the H5 region. *Nature Lond.* **349**: 700-704.
- Yusaf SP, Wray D, and Sivaprasadarao A (1996) Measurement of the movement of the S4 segment during the activation of a voltage-gated potassium channel. *Pflugers Arch.* **433**: 91-97.